GC-MS PROFILING AND IN-SILICO EVALUATION OF PHYTOCONSTITUENTS OF *ANDROGRAPHIS PANICULATA*: MOLECULAR DOCKING AND ADMET PREDICTION AGAINST SARS-COV-2

BY

AKPOMEDAYE EDESIRI

PHA1908455

SUPERVISED BY

DR. VINCENT O. IMIEJE

DEPARTMENT OF PHARMACEUTICAL CHEMISTRY

FACULTY OF PHARMACY

UNIVERSITY OF BENIN

BENIN CITY

NOVEMBER, 2025.

GC-MS PROFILING AND IN-SILICO EVALUATION OF PHYTOCONSTITUENTS OF ANDROGRAPHIS PANICULATA: MOLECULAR DOCKING AND ADMET PREDICTION AGAINST SARS-COV-2

BY

AKPOMEDAYE EDESIRI

PHA1908455

A DISSERTATION SUBMITTED TO THE DEPARTMENT OF PHARMACEUTICAL CHEMISTRY, FACULTY OF PHARMACY, UNIVERSITY OF BENIN, BENIN CITY, IN PARTIAL FULFILMENT OF THE REQUIREMENT FOR THE AWARD OF DOCTOR OF PHARMACY (PHARM.D) DEGREE HONOURS OF THE UNIVERSITY OF BENIN, BENIN CITY, EDO STATE, NIGERIA.

NOVEMBER, 2025.

CERTIFICATION

This is to certify that this work was done by **Akpomedaye Edesiri** in the Department of Pharmaceutical Chemistry, Faculty of Pharmacy, University of Benin, Benin City, Nigeria, in partial fulfillment of the requirements of the award of the Doctor of Pharmacy Degree (Pharm. D).

_____ _____

Dr. Vincent O. Imieje **Date**
(Project Supervisor)

_____ _____

Dr. Vincent O. Imieje **Date**
(Head of Department)

_____ _____

Akpomedaye Edesiri **Date**
(Student)

DEDICATION

This work is dedicated to God Almighty. Blessed is He who has done all things well, and to him be all the glory.

And to my mum, Mrs. Mary Izobo, for her consistent love, support, and prayers throughout my studies. God bless you, Ma. I do not take it for granted.

ACKNOWELEDGEMENT

First and foremost, I am most grateful to the One who does exceedingly above all I could ever ask for and I thank him for his loving-kindness to me.

I would also like to express my most profound appreciation to my project supervisor, Dr. Vincent O. Imieje, for his constant guidance, encouragement, and welcoming aura throughout this study. I truly appreciate you, Sir.

I wish to thank my parents, Mr. Peter and Mrs. Mary Izobo, for their love, prayers, financial and moral support. I owe this achievement to your unwavering belief in me.

My sincere appreciation goes to my project colleagues, Irekhore Ayomide, Kpando Susan, Saibu Nelson, and Ayedogba Bamidele. Thank you all for your outstanding contributions to this project. I am also grateful to my dear friends, Gillow Naomi, Agbonkhese Eghonghon, Ophori Hale, Amratefa Ewomaoghene, Osunde Peter, Ogedengbe Taiwo, Akhideno Omonehizena, Afolabi Jumoke, and Babalola Febisola for all your kind words and encouragement over the years. I would also like to thank my uncle, Engr. Cyril Obukohwo and his family for being my home away from home. Special appreciation to Pst. Mike O. Otayohwo for his constant prayers and support. I am grateful, Sir.

To the distinguished Faculty of Pharmacy, University of Benin, and its staff, thank you for your positive impact on my academic journey.

TABLE OF CONTENTS

LIST OF TABLES

LIST OF FIGURES

LIST OF ABBREVIATIONS

2D: Two-dimensional

3D: Three-dimensional

ADMET: Absorption, Distribution, Metabolism, Excretion and Toxicity

ARG: Arginine

Arom: Aromatic

ASN: Asparagine

ASP: Aspartate

BBB: Blood Brain Barrier

CID: Compound Identification Number

CYP: Cytochrome P450

FDA: Food and Drug Administration

GC-MS: Gas Chromatography- Mass Spectrometry

GI absorption: Gastrointestinal absorption

GLN: Glutamine

GLU: Glutamate

GLY: Glycine

HIS: Histidine

ILE: Isoleucine

LEU: Leucine

LYS: Lysine

MET: Methionine

Num: Number

P-gp substrate: P-glycoprotein substrate

H: Hydrogen

PHE: Phenylalanine

PRO: Proline

RAM: Random Access Memory

ROM: Read-Only Memory

S/N: Serial number

SDF: Structure Data File

SER: Serine

THR: Threonine

TPSA: Topological Polar Surface Area

TYR: Tyrosine

VAL: Valine

WHO: World Health Organization

MIN: Minute

SPA-SE: Specifying and Affinity with Solvation Effect

ABSTRACT

The outbreak of COVID-19, caused by SARS-CoV-2, has created an urgent need for new and more effective antiviral agents, particularly those derived from natural sources. *Andrographis paniculata* (Burm.f.) Nees (Acanthaceae), commonly known as the King of bitters, is a medicinal plant valued for its antiviral and immunomodulatory properties.

This study aimed to investigate the therapeutic potential of phytochemicals from *Andrographis paniculata* as inhibitors of the SARS-CoV-2 virus (PDB ID:7BV2) using molecular docking and ADMET predictions.

The 3D structure of the SARS-CoV-2 protein was obtained from the RCSB PDB. Amino acids at the binding site of the protein were identified using PLIP. The protein was prepared for docking in BIOVIA Discovery Studio. Phytochemicals isolated from the plant and identified using GC-MS were downloaded from PubChem as SDF files and imported into PyRx for molecular docking. Post-docking interaction was analysed in BIOVIA Discovery Studio. The ADMET predictions of the phytochemicals were done using the Swiss ADME web server and ProTox-3.0.

Molecular docking results from 90 isolated compounds and 23 compounds from GC-MS analysis revealed 27 isolated compounds with a binding affinity range of -6.9 to -8.5 kcal/mol against the target protein, as compared to the standard drug (Remdesivir Triphosphate) and co-crystallized ligand (F86) with binding affinities of -7.7 and -6.8 kcal/mol, respectively. These 27 compounds were selected for post-docking analysis and ADMET profiling.

Andrographis paniculata (Burm.f.) Nees (Acanthaceae) possesses phytoconstituents with potential inhibitory activity against the SARS-CoV-2 protein. Methyl 3,4-dicaffeoylquinate, identified as the top compound, along with 5-Hydroxy-7,2',6'-trimethoxyflavone, 5,7,2',6'-Tetrahydroxyflavone, and Apigenin showed good absorption, distribution, metabolism, elimination (ADME), and a comparatively safe toxicity profile. Therefore, further experimental validation is required to confirm their therapeutic potential as antiviral agents against SARS-CoV-2

CHAPTER ONE

INTRODUCTION AND LITERATURE REVIEW

1.1 INTRODUCTION

1.1.1 GLOBAL HEALTH BURDEN OF SARS-CoV-2

Coronavirus (COVID-19), a highly contagious respiratory disease caused by the virus Severe Acute Respiratory Syndrome Coronavirus 2(SARS-CoV-2). The name Corona, derived from the Latin word for 'crown', refers to the crown-like spike projections observed on the viral surface under electron microscopy. Coronaviruses (CoVs) belong to the Coronaviridae family of positive-stranded RNA viruses that infect humans and animals. Alpha, Beta, Gamma, and Delta Covs are the four genera of CoVs; the first two specifically affect humans. Severe Acute Respiratory Syndrome Coronavirus (SARS-CoV) caused an outbreak of SARS (2002-2003) with a 10% death rate, while Middle East respiratory syndrome coronavirus (MERS-CoV) triggered a deadly epidemic in 2012 with a fatality rate of 37% (Aziz *et al.*, 2023; World Health Organization [WHO], 2024). These viruses are widespread across numerous animal species but in several cases they can evolve and infect humans, thus spreading rapidly within the population. Such was the case with SARS-CoV-2, a novel variant of the betacoronaviridae genus that was first identified in Wuhan, China, in late 2019 and quickly spread worldwide, leading to a global pandemic declared by the World Health Organization (WHO) in March 2020.

The COVID-19 pandemic is one of the most severe global crises in history, with over 7 million reported deaths and 778 million reported cases worldwide as of 2025 (Mathieu *et al.,* 2020; WHO, 2025). The source of COVID-19 is not clear, although it was initially believed that bats were the source of the infection (Yin *et al.,* 2018). Reports from the World Health Organization (WHO) show that the Americas have recorded the highest number of COVID-19 cases worldwide, making the region the most affected during the pandemic. While the virus has affected the population worldwide, certain groups remain more susceptible to severe outcomes. These include the elderly, people with pre-existing health problems such as diabetes, hypertension, heart disease, and respiratory disorders, as well as immunocompromised persons.

Symptoms associated with COVID-19

While some patients remain asymptomatic, others present with a variety of symptoms of COVID-19;

- Common symptoms: The most frequent symptoms include fever, cough, fatigue, anorexia, shortness of breath, and myalgias (muscle aches)
- Other non-specific symptoms: patients may experience sore throat, nasal congestion, headache, diarrhea, nausea, and vomiting.
- Neurological manifestations: COVID-19 can be associated with a spectrum of neurological and mental health issues. These include:
  - Anxiety, depression, and sleep problems.
  - Headache, dizziness, and impaired sense of smell (anosmia) or taste preceding the onset of respiratory symptoms
  - Stroke, seizures, and other cerebrovascular disorders.
- Atypical symptoms in specific populations:
  - Older and Immunosuppressed people: these individuals may present with fatigue, reduced alertness, reduced mobility, diarrhea, loss of appetite, and confusion, often without a fever.
  - Children: children generally have milder and less frequent symptoms than adults. Fever and cough are the most common symptoms reported, and infants may have difficulty feeding and fever.
  - Pregnant women: Dyspnoea, fever, gastrointestinal (GI) symptoms or fatigue due to physiologic adaptations in pregnant women, adverse pregnancy events, or other diseases such as malaria, may overlap with symptoms of COVID-19
- Post-COVID-19 Condition (Long COVID): Some individuals experience long term symptoms usually 3 months after the initial infection, including fatigue, muscle or joint pain, breathlessness, impaired sleep, depression, anxiety, loss of smell and taste, headache, and brain fog (WHO, 2023).

Modes of COVID-19 transmission

Human-to-Human Transmission

- ❖ Aerosol: The virus can spread through aerosols from expired air, coughs, and sneezes. These virus-containing aerosols can persist in the air for extended periods, especially in closed environments, increasing the rate of transmission. Asymptomatic individuals can also be a source of aerosol transmission.
- ❖ Droplets: Droplets expelled from the oral cavity and respiratory tract through coughing and sneezing can contain the virus. People can get infected by inhaling or ingesting these droplets, or by having them land on their mucous membranes.
- ❖ Direct contact: Transmission can occur through direct contact with virus-contaminated objects or surfaces, which then infect a person through their mouth, nose, or eyes. Fomites are suspected to be a primary source of infectious particles in this mode.

Other Potential Modes of Transmission

- ❖ Faecal-Oral Transmission: The virus can be transmitted through faeces. The gastrointestinal system is considered a crucial route for the virus's spread. Viral RNA can be found in a person's stool for a long time, even after the virus is no longer present in their respiratory tract.
- ❖ Animal-to-Human Transmission: The virus is believed to have originated from animals. Therefore, close contact with infected animals can cause infection.
- ❖ Vertical Transmission: The virus can be transmitted from a pregnant mother to her fetus, potentially causing infection (Rahman *et al.,* 2020).

1.1.2 WHO's definitions of the disease severity of COVID-19

- Critical COVID-19 – Defined by the criteria for acute respiratory distress syndrome (ARDS), sepsis, septic shock, or other conditions that would typically require the provision of life-sustaining therapies such as mechanical ventilation (invasive or non-invasive) or vasopressor therapies
- Severe COVID-19 – defined by any of:
  - Oxygen saturation < 90% on room air;
  - Severe pneumonia
  - Signs of respiratory distress
- Non-severe COVID-19 – absence of any criteria for severe or critical COVID-19

1.1.3 Prevention and Clinical Management of COVID-19

Prevention and clinical management of COVID-19 involve measures to reduce the spread of the disease and to provide proper treatment for those affected. Below are key aspects of COVID-19 management:

1.1.3.1 Diagnosis of COVID-19

- Reverse transcriptase-polymerase chain reaction (RT-PCR), which identifies viral RNA in respiratory samples.
- Rapid antigen tests provide quicker results and are widely used for screening, though they are less sensitive than RT-PCR.
- Computed tomography (CT) scans are essential in patients with severe disease.
- Clinical diagnosis also considers a history of exposure, presenting symptoms such as fever, cough, and shortness of breath, and laboratory findings, including elevated inflammatory markers.

1.1.3.2 Preventive strategies for COVID-19

Preventing the spread of COVID-19 involves both pharmacological and non-pharmacological measures.

- Pre-exposure prophylaxis and Vaccination (Centers for Disease Control and Prevention [CDC], 2025).
- Personal Hygiene: frequent handwashing with soap and water or use of alcohol-based hand sanitizer
- Respiratory protection: the use of face masks, particularly in crowded environments.
- Physical distancing and ventilation: avoiding close contact, maintaining adequate ventilation in indoor spaces, and avoiding mass gatherings.
- Symptom-based isolation and testing: Individuals with symptoms are advised to isolate promptly and undergo diagnostic testing until symptom resolution.

1.1.3.3 Medications Used in Management

According to the WHO clinical practice guidelines 2025, several medications are used in the management of COVID-19 depending on disease severity.

- Antiviral agents:

- Remdesivir has been approved for hospitalized patients requiring supplemental oxygen.
- Nirmatrelvir-Ritonavir (Paxloid) and Molnupiravir are oral antivirals used in patients at risk of progression to severe disease.

- Anti-inflammatory and immunomodulatory agents:
  - Dexamethasone (or equivalent steroid) is indicated for all patients needing oxygen or ventilatory support.
  - Tocilizumab and Baricitinib are used in select severe cases to modulate excessive immune response.
- Antipyretic agents:
  - Use of NSAIDs or acetaminophen to allay fever and pain is recommended for patients with mild COVID-19.
- Anticoagulants:
  - Prophylactic low-molecular-weight heparin is advised for hospitalized patients to prevent thromboembolic complications.

1.1.3.4 Supportive care

- Oxygen Therapy: for patients with hypoxemia
- Fluid and Electrolyte Balance: careful monitoring to avoid fluid overload while maintaining hydration.
- Nutritional support: adequate caloric and protein intake supports immune function and recovery
- Monitoring and Treatment of Complications: early recognition of acute respiratory distress syndrome (ARDS), sepsis, and multi-organ failure is vital (WHO, 2023).

1.1.3.5 Current approved antiviral medications used in the management of COVID-19.

As stated earlier, effective prevention and management of COVID-19 are crucial for reducing the burden of the disease on the general population. There are several drugs that are currently approved for the treatment of COVID-19. Here, we discuss the current drugs used to manage COVID-19, highlighting their mechanisms of action, indications, and potential side effects.

1. Remdesivir: A nucleotide analog prodrug that is metabolized intracellularly to Remdesivir Monophosphate (RMP) and to the active form Remdesivir Triphosphate (RTP), which competes with Adenosine Triphosphate (ATP) and incorporates into

viral RNA, causing premature termination of viral RNA synthesis by inhibiting SARS-CoV-2 RNA-dependent RNA polymerase (RdRp). It is indicated for patients with non-severe COVID-19 in high-risk outpatients and also for hospitalized patients with severe COVID-19 who require supplemental oxygen but are not yet on mechanical ventilation. Common side effects include elevated liver enzymes and gastrointestinal symptoms (CDC,2025; Malin *et al.,* 2020).

2. Nirmatrelvir/Ritonavir (Paxloid): Nirmatrelvir is a protease inhibitor that targets the SARS-CoV-2 protein, preventing cleavage of viral polyproteins required for replication, while Ritonavir is not active against SARS-CoV-2 but acts as a potent CYP3A4 inhibitor, boosting plasma levels of nirmatrelvir. It is indicated for high-risk non-severe COVID-19 in adult and adolescent patients (CDC, 2025; Wikipedia, 2025). Major caution is significant drug-drug interaction due to Ritonavir.

3. Molnupiravir: A prodrug of beta-D-N4-hydroxycytidine (NHC), which is converted in cells to the active ribonucleotide triphosphate. It is incorporated into viral RNA by RdRp, leading to the accumulation of mutations that render the viral genome nonfunctional. It is indicated for non-severe COVID-19 in high-risk patients when preferred options are not available or contraindicated. However, it is contraindicated in pregnancy and not recommended for children under 18 years (CDC, 2025; Wikipedia, 2025; WHO, 2022).

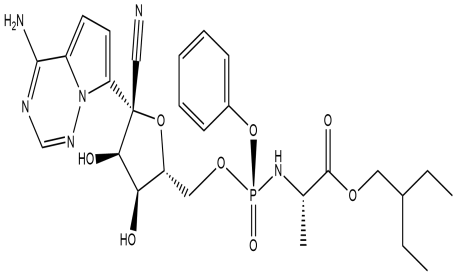

A

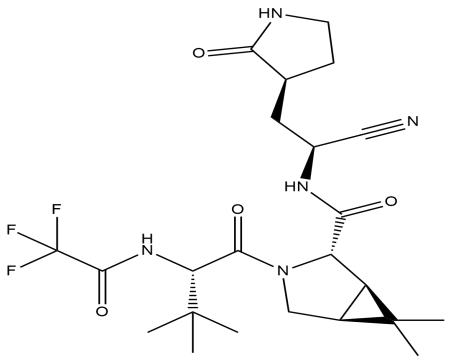

B

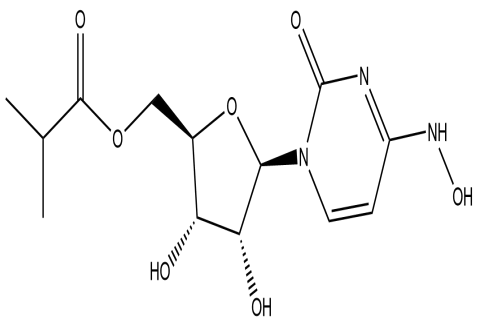

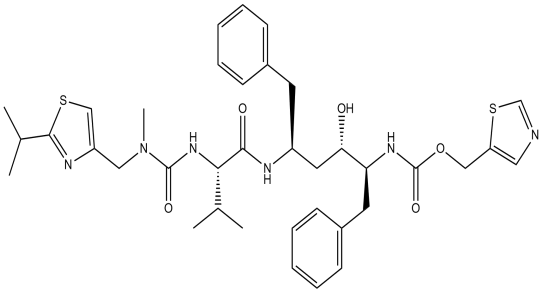

C **D**

Figure 1.1 Chemical Structure of Antiviral Agents Currently Used in Management of COVID-19

(A) Chemical structure of Remdesivir (**B**) Chemical structure of Nirmatrelvir (**C**) Chemical structure of Ritonavir (**D**) Chemical structure of Molnupiravir

1.1.4 Historical Exploration of Medicinal Plants in Human Health

From ancient civilization to modern-day pharmaceutics, medicinal plants have played major roles in human health. Medicinal plants have been a fundamental source of healing, providing not only traditional cures but also the basis for some of the most life-saving drugs in modern medicine. A substantial number of today's most effective drugs are either derived directly from plants or are synthetic versions of plant-based compounds (Newman *et al.,* 2012). Historically, the earliest records of herbs are found from the Sumerian civilization, where hundreds of medicinal plants, including opium, were listed on clay tablets, c.3000 BC. The Ebers Papyrus from ancient Egypt, c.1550 BC, describes over 850 plant medicines. The Greek physician Dioscorides documented over 1000 recipes using over 600 medicinal plants in De materia medica, c.60AD; this formed the basis of pharmacopoeias for some 1500 years (Wikipedia, n.d.). In India, the Atharvaveda and the Charaka Samhita laid the foundation of Ayurveda, while in China, the Shennong Bencao Jing became a cornerstone of Traditional Chinese Medicine (Khan, 2014).

Ethnobotanical knowledge is often applied in drug development to identify plants with potential therapeutic value. This approach has contributed to the discovery of numerous pharmacologically active compounds. Examples of plant-derived medicines include:

1. Artemisinin: extracted from leaves of *Artemisia annua* (sweet wormwood), it is a potent antimalarial.
2. Reserpine: isolated from the roots of *Rauwolfia serpentina* (Indian snakeroot). It is used as an antihypertensive
3. Morphine: isolated from the seeds of *Papaver somniferum* (Opium poppy). It is a potent analgesic
4. Atropine: isolated from leaves and roots of *Atropa belladonna* (deadly nightshade). It is an anticholinergic; used in ophthalmology and as an antidote for poisoning.

5. Vinca alkaloids: isolated from leaves of *Catharanthus roseus* (Madagascar periwinkle). It is an anti-cancer agent.

Conclusively, medicinal plants have remained a cornerstone of healthcare. Through extraction, isolation, and derivatization techniques, plants have provided active compounds effective for conditions ranging from infectious diseases to cancer and cardiovascular disorders. Presently, they continue to serve as a valuable resource for drug discovery, providing new possibilities for addressing emerging health challenges.

1.1.5 Medicinal Plants Used in the Management of COVID-19

The use of medicinal plants in traditional practices is often deeply rooted in a community's culture and history. Medicinal plants are valued for their recognized role in managing multiple disease conditions and infections with minimal side effects. During the COVID-19 pandemic, individuals turned to herbal medicines and plants due to limited availability of specific treatments, the easy accessibility and affordability of these remedies, and the belief in their potential to boost immunity and relieve symptoms. Many of these plants have demonstrated anti-COVID activities, and their isolated compounds show promise (Demeke *et al.,* 2021). Some of these plants include;

1. *Nigella sativa*
2. *Allium sativa*
3. *Allium cepa*
4. *Curcuma longa*
5. *Zingiber officinale*
6. *Capsicum annuum*
7. *Astragalus membranceus*
8. *Mentha piperita*

1.1.6 HISTORICAL BACKGROUND OF DRUG DISCOVERY

The history of drug discovery dates back to ancient human civilization. It is a rigorous, lengthy, and expensive process that involves identifying a lead compound with therapeutic activity. In the fields of medicine, biotechnology, and pharmacology, drug discovery is the process by which new candidate medications are identified (US Food and Drug Administration [FDA], 2018). In the ancient past, the primary sources of medicine for treating disease were plants, animals, and microbes, which were mostly discovered through

observation and chance. This approach was based on the trial-and-error method, which involves testing natural products on oneself to understand their effects. Among these natural products was the juice from the opium poppy plant (Papaver somniferum) dating from ~3000 BC that contained the all-powerful painkiller morphine (Dailey, 2025; Drews, 2000; Jones, 2011). However, in the 18th century, the practices of clinical trials and preventive medicine were started when James Lind reported his study on the prevention of scurvy with his first established controlled clinical study in 1753. In the 19th century, advances in chemistry enabled the extraction and isolation of active substances from herbal plants, bringing small-molecule drug discovery to the forefront. This led to the extraction and isolation of important active substances such as alkaloids, morphine, atropine, and quinine. Between the late 19th and early 20th centuries, advances in chemical knowledge stimulated subsequent investigations in medicinal chemistry and led to the development of novel concepts such as ligand-receptor interactions. The 1950s marked the rise of rational drug design, followed by quantitative structure-activity relationships in the 1960s. Computational-aided drug design (CADD) gained attention in the 1980s. It contributed to the approval of drugs such as captopril for hypertension, dorzolamide for glaucoma, saquinavir, ritonavir, and indinavir for HIV, and zanamivir for influenza virus. Other advances include combinatorial chemistry, recombinant DNA technology, and automated high-throughput screening, giving way to target-based drug discovery. Also, the late 20th century and early 21st century saw breakthroughs in molecular biology-directed drug discovery, with the initiation of the Human Genome Project and the first successful clinical trial of gene therapy in 2011. After identifying promising compounds, clinical trials are conducted to establish safety, efficacy, and appropriate dosage, after which regulatory authorities such as the FDA critically assess the data before approving for clinical use (Pina *et al.,* 2009; Xu *et al*., 2024).

1.1.7 COMPUTER-AIDED DRUG DESIGN (CADD)

CADD refers to all computer-assisted techniques used to discover, design, and optimize compounds with desired structures and properties. CADD comprises various processes, including target identification, virtual screening of chemical libraries, optimization of lead compounds, and evaluation of potential toxicity, all performed through computational simulation. Based on different principles, computer-aided drug design is broadly categorized into structure-based drug design (SBDD) and ligand-based drug design (LBDD). The SBDD concept applies in situation where the structure of both ligand molecules and protein targets are known. In contrast, the LBDD concept applies when the structure of the ligand molecule

is known but the structure of the target site is not (Pattnaik & Siddharta, 2022). SBDD approaches include molecular docking, molecular dynamics (MD) simulations, structure-based virtual screening, and de novo drug design (the creation of novel synthetic compounds), while LBDD methods include quantitative structure-activity relationship (QSAR) models, similarity searching, and pharmacophore models. In addition, fragment-based drug design (FBDD) is a common drug design method that involves fragment growing, linking, and merging. The ultimate goal of CADD is to facilitate the virtual screening of large compound databases to generate hit and lead compounds, or to optimize known lead compounds, transforming bioactive molecules into suitable drug candidates by enhancing their physicochemical characteristics and pharmacokinetic profiles (absorption, distribution, metabolism, excretion, and toxicity). SBDD uses computational chemistry tools and requires the target protein's three-dimensional structure to examine and exploit the binding pocket for screening and designing suitable ligands, which can be experimentally validated and optimized (Macalino *et al.,* 2020). In research, using the molecular operating environment, structure-based virtual screening has been carried out on SARS-CoV-2 proteins (Wu *et al*., 2024). The purpose is to conceive ligands with specific electrostatic and stereochemical attributes to achieve high receptor binding affinity. Selective modulation of a validated drug target by high-affinity ligands interferes with specific cellular processes, ultimately leading to desired pharmacological and therapeutic effects (Yu and MacKerell, 2017). Molecular dynamics simulations model the behaviour of complex molecular systems based on the fundamental properties of chemical entities and their interactions, providing a more dynamic view of interactions between compounds and their target proteins (Batool *et al.,* 2019). The advent of molecular dynamics complements the information obtained from docking analysis and thus provides a robust tool for screening potent lead molecules. The molecular dynamics tool not only provides insight into ligand-target protein interactions through energy calculations but also confirms the stability associated with the formation of the ligand-protein complex (Pattnaik & Siddharta, 2022).

1.1.7.1 Molecular Docking

Molecular docking is one of the most frequently used methods in SBDD because of its ability to predict the conformation of small-molecule ligands within the appropriate target binding site with a substantial degree of accuracy (Yu & MacKerell, 2017). The site n the protein that is targeted is referred to as a binding site, defined by the surrounding amino acids. Usually, the binding site location docking calculations is known. However, when the binding region

information is missing, two commonly employed approaches are used: either the most probable binding sites are algorithmically predicted, or a blind docking simulation is performed (Torres *et al.,* 2019). During docking calculations, a common strategy is to employ a grid representation that includes precalculated potential energies for interaction within the target binding site. When compounds/ligands are computationally made to fit the binding site, this is often referred to as molecular docking. This calculates the conformation and orientation (or so-called 'docking pose') of compounds at the targeted binding site. Docking algorithms predict binding energies and rank ligands using various scoring functions. The appropriate ligand-binding conformation depends on two factors: (i) large conformational space defining possible binding poses and (ii) explicit prediction of binding energy correlating with each conformation. Multiple iterations are performed until the minimum-energy state is attained, and ligand binding is assessed using various scoring functions (Batool *et al.,* 2019).

There are three significant types of docking, and they include;

1. Rigid docking**:** In rigid docking, the primary structure of both the target and the ligand remains unchanged and fixed through the docking analysis. This approach is based on Emil Fischer's lock-and-key hypothesis (1894) and is therefore referred to as lock-and-key docking. However, this approach has its limitations. Ligand-target docking analysis is very significant for understanding drug-target interactions. Still, when a ligand attempts to dock into the binding pocket of a receptor protein, the absence of structural flexibility makes it difficult to accurately model the interactions or determine the ligand's optimal conformation. In some cases, ligands do not fit into the binding site, resulting in weak interactions and unsatisfactory results. Internal flexibility is essential for good docking interaction. In various cases, the structural modifications are negligible. Rigid docking is only enough to observe the interaction. Nonetheless, rigid docking remains valuable due to its simplicity and relatively short runtime (Azads, 2023).
2. Flexible docking: In flexible docking, both the ligand and protein side chains are allowed to adopt different conformations. This method follows the induced-fit hypothesis proposed by Daniel Koshland in 1958, and is often referred to as "induced-fit docking". In this method, the binding energies of multiple possible ligand conformations are evaluated within the receptor's binding pocket. Furthermore, the target protein should also be flexible enough to adapt to the conformational changes

of both the receptor and ligand. Because it accounts for these structural adjustments, flexible docking is considered the most accepted and accurate technique; however, it is time-consuming and costly at the same time (Azads, 2023).

3. Semi-flexible docking: in this method, the ligand is flexible, while the protein remains rigid. Along with the six translational and rotational degrees of freedom, the conformational degrees of the ligands are also tested. This method assumes that a protein in a fixed conformation can recognize the ligands to be docked (Azads, 2023).

Softwares used for molecular docking include **PyRx, PyMol, Chimera, Discovery Studio AutoDock, AutoDock Vina, DockThor, GOLD, FlexX, Molegro Virtual Docker, GLIDE, LeDock, and MOE-Dock**. Several software and website servers can be used to detect binding sites this including **PLIP, CASTp, MolDock, and PyMol**.

1.1.7.2 Post Docking Analysis

After the ligands have been docked to the protein, the results are analyzed to identify the most promising candidates for further study. The binding affinity of each ligand is calculated based on the predicted interaction energy, and the ligands are ranked based on their affinity scores. The docked structures are also analyzed to identify key interactions between the ligands and the protein, including hydrophobic, hydrogen-bonding, and electrostatic interactions. These interactions provide insights into the ligands' mechanism of action and guide further optimization of the compound (Azads, 2023).

1.1.7.3 General Application of Molecular Docking

A binding interaction between a target enzyme and a ligand can activate or inhibit the enzyme. If the protein is a receptor, ligand binding may result in agonism or antagonism (Eweas, 2014). Docking may be applied to the following:;

1. Hit identification: Molecular docking is widely used in drug discovery. It helps in identifying potential drug candidates by predicting the binding affinity of small molecules to a protein or receptor of interest. Docking can be used to screen a large database of small molecules to identify those that can bind to a protein of interest with high affinity (Eweas, 2014)
2. In. In bioremediation, molecular docking is used to predict the binding affinity of small molecules to enzymes involved in the degradation of environmental pollutants.

Docking can help in designing inhibitors or activators of these enzymes to enhance bioremediation efficacy (Eweas, 2014)

3. Structure elucidation: Molecular docking can be used to elucidate the structure of proteins with unknown structures. Docking can be used to predict the binding modes of small molecules to the protein and to generate a homology model of the protein based on these predictions. The generated model can then be refined using experimental data to obtain an accurate protein structure (Eweas, 2014).
4. Molecular dynamics simulation: molecular docking can be combined with molecular dynamics simulations to study the dynamic behaviour of protein-ligand complexes. The simulations can help in understanding the conformational changes that occur upon ligand binding and the stability of the complex. They also allow exploration of protein-ligand interactions over time and the analysis of their dynamic behaviour (Agu *et al.,* 2023).
5. Searching for lead structures for protein targets (Eweas, 2014).
6. Prediction of Adverse Drug Reactions: molecular docking helps in toxicity prediction of compounds at an early stage of drug discovery (Pinzu *et al.,* 2019)

1.1.7.4 Advantages of CADD

-aided Drug Design has emerged as an efficient and thriving approach in drug discovery, providing innovative solutions to the challenges associated with traditional drug discovery. Below are some key advantages of CADD:

1. Time Efficiency: CADD significantly reduces time in drug discovery by enabling rapid screening and optimization of large numbers of compounds for efficacy and safety (Ajjarapu, 2023).
2. Cost Reduction: CADD minimizes the number of compounds synthesized in the laboratory by predicting molecular interactions and properties. This allows researchers to focus on the most promising drug candidate and reduce financial burden (Ajjarapu, 2023).
3. Facilitates rational drug design: CADD supports the drug design based on structural and chemical insights of lead compounds, moving beyond the trial-and-error method and promoting rational drug design (Macalino *et al*., 2015)
4. Lead optimization: CADD assists in lead optimization by enabling researchers to refine the pharmacokinetic properties of compounds (Ajjarapu, 2023).

5. Support in Repurposing Drugs: Through CADD, researchers can identify novel therapeutic indications for existing drugs, thereby providing timely treatment options while novel drugs are in development (Pattnaik & Siddharta, 2022).
6. Reduced Toxicity: By identifying potential toxic interactions early in the design process, CADD helps researchers eliminate harmful compounds at an early stage and also optimize potentially toxic compounds to increase their safety. (Ajjarapu, 2023).
7. Predictive Power: CADD enables researchers to predict a compound's activity before laboratory experiments. In CADD, researchers use software tools to model the molecular structures of drugs and their target proteins, simulate interactions, and predict properties such as binding affinity, bioavailability, solubility, and toxicity, which helps prioritize compounds for further testing, saving time and resources. (Ece, 2023).

1.1.7.5 TOOLS USED IN CADD

The various tools (software) and websites used in CADD include;

Autodock, GOLD, Glide, and **Vina** perform ligand-receptor docking simulations.

LigandScout, MOE, and **Discovery Studio** create pharmacophore models.

ADMET Predictor and **SwissADME** estimate absorption, distribution, metabolism, excretion, and toxicity.

GROMACS, AMBER, and **NAMD** simulate protein-ligand interactions under physiological conditions.

Derek Nexus, ProTox II and **Toxtree** predict toxicity.

ChemDraw, ChemAxon, and **RDKit** are used to analyze and draw/construct chemical structures (Ajjarapu, 2023).

1.1.7.6 CHALLENGES AND PROSPECTS

Advances in docking protocols and scoring functions have established SBDD as a valuable tool for lead compound discovery; however, it still faces several challenges. Protein flexibility should be accounted for throughout the modelling phase. In some experimental and SBDD methods, proteins are presented as static, whereas in nature they are dynamic, and ligand binding to the active site can alter the protein's substantial conformation. Flexible

docking and molecular dynamics simulations have been developed to address this issue. Additionally, structured water molecules and solvation effects influence protein-ligand interactions. Key water molecules should be taken into account to improve the accuracy of molecular docking. Still, it is difficult to accurately predict which water molecules play important roles in binding and which can be ignored. Similarly, solvation significantly influences binding energetics, but quantifying its contribution within scoring functions is challenging, often reducing the precision of docking predictions. Improved protocols, such as SWRosettaLigand, and novel scoring functions, such as SPA-SE, have been developed to incorporate these factors and enhance docking results.

Beyond these technical hurdles, accompanied by the development of biological technology, computational methods have gained massive recognition and expansion in selecting new drugs from large-scale databases, identification of new drug targets, and predicting synergistic drug combinations, thereby overcoming drug resistance, increasing treatment efficacy, and decreasing drug dosage to avoid toxicity (Wang *et al.,* 2018).

1.8 DRUG LIKENESS

Drug likeness is a qualitative measure used in drug design to predict how “druglike” a chemical compound is, based on its physicochemical properties and molecular structure. This simply means how similar a lead compound's properties are to those of existing drugs. Drug-likeness is a set of guidelines that align the properties of lead compounds with those of successfully developed drugs. Researchers evaluate the properties of potential lead drugs to assess their safety, efficacy, and bioavailability. A common rule in drug discovery is the Lipinski rule of five, and the pharmacokinetic (Absorption, Distribution, Metabolism, Excretion, and Toxicity) profiles must be evaluated.

1.1.8.1 Lipinski's Rule of Five

Lipinski's rule of five, also referred to as **Pfizer's rule of five** or simply the **rule of five** (RO5), is a computational rule of thumb used to assess the drug-likeness of a potential drug candidate. It helps determine whether a chemical compound exhibiting a specific pharmacological or biological activity possesses properties conducive to oral activity in humans. Christopher A. Lipinski formulated this rule in 1997, noting that the majority of orally administered drugs are relatively small, moderately lipophilic molecules (Lipinski, 2004).

The rule outlines chemical and physical properties crucial for a drug to be orally bioavailable within the human body, encompassing aspects such as absorption, distribution, metabolism, and excretion ("ADME"). It is important to note that the rule does not forecast a compound's pharmacological activity.

This rule becomes significant in the drug discovery process, particularly when optimizing a pharmacologically active lead compound to enhance its activity and selectivity. It ensures that the compound maintains drug-like physicochemical properties, as stipulated by Lipinski's rule (Oprea *et al*., 2001). Drug candidates that adhere to the RO5 typically exhibit lower attrition rates in clinical trials, increasing the likelihood of reaching the market (Lipinski, 2004; Leeson & Springthorpe, 2007).

1.1.8.2 Key Component of Lipinski's Rule

Lipinski's rule states that, in general, an orally active drug should have no more than one violation of the following criteria:

Hydrogen Bond Donors: No more than **5 hydrogen bond donors** (the total number of nitrogen–hydrogen and oxygen–hydrogen bonds).

Hydrogen Bond Acceptors: No more than **10 hydrogen bond acceptors** (all nitrogen or oxygen atoms).

Molecular Mass: A molecular mass **less than 500 daltons**.

Calculated Octanol-Water Partition Coefficient (Clog P): A Clog P value that **does not exceed 5**.

Note that all these numbers are multiples of five, which is the origin of the rule's name. As with many other rules of thumb, there are exceptions (Lipinski *et al*., 2001), but adhering to Lipinski's rule tends to increase the likelihood that a candidate drug will reach the market.

1.1.8.3 Variants and Extensions

To improve the predictions of druglikeness, several variants and extensions of Lipinski's rule have been proposed. One such addition is **Veber's Rule**, which includes additional criteria:

Number of Rotatable Bonds: The number of rotatable bonds is less than or equal to 10

Polar Surface Area: Topological Polar Surface Area is less than or equal to 140 A (or total hydrogen bond donors + acceptors less than or equal to 12 (Verber *et al.,* 2002)

1.1.8.4 ADMET Properties

An ADMET study assesses the pharmacokinetics of a drug, including Absorption, Distribution, Metabolism, Excretion, and Toxicity (Flores-Holguín *et al*., 2021). This assessment plays a crucial roles in the process of drug discovery and development. A high-quality potential drug candidate should not only exhibit sufficient efficacy against the therapeutic target but also demonstrate appropriate ADMET properties at a therapeutic dose. Numerous in silico models have been developed to predict ADMET properties of compounds (Guan *et al*., 2018); however, evaluating drug-likeness based on multiple ADMET properties remains challenging, and the predictive capacity of computational methods for ADMET assessment remains limited.

Predicting a lead compound's pharmacokinetic behaviour is a critical step in drug discovery. The evaluation of ADMET (absorption, distribution, metabolism, excretion, and toxicity) properties is vital to optimizing potential drug candidates, ensuring their safety and optimal therapeutic efficacy during clinical use. Poor absorption can impact distribution and metabolism, thereby leading to neurotoxicity and nephrotoxicity. Ultimately, ADMET profiling provides insights into how a potential lead compound/drug molecule is distributed within an organism. Therefore, ADMET analysis is considered one of the most essential components of computational drug design (Flores-Holguin *et al.,* 2021). Software tools that can be employed for the assessment of ADMET properties include ADMET Predictor, SwissADME, ProTox-II/Protox-3.0, admetSAR, and ToxT**ree.**

1.2 LITERATURE REVIEW

1.2.1.Andrographis paniculata (Burm.f.) Nees., (Acanthaceae).

1.2.1.1 Introduction

Andrographis paniculata, commonly known as creat or green chiretta and king of bitters, is an herbaceous plant in the family Acanthaceae, native to India and Sri Lanka. It is widely cultivated in Southern and Southeastern Asia and is found in a variety of habitats, including plains, hillsides, coastlines, and disturbed and cultivated areas, including roadsides and farms. The plant grows as an erect herb to a height of 30–110 cm in moist, shady places, with longitudinal furrows and produces small, pinkish or white flowers in racemes or panicles. The fruit is a slender capsule containing numerous yellow brown seeds. The bitterness is

attributed to its major bioactive constituent, andrographolide. The plant is valued in traditional medical systems such as Ayurveda, Siddha, and Traditional Chinese Medicine. This literature review aims to provide a comprehensive overview of the ethnomedicinal uses, phytochemistry, and pharmacological activity of *Andrographis paniculata.*

A B

Figure 1.2 Pictures of *Andrographis paniculata*

(A) *Andrographis paniculata* plant (B) Leaves of *A. paniculata*

1.2.1.2 Ethnomedical uses

Andrographis paniculata is known as a bitter wonder plant, as it is known for its immunostimulant and other properties in humans (Ameh, 2010). The herb, whose bitterness and other properties are known to vary with habitat, was introduced to the National Institute for Pharmaceutical Research and Development (NIPRD), Nigeria, from India in the late 1990s. It has since been cultivated in the institute's garden for drug research and development (Ameh, 2010). In Nigeria, the plant is widely used to treat pyrexia, inflammation, and intermittent fever (Okhuarobo *et al*., 2014). In the southern part of Nigeria, it is locally referred to as 'ewe meje', and used to treat malaria by direct consumption of the leaves in pulverized form, chewing of the leaf directly or through decoction, which is orally administered for treatment of malaria (Adedayo *et al.,* 2024; Faluyi, 2021). It is also used locally to treat various types of respiratory infections. Its bitter properties are believed to cleanse the body and have a therapeutic effect on the gastrointestinal tract, making it a traditional remedy for diarrhea and dysentery (Dwivedi *et al.*, 2021). Also, it is used in the management of chronic conditions with reported effects in lowering blood pressure and regulating blood sugar in diabetes (Mshebelwala *et al.,* 2013; Yusuf *et al.*, 2022).

1.2.1.3 Phytochemistry

Andrographis paniculata contains diverse compounds in its aerial parts, roots, leaves, and the whole plant, which are commonly used for extracting its active constituents. The chemical composition varies due to diverse factors such as geographical region, harvest time, and processing method. Phytochemical studies of *A. paniculata* have led to the isolation of various plant compounds. Key compounds include terpenoids (ent-labdane diterpene lactone), which are majorly responsible for the plant's therapeutic effects. Other categories of compounds that have also been isolated include flavonoids, noriridoides, xanthones, polyphenols, as well as trace and macro elements (Okhuarobo, 2014).

The various groups of compounds found in Andrographis paniculata are as follows;

1. **Terpenoids**

   Diterpenoid lactones are the most commonly isolated terpenoid compounds from Andrographis paniculata. These are found in the plant's aerial parts and roots. Among them, andrographolide is the most abundant and widely occurring. It is colourless, crystalline, and extremely bitter. Other notable diterpenoids include 14-deoxyandrographolide, Neoandrographolide, Andrographoside, 19-O-β-D-glucopyranosyl-ent-labda-8(17),13-dien-15,16,19-triol, Andrographolactone, 8α-methoxy-14-deoxy-17β- hydroxy andrographolide,13-diene-16, 15-olide, 3,7,19-trihydroxyl-8,11, 13- ent-labdatriene-15, 16-olide and Andrograpanin. Terpenoids have shown various activities, including anti-inflammatory effects by inhibiting cyclooxygenase enzyme activity. Andrographolide and 14-deoxy-11,12-didehydroandrographolide have also demonstrated anti-diabetic activity. They also possess anti-oxidant activity (Okhuarobo, 2014).

2. **Flavonoids**

   Flavones are the major flavonoids that have been isolated from the aerial parts, roots and whole plant of *A. paniculata.* They include the following compounds; 5, 7, 2', 3'-tetramethoxyflavone, 7-O-methyldihydrowogonin, 7-O-methylwogonin, Flavone-1, 2'methylether, 7-O-methylwogonin-5-glucoside, Dihydroskullcapflavone, and 5-hydroxy-7, 8, 2, 3' tetramethoxyflavone. Flavonoids such as 7-O-methylwogonin and skullcapflavone-1 have been shown to have anti-inflammatory and anti-allergic activity (Okhuarobo, 2014).

3. **Xanthone**

Xanthones are naturally produced organic compounds found in plants. They are classed as miscellaneous compounds because of their minor occurrence in the plant. However, 1,2-dihydroxy-6,8-dimethoxy xanthone has shown anti-plasmodial activity against Plasmodium falciparum and Plasmodium berghei. Other xanthones that were isolated from the plant include; 1, 8-dihydroxy-3,7-dimethoxy-xanthone, 4,8-dihydroxy 2,7-dimethoxy-xanthone, and 3,7,8-trimethoxy-1-hydroxy-xanthone (Okhuarobo, 2014).

4. **Noriridoids**

   These are also miscellaneous compounds isolated from the plant's roots. They include andrographolide A, B, C, D, E, and Curvifloruside (Okhuarobo, 2014).

Other miscellaneous components isolated from the plant included trace elements such as Cr, Mn, Co, Ni, Zn, Cu, Se, Rb, Sr, and Pb, and macroelements such as potassium and calcium, which were identified and quantified in the roots. Cinnamic acid, caffeic acid, ferulic acid, and chlorogenic acid are phenolic acids that were isolated from the whole plant. Arabinogalactan proteins were also isolated from the plant's dried herbs, and these demonstrated antibacterial and antifungal activity (Okhuarobo, 2014).

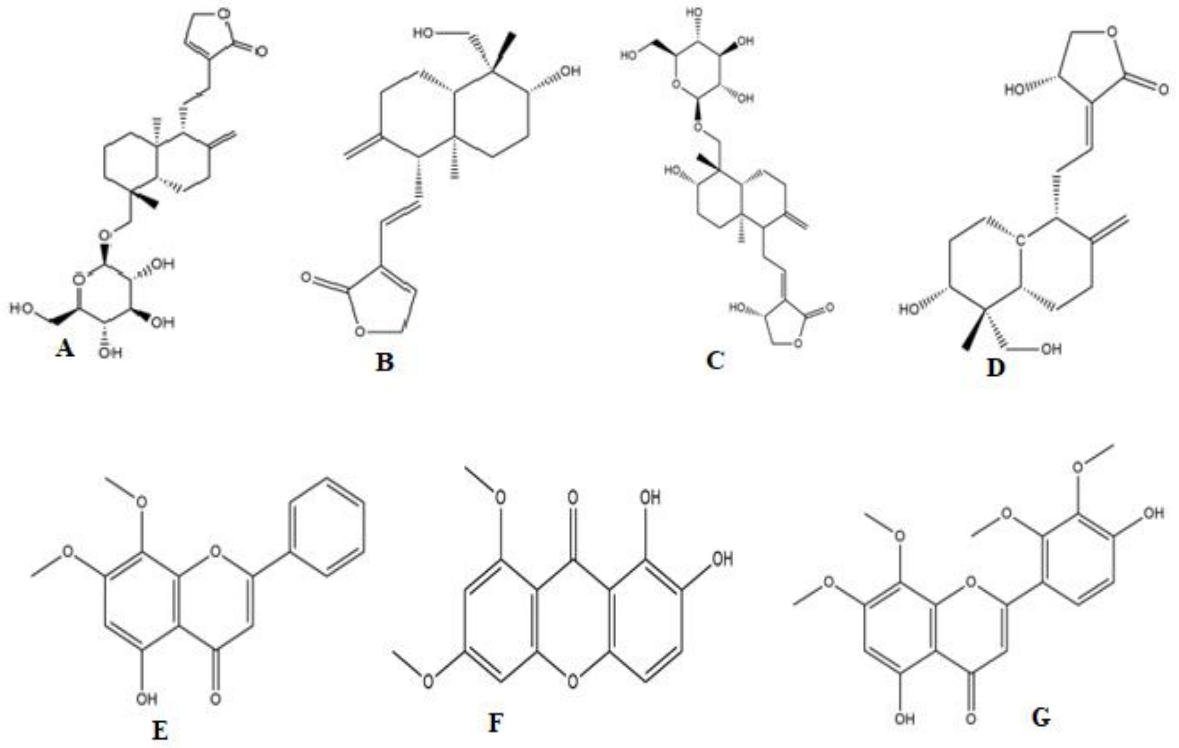

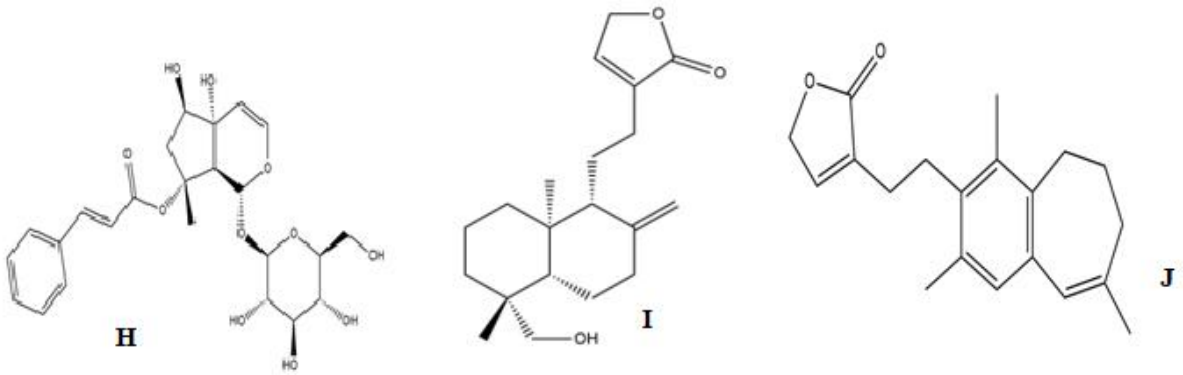

FIGURE 1.3: Structures of some phytochemical constituents present in *Andrographis paniculata*

(**A**) Chemical structure of Neoandrographolide (**B**) Chemical structure of 14-deoxy-11,12-didehydroandrographolide (**C**) Chemical structure of Andrographoside (**D**) Chemical structure of Andrographolide (**E**) Chemical structure of 7-O-methylwogonin (**F**) Chemical structure of 1,2-dihydroxy-6,8-dimethoxy xanthone (**G**) Chemical structure of 5, 7, 2', 3'-tetramethoxyflavone (**H**) Chemical structure of Curvifloruside (**I**) Chemical Structure of Andrograpanin (**J**) Chemical Structure of Andrographolactone

1.2.1.4 Therapeutic Application

The various phytochemicals in Andrographis paniculata contribute to its wide range of medicinal properties and pharmacological activities. These include hepatoprotective, immunostimulatory, antipyretic, antioxidant, hypotensive, antidiabetic activity, anti-inflammatory, antibacterial, anti-plasmodial, antiviral, antivenom, anti-malaria, anticold, and immunomodulatory (Nyeem *et al.,* 2017). Some of the pharmacological activities revealed by experimental studies validate the various traditional uses of the plant.

Hepatoprotective Activity

Experiments showed that crude extracts and isolated compounds (particularly andrographolide, andrographiside, and neoandrographolide) protect against liver damage induced by various toxins. This indicates that *Andrographis paniculata* has a broad spectrum of hepatoprotective effects (Nyeem *et al.,* 2017).

Immunostimulatory and Immunomodulatory Activity

Studies have shown that both crude extracts and isolated compounds of *A. Paniculata* enhances antibody production, delayed-type hypersensitivity responses, and stimulates nonspecific immune functions, indicating that the plant possesses immunostimulatory activity (Nyeem et al*.,* 2017).

Antipyretic Activity

Studies confirm that *A. Paniculata* compounds reduce fever in animals, demonstrating antipyretic effects comparable to those of aspirin without notable toxicity (Nyeem *et al.,* 2017).

Antioxidant Activity

Experimental studies show that *A. paniculata* enhances antioxidant enzyme activity, reduces oxidative stress, and provide cardioprotective effects (Nyeem *et al.,* 2017).

Hypotensive Activity

Research revealed that *A. paniculata* lowers blood pressure by acting through beta-adrenoceptors, inhibiting the Angiotensin Converting Enzyme (ACE), and improving endothelial Nitric Oxide (NO) function. Its effects are equivalent to those of verapamil, a calcium channel blocker (Nyeem *et al.,* 2017).

Antidiabetic Activity

Both aqueous and ethanolic extracts, as well as isolated compounds, show antihyperglycemic effects, reduce oxidative stress, and help restore normal functions in diabetic rats (Nyeem *et al.,* 2017).

Anti-Inflammatory Activity

Research studies showed that *A. paniculata* inhibits inflammatory mediators. It was also shown to inhibit tumor-specific angiogenesis by modulating the production of various pro- and anti-angiogenic factors in both in vivo and in vitro studies. it was also found to be safe and efficacious for the relief of symptoms of uncomplicated upper respiratory tract infection (Nyeem *et al.,* 2017).

Anti-Bacterial Activity

A. paniculata leaf extracts showed in vitro inhibitory effects against Escherichia coli and Staphylococcus aureus. However, no *in vitro* antibacterial activity was observed when dried powder from the aerial parts was tested against *E. coli, Staphylococcus aureus, Salmonella typhi* or Shigella species (Nyeem *et al.,* 2017).

Anti-Plasmodial/ Malaria Activity

Extracts and active compounds of *A. paniculata*, including andrographolide, neoandrographolide, and xanthones, have shown significant antimalarial and antiplasmodial effects by inhibiting in vitro Plasmodium falciparum growth and reducing *P. berghei* parasitaemia in animal models, confirming its potential as an antimalarial agent (Nyeem *et al.,* 2017).

Antiviral Activity

Study revealed that aqueous and methanol extracts of *A. paniculata* inhibited HIV infection, replication, and syncytia formation in cell models, while Dehydroandrographolide showed direct anti-HIV effects. In addition, Andrographolide, neoandrographolide, and 14-deoxy11,12-didehydroandrographolide were reported to exhibit virucidal activity against herpes simplex virus 1 (HSV-1) without causing significant cytotoxicity at virucidal concentrations (Nyeem *et al.,* 2017).

Antivenom Activity

Ethanol extracts of the plant delayed cobra venom-induced respiratory failure and death in mice. It also showed significant muscarinic activity in guinea pig ileum, supporting its anti-venom potential (Nyeem *et al.,* 2017).

Anticold Activity

A standardized *A. paniculata* preparation reduced the incidence of the common cold in a clinical trial, demonstrating protective effects after a 3-month observation period (Caceres *et al.,* 1997).

1.3 JUSTIFICATION OF THE STUDY

Several research publications have demonstrated the potential antiviral properties of *Andrographis paniculata* through in silico, in vitro, and in vivo studies (Gupta *et al.,* 2017; Jiang *et al.,* 2021). The COVID-19 pandemic, caused by the SARS-CoV-2 virus, emerged unexpectedly and led to widespread mortality due to the limited availability of effective

antiviral agents. Since its onset in 2019, there has been a continuous emergence of new viral variants posing challenges to treatment and further contributing to global death despite progress in vaccine development and drug repurposing. Through *in silico* studies, cost-effective tools have been provided to researchers to investigate the bioactivity, toxicity, and other pharmacokinetic parameters of drug molecules. The current research is carried out to investigate potential phytoconstituents from *Andrographis paniculata* with anti-COVID activity, their molecular targets in the SARS-CoV-2 protein, and to identify their ADMET properties through molecular docking to discover new and potent antiviral agents for development into a pharmaceutical product.

1.4 AIM AND OBJECTIVES

This study aimed to assess the anti-COVID-19 potential of phytoconstituents from *Andrographis paniculata* using *in silico* methods to identify a potential source of new drugs for treating COVID-19.

1.4.1 Specific Objectives

The specific objectives were to:

1. Obtain phytoconstituents isolated from the plants.
2. Carry out molecular docking studies of the phytoconstituents obtained against a selected protein target (SARS-CoV-2 RdRp. PDB ID:7BV2).
3. Determine the ADMET properties of the chosen compounds/ligands with good docking scores.
4. Perform post-docking analysis

CHAPTER TWO

MATERIALS AND METHODS

2.1 MATERIALS

2.1.1 PyRx

PyRx (Python Prescription) is a computational application designed for drug discovery, and built explicitly for virtual screening. It analyses a large database of compounds against potential drug targets, aiding research in Computational Drug Discovery.

Virtual screening (VS) is a computer-based approach used to screen a large number of database molecules to identify potential lead compounds. By placing the most promising compounds, it reduces the time and resources needed to test the entire database of compound experimentally. Docking-based virtual screening (DBVS) further investigates how small molecules/ligands interact with the binding/active sites of targets, enabling the selection of those with the strongest predicted interactions for further experimental validation. (Kondapuram *et al.,* 2021)

PyRx uses a large body of established open-source software, including:

- AutoDock 4 and AutoDock Vina are used as docking software.
- AutoDockTools is used to generate input files.
- Python is a programming/scripting language.
- wxPython for cross-platform GUI.
- The Visualization ToolKit (TVTK) by Kitware, Inc.
- Enthought Tool Suite, including Traits, for application building blocks.
- Open Babel for importing SDF files, removing salts, and energy minimization.
- matplotlib for 2D plotting

In this study, Autodock Vina (version 0.8) in PyRx was used.

2.1.2 RCSB PDB

The Research Collaboratory for Structural Bioinformatics Protein Data Bank (RCSB PDB), funded by the United States National Science Foundation, National Institutes of Health, and Department of Energy, provides assistance to structural biologists and users of Protein Data Bank (PDB) information worldwide (Burley *et al.,* 2022).

As a pioneer member of the Worldwide Protein Data Bank (wwPDB) consortium, the RCSB PDB functions as the primary United States-based repository for the global PDB collection, housing three-dimensional (3D) structural data for biological macromolecules derived from experimental methods. In its role as the designated Archive Keeper for wwwPDB, the RCSB PDB is tasked with ensuring the security of PDB data and with regularly updating the archive weekly. Annually, the RCSB PDB serves a multitude of data contributors using various techniques, including macromolecular crystallography, nuclear magnetic resonance spectroscopy, electron microscopy, and micro-electron diffraction, spanning all continents with permanent human habitation.

The 3D structure of RNA-dependent RNA polymerase co-complexed with inhibitor F86 (Remdesivir Nucleoside Monophosphate) was obtained from this database, with ID 7BV2 and DOI: https://doi.org/10.1126/science.abc1560 (Yin *et al.,* 2020).

2.1.3 PLIP

PLIP (Protein Ligand Interaction Profiler) is an accessible active software/webserver tool designed for profiling of non-covalent 3D molecular interactions in protein structures, including interactions between proteins and small molecules (protein-ligand), protein-DNA, protein-RNA, and protein-protein complexes. The software identifies -covalent interactions such as hydrogen bonds, hydrophobic interactions, salt bridges, halogen bonds, water bridges, pi-stacking, and pi-cation interactions, thereby providing a complete picture of the binding site. Its user-friendly interface and high adaptability make PLIP one of the most versatile tools for molecular interaction profiling in computational drug discovery (Schake *et al*., 2025).

The PLIP software was used to identify binding/active amino acid residues for site-directed docking.

PLIP is available both as a web server (https://plip-tool.biotec.tu-dresden.de) and as a downloadable software. The web server was used in this study.

2.1.4 BIOVIA Discovery Studio Visualizer 2020

This software tool is used for analyzing and modeling molecular structures, conducting pharmacophore modeling, performing Quantitative Structure-Activity Relationship (QSAR) analyses, and running various simulations. Biovia Discovery Studio Visualizer enables users to visualize and modify molecular structures, sequences, sequence alignments, and Perl scripts generated with Discovery Studio and other associated applications.

Discovery was used to prepare the target protein (RdRp) before docking using PyRx. It was also used to view and analyze the active/binding site protein and the ligand, and to visualize various binding models of each ligand.

In this study, version 20.1.0.19295 of BIOVIA Discovery Studio Visualizer, released in 2020, was used.

2.1.5 SwissADME

This website allows users to compute physicochemical descriptors and predict ADME parameters, pharmacokinetic properties, druglike nature, and medicinal chemistry friendliness for one or multiple small molecules to support drug discovery (Daina *et al.,* 2017).

2.1.6 ProTox 3.0

ProTox is a virtual laboratory designed to predict the toxicity of small molecules —an essential step in drug development and design. Using molecular similarity, fragment tendencies, machine learning, and pharmacophore models, it predicts various toxicity endpoints, including acute toxicity; organ toxicity (such as LD50, hepatotoxicity, neurotoxicity, nephrotoxicity, respiratory toxicity, cardiotoxicity, carcinogenicity, immunotoxicity, mutagenicity, and cytotoxicity); adverse outcomes; and toxicity targets. It also predicts which common enzymes that it inhibits (Banerjee *et al.,* 2018).

It is **version 3.0** of **ProTox,** which is a very recent update to the site that was used in this study.

2.1.7 Analytical and Computer Systems

2.1.7.1 Instrumentation and Chemicals for GC-MS Analysis

- Machine model: 7890A GC system, 5675C Inert MSD with triple–axis detector
- Packing material: Capillary column
- Carrier gas: Helium gas
- Flow rate: in the instrumentation parameter
- Temperature programme:
- Column length: 30m
- Dimension: 30mx250umx 0.25um
- Column: Agilent 19091-433HP-5Ms 5%phenyl methyl silox

2.1.7.2 Computer System for Molecular Docking

The experiment was run on a computer system, and its specifications are as follows:

- Model: Dell latitude 3350
- Processor: Intel(R) Core (TM) i3-5005U CPU @ 2.00GHz
- RAM: 8.00 GB (7.63 GB usable)
- ROM: 500 GB (464 GB usable)
- System type: 64-bit operating system, x64-based processor
- Operating System: Windows 11 Pro

The study used the following software: PyRx, PLIP, ProTox-3.0, Biovia Discovery Studio 2020, and SwissADME and ProTox3.0 online web servers; the databases used were Protein Data Bank (PDB) and PubChem.

2.2 METHOD

2.2.1 Plant collection and authentication

Plant collection and identification are presented in Table 2.1 below.

Table 2.1: Plant collection and identification.

S/N	Plant name	Plant part	Place of collection	Date of Collection	Plant ID*
1	*Andrographis paniculata*	Leaves	Ekosodin Edo State	Feb, 2021	UBH-P290

* UBH= University of Benin, Herbarium number.

2.2.2 Plant Preparation and Extraction

The plant materials (leaves; Table 1) were air-dried for 3 weeks, ground to a powder, and stored in an airtight container until ready. The powdered plant material (200 g) was extracted and separated by maceration in dichloromethane (2 L) at room temperature for 1 week. The extracts were concentrated *in vacuo* using a rotary evaporator at 45℃ and then stored at 4℃ in a refrigerator until further use.

2.2.3 Sample Analysis (GC-MS)

Gas chromatography from Agilent USA was hyphenated to a mass spectrometer (5975C) with a triple-axis detector equipped with an autoinjector (10 µl syringe). Helium was used as the carrier gas.

All chromatographic separations were performed on a capillary column with the following specifications: length, 30m; internal diameter, 0.2 µm; thickness, 250 µm; treated with phenylmethylsilox. Other GC-MS conditions are ion source temperature (EI), 250^0c, interface temperature, 300 ℃, pressure, 16.2 psia, out time, 1.8mm, 1 µL injector in Split mode with split ratio 1:50, with injection temperature of 280 ℃ the column temperature started at 50^0c for 2mins and changed to 100^0c at the rate of 20^0c/min. The temperature was raised to 2500 °C at a rate of 200 °C/min and held for 5 min. The total elution was 19minutes. The Ms Solution software provided by the supplier was used to control the system and acquire data; identification of the compounds was carried out by comparing the mass spectra obtained with those of the standard mass spectra from the NIST library (NIST II).

2.2.4 Identification and Preparation of Ligands

The 3D structure data files (SDF) of the bioactive compounds of *Andrographis paniculata,* identified by GC-MS, were downloaded from the PubChem database and imported into PyRx using the Open Babel plugin. They were minimised, converted to Autodock ligands (pdbqt), and used for molecular docking.

2.2.5 Preparation of Protein Target

The target protein, SARS-CoV-2 (PDB ID:7BV2) was obtained using the RCSB PDB https://rcsb.org). Preparation of the target protein was performed in Biovia Discovery Studio Visualizer 2020 to remove all non-standard residues (such as the co-crystallized ligand RMP, ID: F86) and water molecules that could interfere with molecular docking. Hydrogen atoms

were added to the protein thereafter to complete the protein preparation for molecular docking. The prepared protein was thereafter saved in the PDB format.

2.2.6 Identification of Binding Site

The active/binding-site amino acids were identified using the Protein Ligand Interaction Profiler (PLIP), which was possible because the protein is complexed with F86, its co-crystallized ligand. Biovia Discovery Studio Visualizer 2020 was also used to view and analyze the protein's active/binding site. This step is very important in this study, as a site-directed docking approach was used. Therefore, it is essential to identify the amino acids at the protein's active or binding site for accurate docking.

2.2.7 Molecular Docking

The protein target, previously prepared and saved in PDB format, was loaded into PyRx and converted to a macromolecule; all ligands were also imported into PyRx. The binding amino acids on the macromolecule ere then labelled, and the AutoDock Vina plug-in was used for docking, with the grid box placed on the binding amino acids. This was carried out at an exhaustiveness of 8.

2.2.8 Post-Docking Analysis

The various binding conformations of each ligand with binding affinity $\leq$ -6.9 against the protein were extracted from PyRx in the PDB format.

The binding site and ligand interaction between the identified binding amino acid residues and the ligands were then analyzed using Biovia Discovery Studio Visualizer 2020. 3-dimensional and 2-dimensional analysis were done to visualize the various binding models of each ligand, and compared with those of the co-crystallized ligand and the standard drug (F86 and RTP), and to also determine the ligands with higher potential of anti-COVID activity

2.2.9 ADMET Analysis

Selected compounds were chosen for ADMET analysis. The absorption, distribution, metabolism, excretion, and toxicity (ADMET) properties of the test ligands, including physicochemical and lipophilicity parameters, along with their toxicity profiles, were determined using in silico integrative software such as SwissADME and the ProTox3.0

webserver. The predicted toxicity was obtained and examined using the Lipinski rule of five for drug-likeness properties.

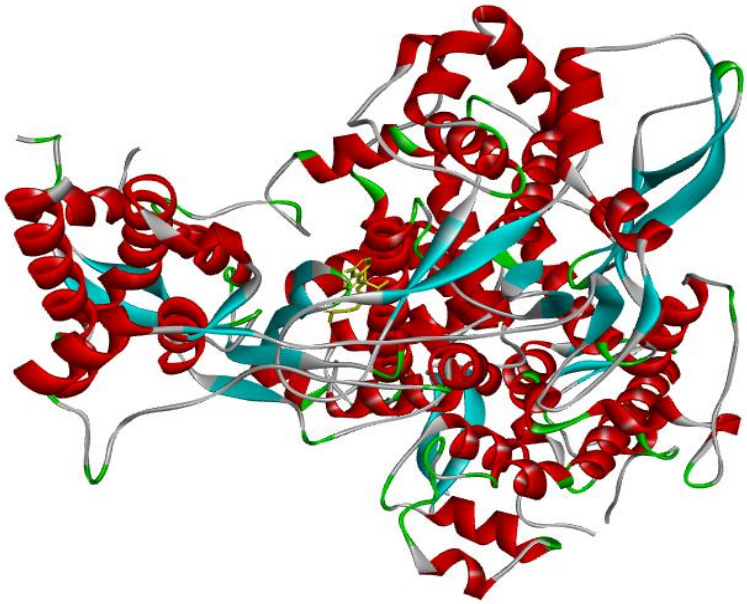

Figure 2: Crystal structure of SARS-CoV-2 RNA-dependent RNA polymerase (RdRp) protein (PDB ID:7BV2) complexed with inhibitor F86 from Biovia Discovery Studio Visualizer

CHAPTER THREE

RESULTS

3.1 GC-MS Analysis

The compounds obtained from GC-MS analysis of *Andrographis paniculata* are shown in Table 3.1.

The chromatogram of the GC-MS analysis of *Andrographis paniculata* using Dichloromethane extract is shown in Figure 3.1

3.2 Binding Affinities

The results of the binding site amino acids identified with the aid of PLIP are shown in Table 3.2.

The binding affinities of all selected compounds from *Andrographis paniculata,* with binding affinity values of ≤ -6.9 kcal/mol when docked against the protein target RdRp (7BV2) are shown in Table 3.2

The binding affinity of the standard drug and the co-crystallized ligand is shown in Table 3.3

The chemical structures of compounds from *Andrographis paniculata* with binding affinities ≤ -6.9 are shown in Figure 3.2.

3.3 The 2D, 3D, and H-bonds Binding Interactions of the Phytoconstituents of *Andrographis paniculata* with 7BV2.

The images show the molecular interactions between the ligands and the amino acids of the target protein, with binding affinity scores < -6.9 kcal/mol (Figure 3.3–Figure 3.7). The interaction of the co-crystallized ligand (F86) and the standard drug (Remdesivir Triphosphate) with the target protein are also shown below.

3.4 Post-Docking Analysis

The amino acids that the ligands from *Andrographis paniculata,* the co-crystallized ligand, and the standard drug interact with via Conventional Hydrogen bonds, Van der Waals interactions, and other interactions on the protein are presented in Tables **3.5** and **3.6,** respectively.

Table 3.1 Compounds identified from GC-MS Analysis of *Andrographis paniculata* Dichloromethane Extract

S/N	Name	Pubchem CID	Molecular Weight(g/mol)	Molecular formula	Retention Time(min)	Area (%)
1	Benzoic acid, methyl ester	7150	136.15	$C_6H_5COOCH_3$	5.164	7.68
2	Undecane	14257	156.31	$C_{11}H_{24}$	5.033	3.03
3	O-veratramide	220089	181.19	$C_9H_{11}NO_3$	5.445	1.19
4	Decane	15600	142.28	$C_{10}H_{22}$	5.113	2.16
5	1-Cyclohexene, 1,3,3-trimethyl-2-(1-methylbut-1-en-3-on-1-yl)-	5375216	206.32	$C_{14}H_{22}O$	10.165	1.75
6	6-epi-shyobunol	520758	222.37	$C_{15}H_{26}O$	13.839	1.68
7	Hexadecanoic acid, methyl ester	8181	270.5	$C_{17}H_{34}O_2$	14.045	10.33
8	N-Hexadecanoic acid	985	256.42	$C_{16}H_{32}O_2$	14.463	11.7
9	9,17-Octadecadienal	6431297	264.4	$C_{18}H_{32}O$	15.504	4.62
10	Methyl stearate	8201	298.5	$C_{19}H_{38}O_2$	15.727	4.94
11	9-Octadecenoic acid,E	637517	282.5	$C_{18}H_{34}O_2$	15.95	29.31
12	1,9-Cyclohexadecadiene	44148196	220.39	$C_{16}H_{28}$	16.053	5.59
13	2-Methyl-Z,Z-3,13-octadecadienol	5364412	280.5	$C_{19}H_{36}O$	16.254	2.25
14	Acetic acid, trifluoro-, dodecyl ester	6428482	282.34	$C_{14}H_{25}F_3O_2$	16.299	1.52
15	Isobutyl nonyl carbonate	6420744	244.37	$C_{14}H_{28}O_3$	5.164	2.38
16	Pentadecanoic acid	13849	242.4	$C_{15}H_{30}O_2$	14.463	14.05
17	Z-1,6-Tridecadiene	5364461	180.33	$C_{13}H_{24}$	15.453	2.17
18	Oxacycloheptadec-8-en-2-one, (8Z)-	5365703	252.39	$C_{16}H_{28}O_2$	15.504	5.81
19	2-Methyl-Z,Z-3,13-octadecadienol	5364412	280.5	$C_{19}H_{36}O$	15.561	3.08
20	Methyl 8,10-dimethyl-hexadecanoate	91697161	298.5	$C_{19}H_{38}O_2$	15.727	4.6
21	Butyl 9-tetradecenoate	87382688	282.5	$C_{18}H_{34}O_2$	15.973	36.8
22	Oleic Acid	445639	282.5	$C_{18}H_{34}O_2$	16.168	8.44
23	17-Octadecynoic acid	1449	280.4	$C_{18}H_{32}O2$	16.248	1.62

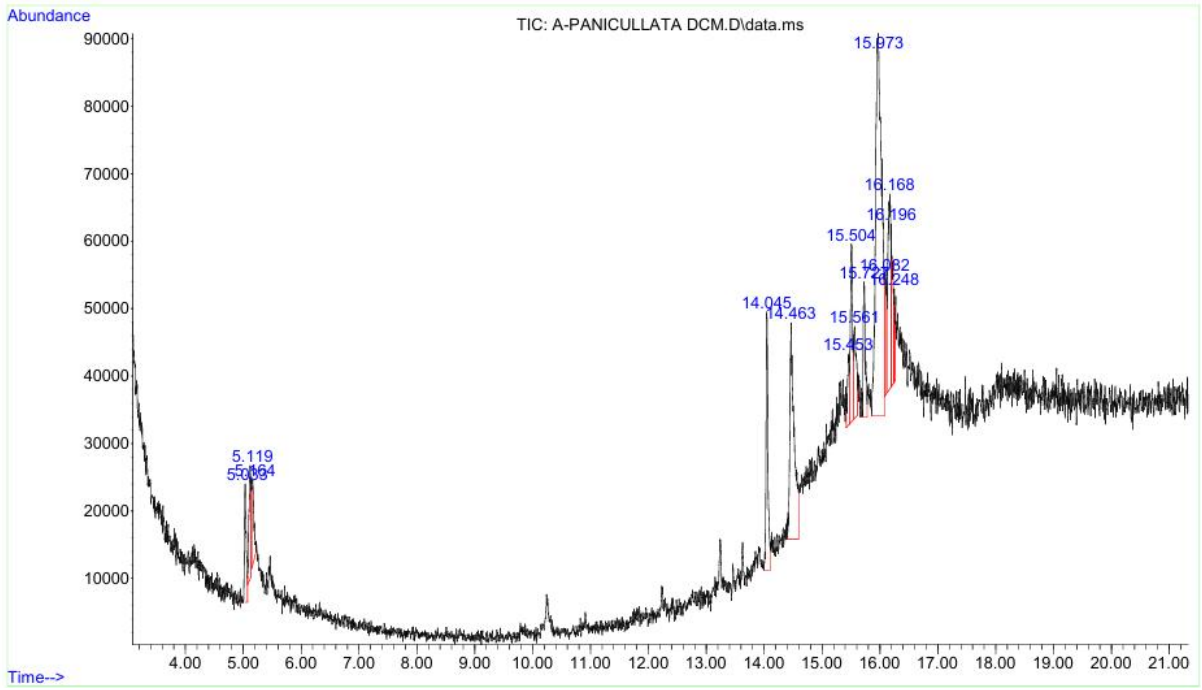

Figure 3.1: GC-MS Analysis result of the Dichloromethane extract of *Andrographis paniculata*

Table 3.2. Identified Binding Site Amino Acids in the SARS-CoV-2 Protein (PDB ID:7BV2)

S/N	Binding Site Amino Acids
1	ARG555
2	ASN691
3	ASP760
4	SER759
5	SER814

Table 3.3. Binding Affinities of *Andrographis paniculata* Compounds

S/N	NAME OF COMPOUNDS	PUBCHEM CID	BINDING AFFINITY(Kcal/mol)
1	Oleanolic Acid	10494	-7.4
2	3-O-beta-D-Glucopyranosylandrographolide	11519131	-6.9
3	Andrographidin B	11968627	-7.3
4	Bisandrographolide C	154704215	-7.9
5	Andrographidin A	13963762	-7.3
6	14- Deoxy-11,12-didehydroandrographiside	44575271	-7.4
7	Chlorogenic Acid	1794427	-7.2
8	2',3',4',5,7-Pentamethoxyflavone	373146	-6.9
9	Echioidin	44257608	-7.7
10	14-Deoxyandrographoside	44575270	-7.0
11	Andrographiside	44593583	-7.0
12	Quercetin	5280343	-7.7
13	Apigenin	5280443	-7.3
14	Luteolin	5280445	-7.5
15	Apigetrin	5280704	-8.4
16	Wogonin	5281703	-7.2
17	4,5-Dicaffeoylquinic acid	5281780	-8.4
18	5-Hydroxy-7,2',6'-trimethoxyflavone	5318369	-6.9
19	Andrographidine C	5318484	-7.4
20	Andrographidine E	5318498	-7.3
21	5,7,2',6'-Tetrahydroxyflavone	5321865	-7.0

22	Andrographoside	6439612	-7.4
23	Methyl 3,4-dicaffeoylquinate	91666355	-8.5
24	Neoandrographolide	9848024	-6.9
25	Bisandrographolide B	44575280	-7.2
26	7-O-Methylvitexin	44258317	-7.6
27	Eleutheroside E1	443024	-7.0

Table 3.4 Binding Affinities of Co-crystallized Ligand and Remdesivir Triphosphate (standard drug)

S/N	NAME OF COMPOUND	PUBCHEM CID	BINDING AFFINITY (KCAL/MOL
1	Remdesivir Monophosphate	121310009	-6.8
2	Remdesivir Triphosphate	56832906	-7.7

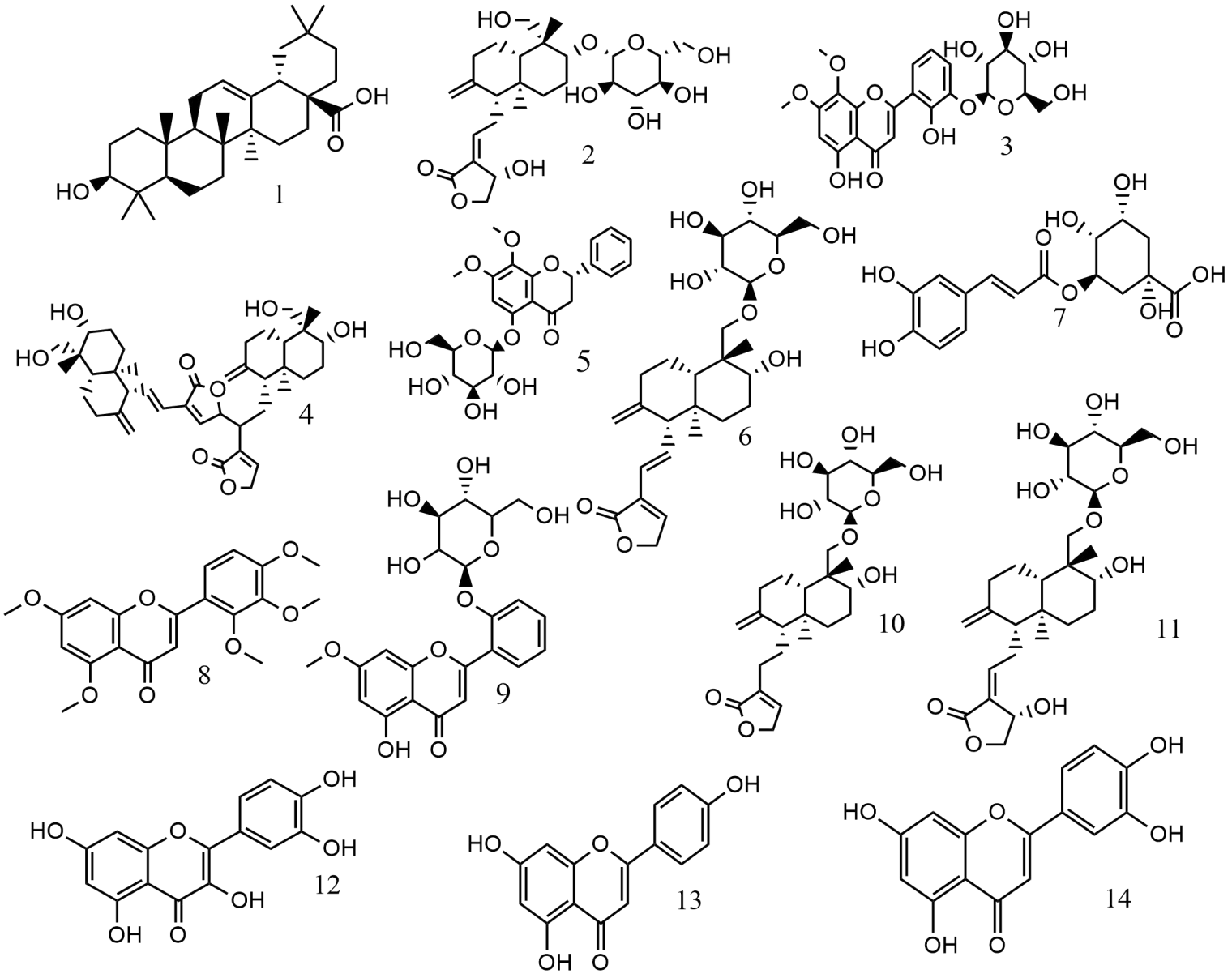
1
2
3
4
5
6
7
8
9
10
11
12
13
14

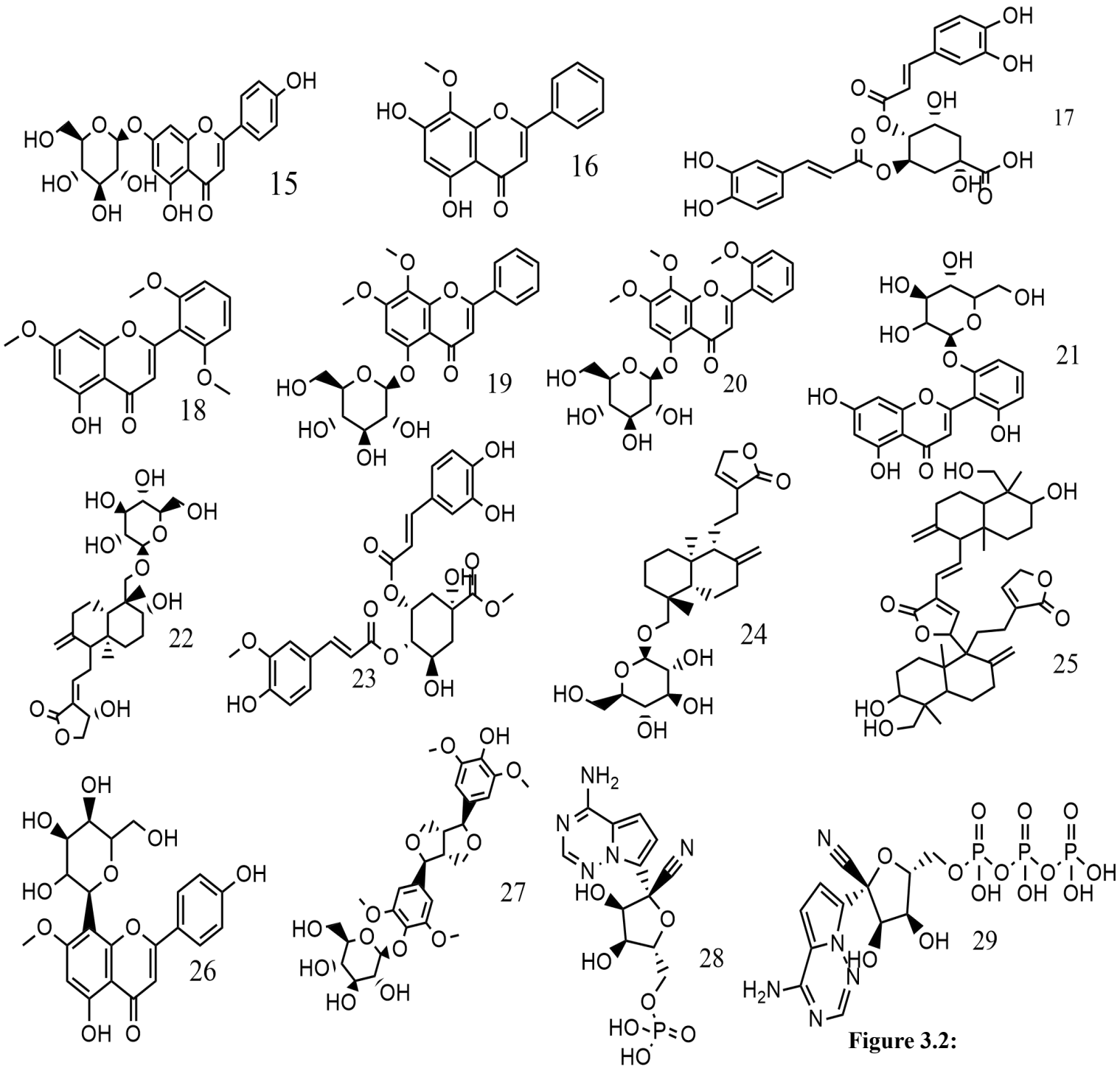

Figure 3.2:

Showing the chemical structures of compounds 1-27 from *Andrographis paniculata* and 28-29 for the co-crystallized ligand and Remdesivir Triphosphate respectively (Table 3.2 and 3.3 respectively).

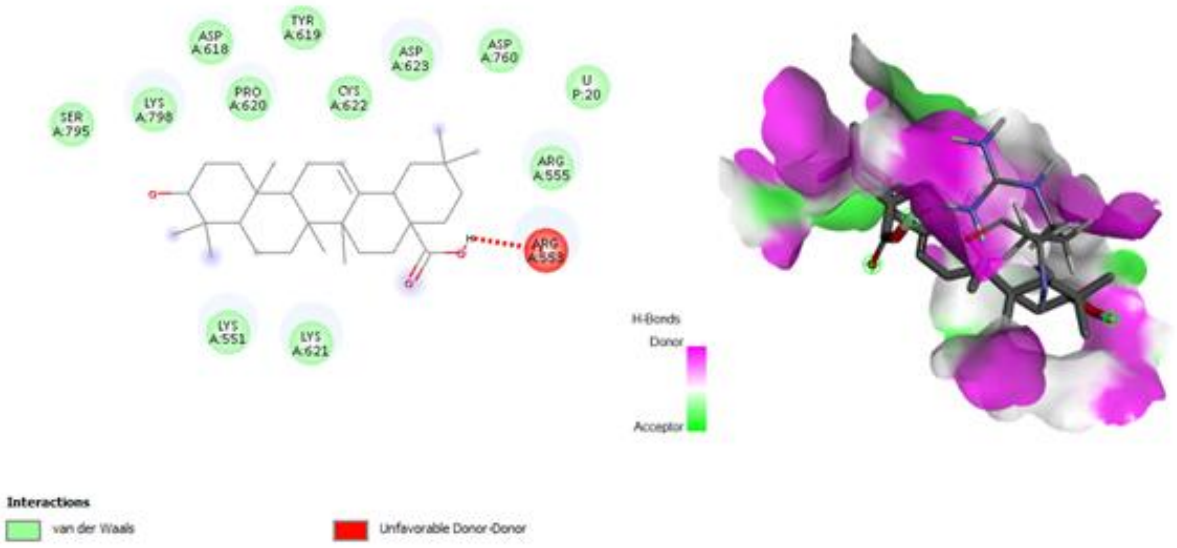

Oleanolic Acid

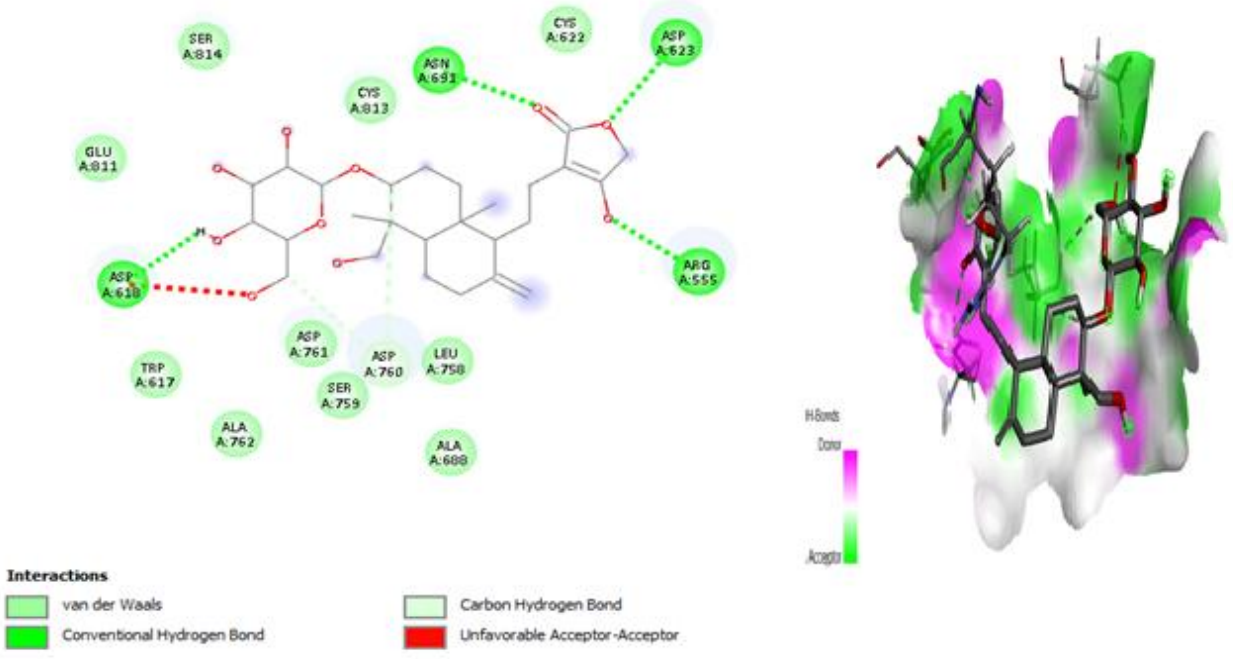

3-O-beta-D-Glucopyranosylandrographolide

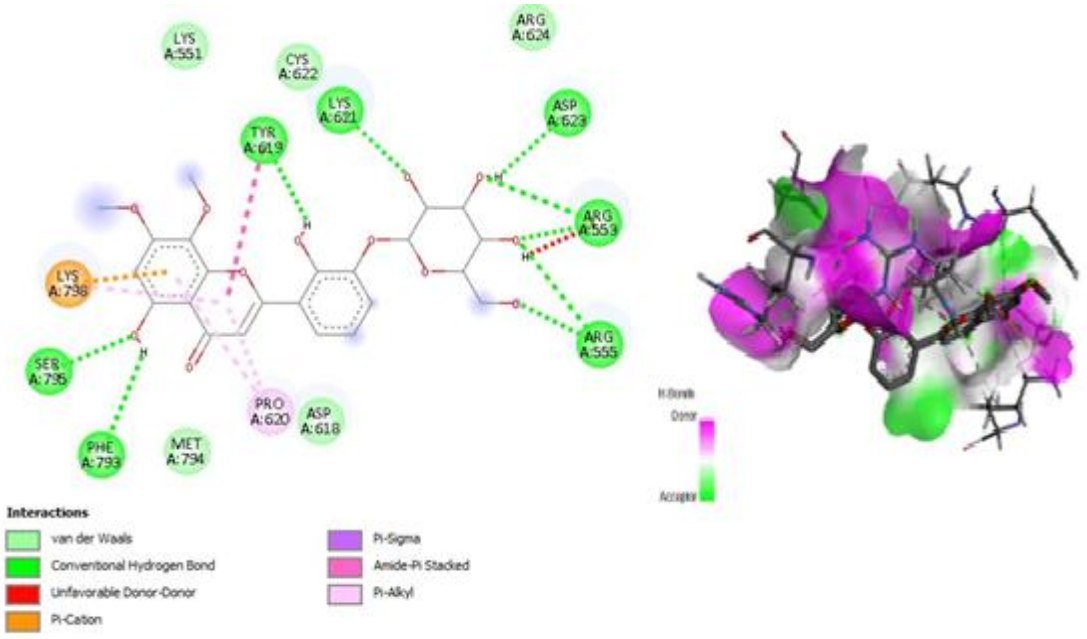

Andrographidin B

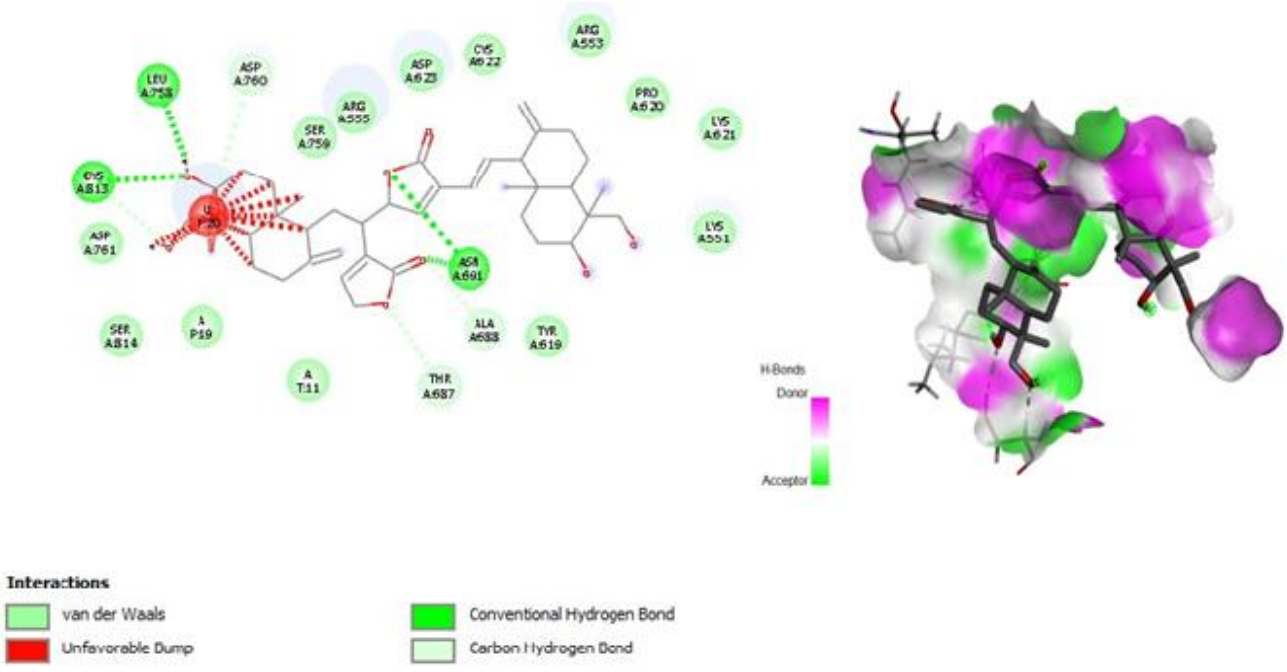

Bisandrographolide CFigure 3.3: 2D (left) and 3D (right) views of the molecular interactions of compounds **1-4** from *Andrographis paniculata* (Table 3) with the amino-acid residues of SARS-CoV-2 protein.

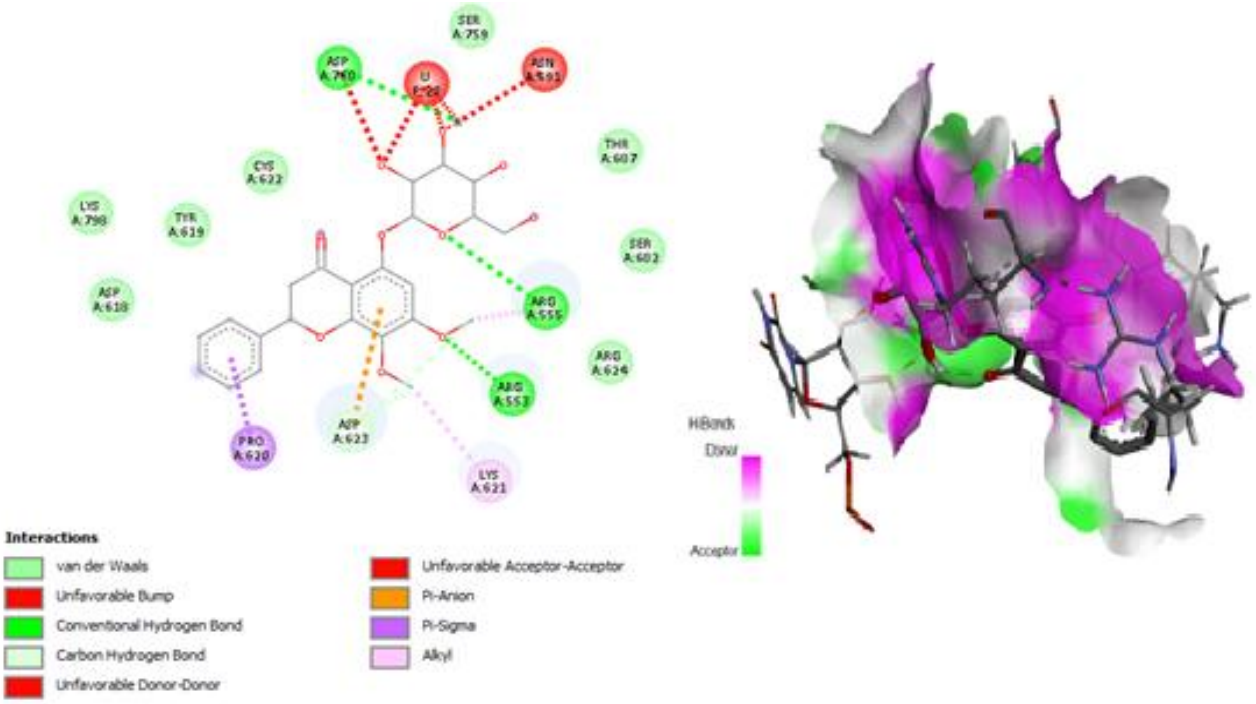

Andrographidin A

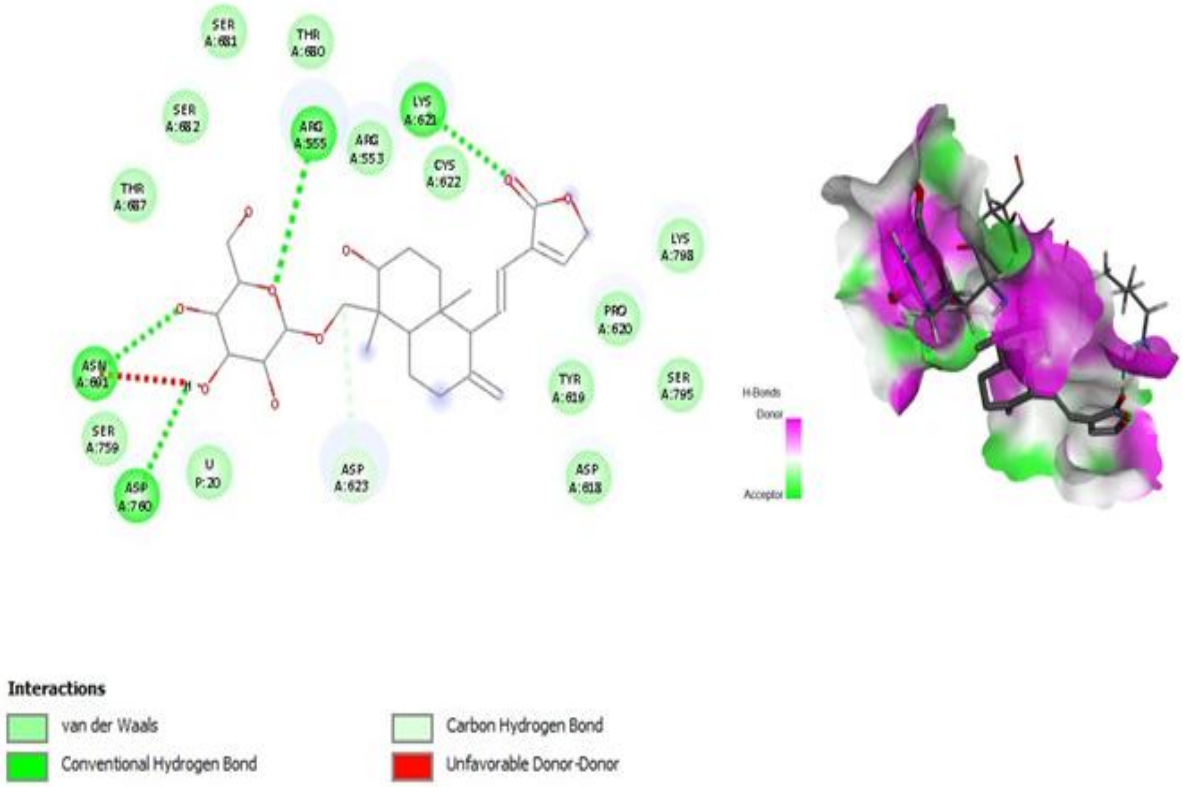

14- Deoxy-11,12-didehydroandrographiside

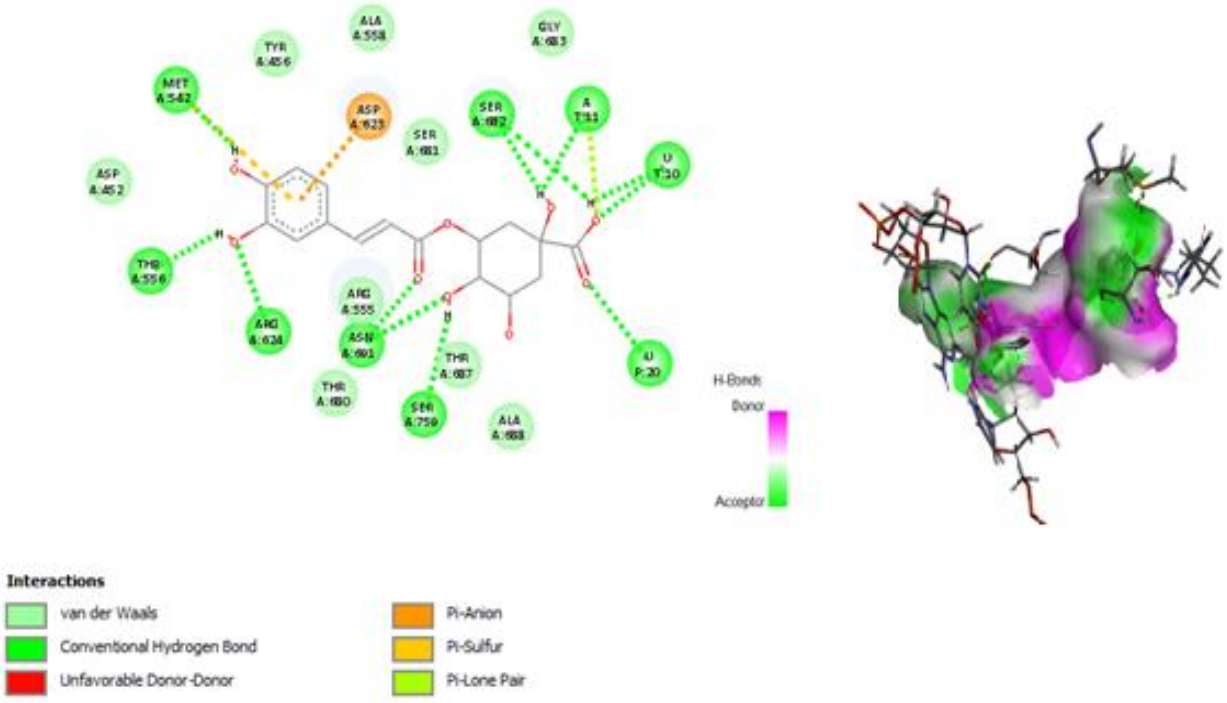

Chlorogenic Acid

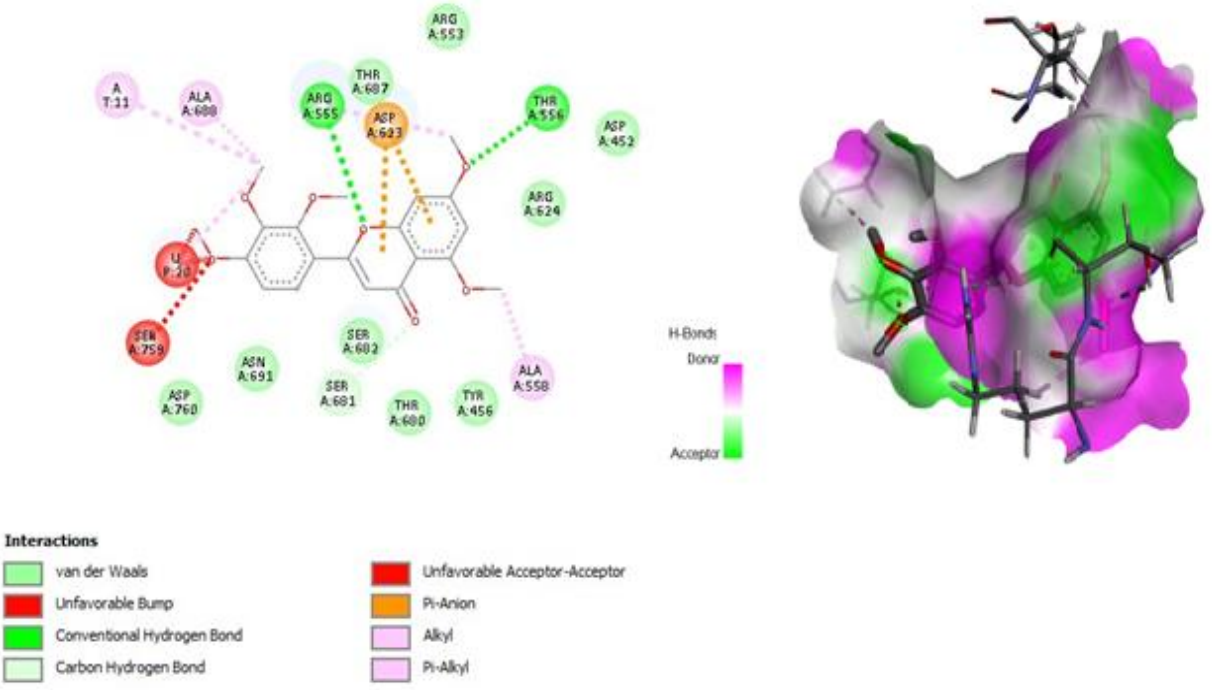

2',3',4',5,7-Pentamethoxyflavone

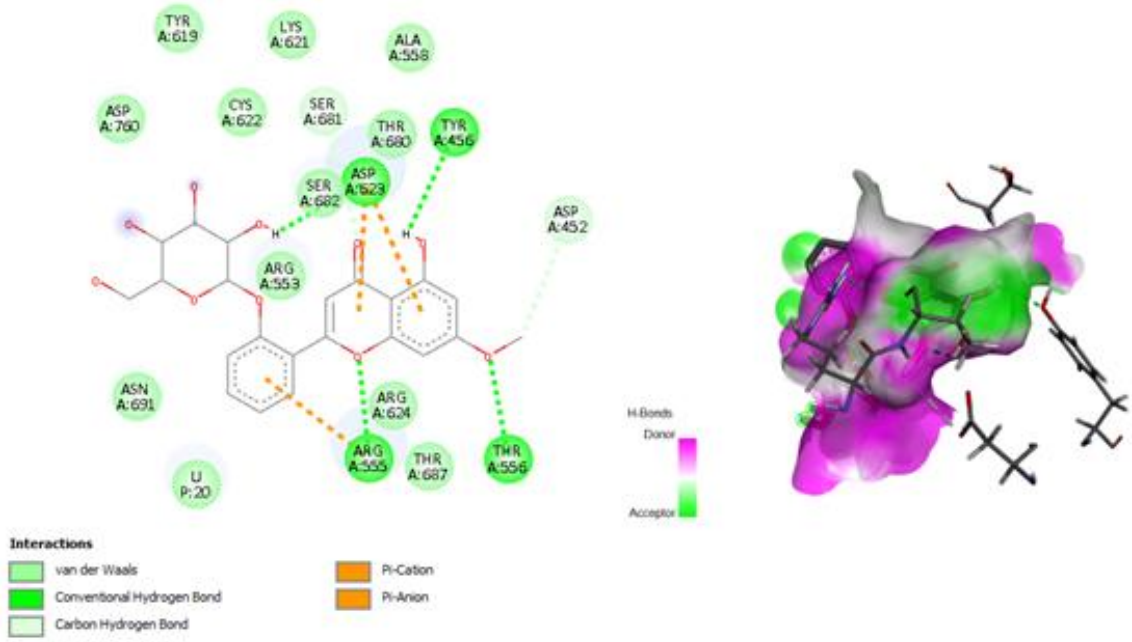

Echioidin

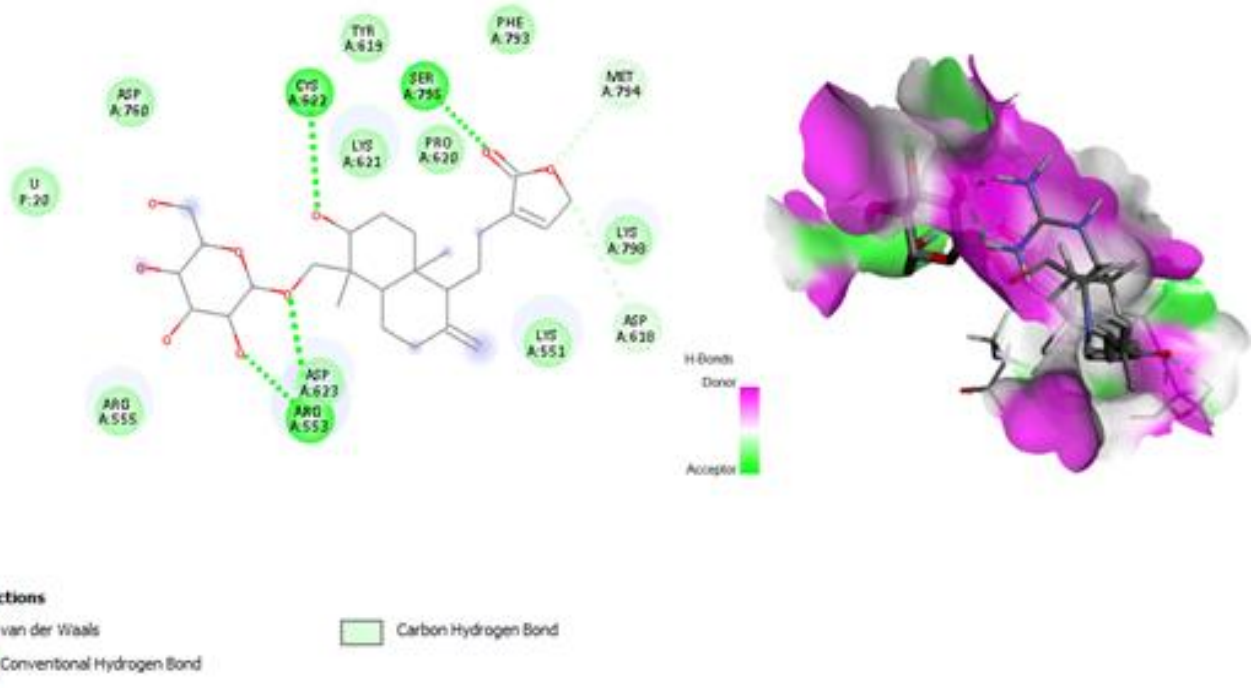

14-DeoxyandrographosideFigure 3.4: 2D (left) and 3D (right) views of the molecular interactions of compounds **6-10** from *Andrographis paniculata* (Table 3) with the amino-acid residues of SARS-CoV-2 protein.

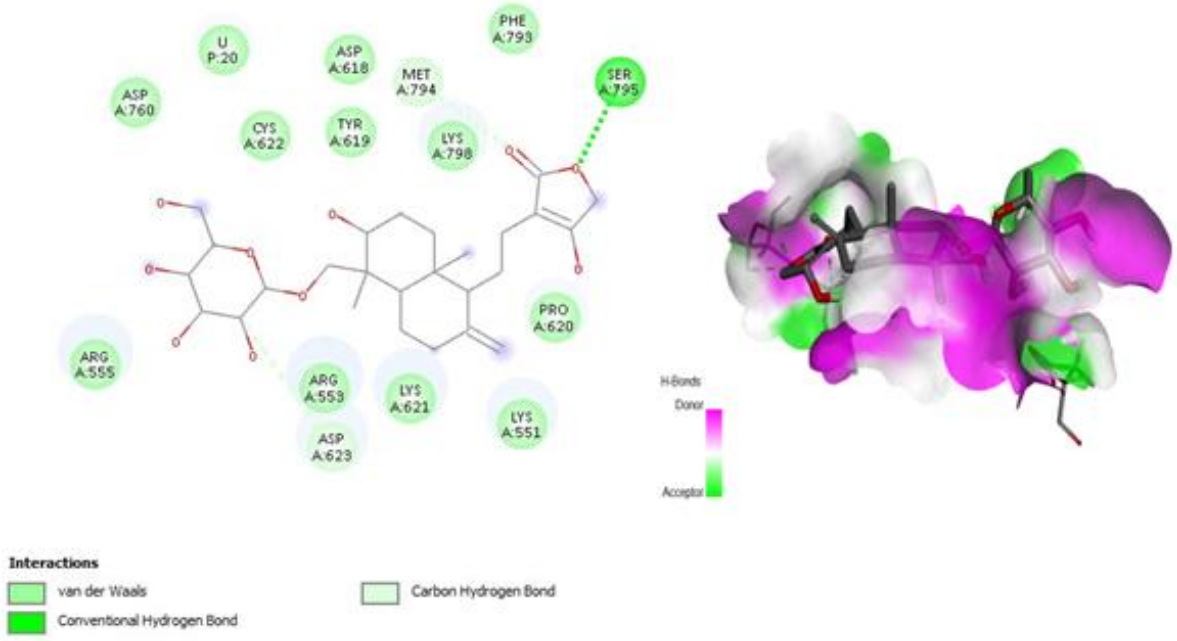

Andrographiside

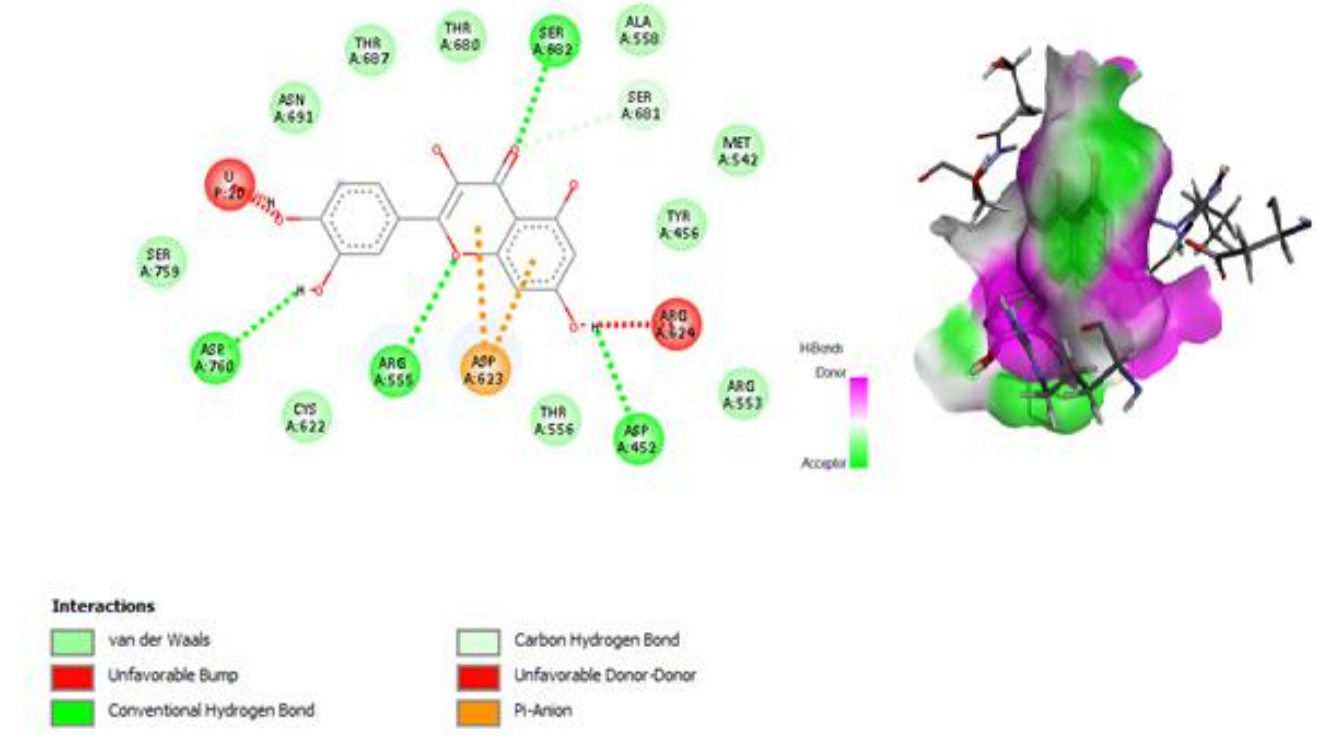

Quercetin

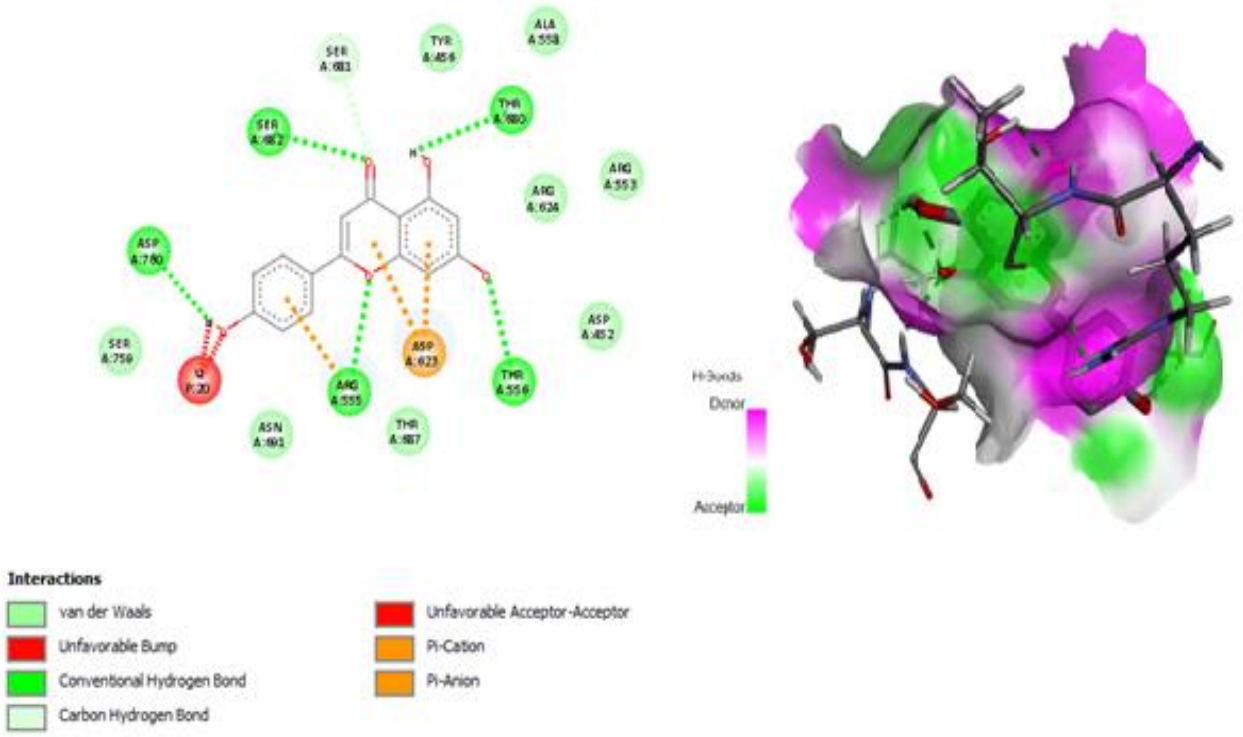

Apigenin

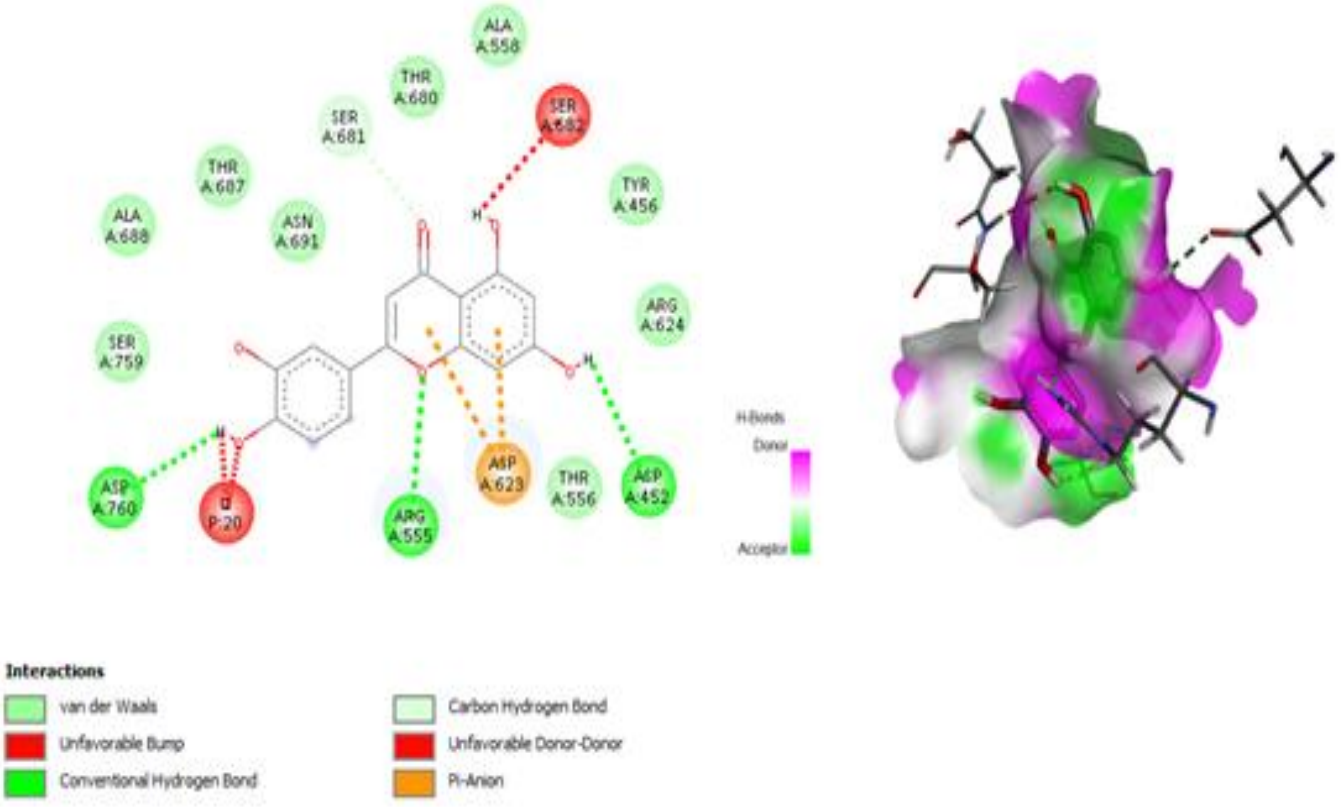

Luteolin

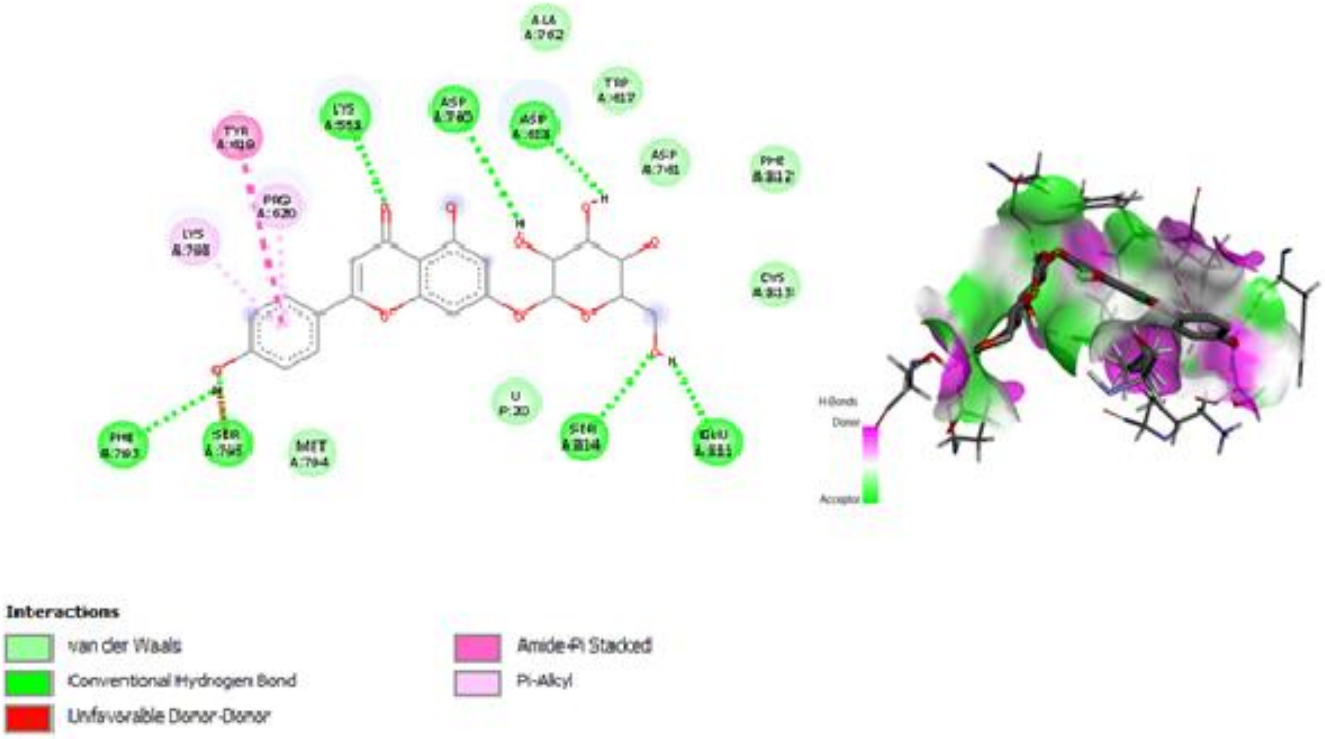

Apigetrin

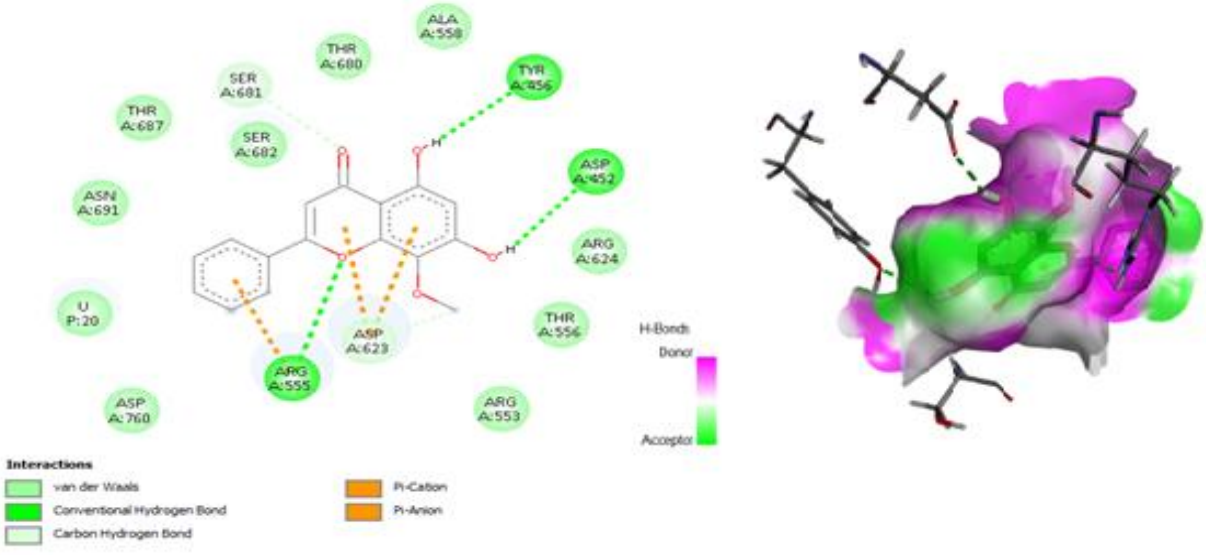

WogoninFigure 3.5: 2D (left) and 3D (right) views of the molecular interactions of compounds **11-16** from *Andrographis paniculata* (Table 3) with the amino-acid residues of SARS-CoV-2 protein.

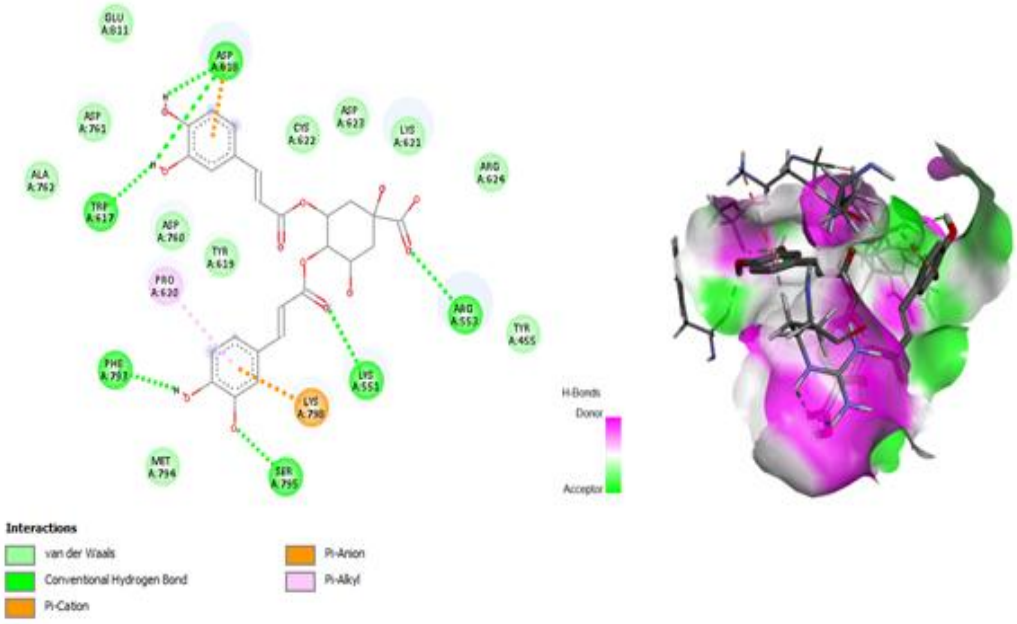

4,5-Dicaffeoylquinic acid

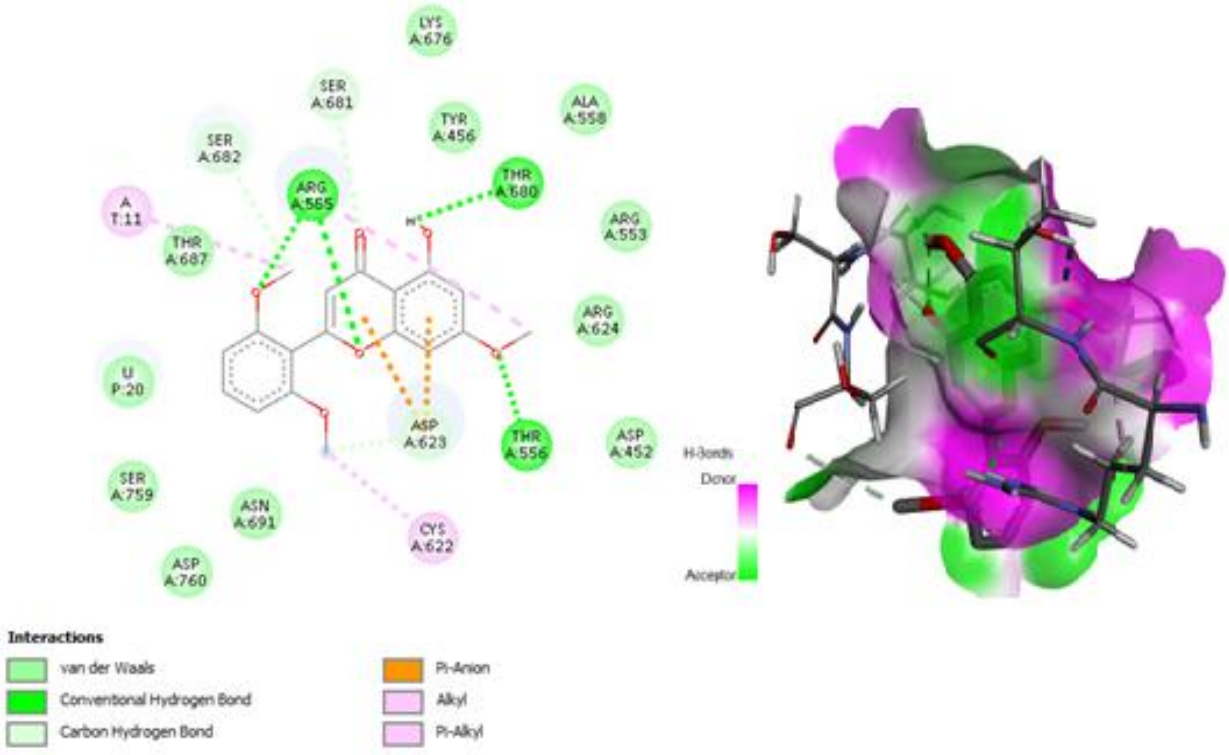

5-Hydroxy-7,2',6'-trimethoxyflavone

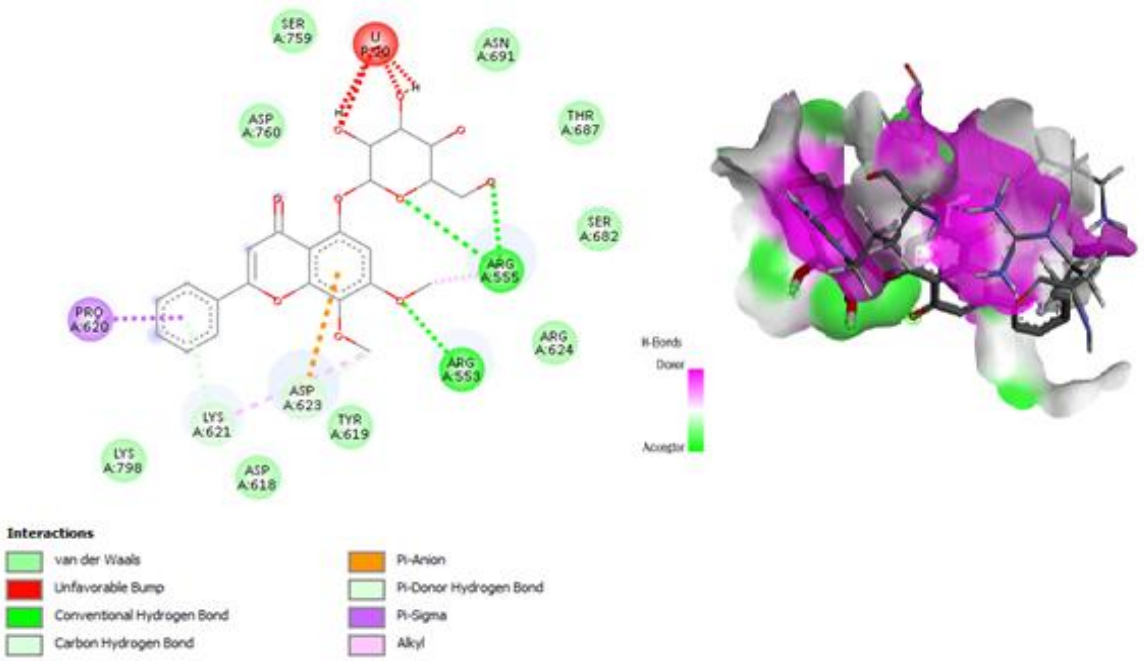

Andrographidine C

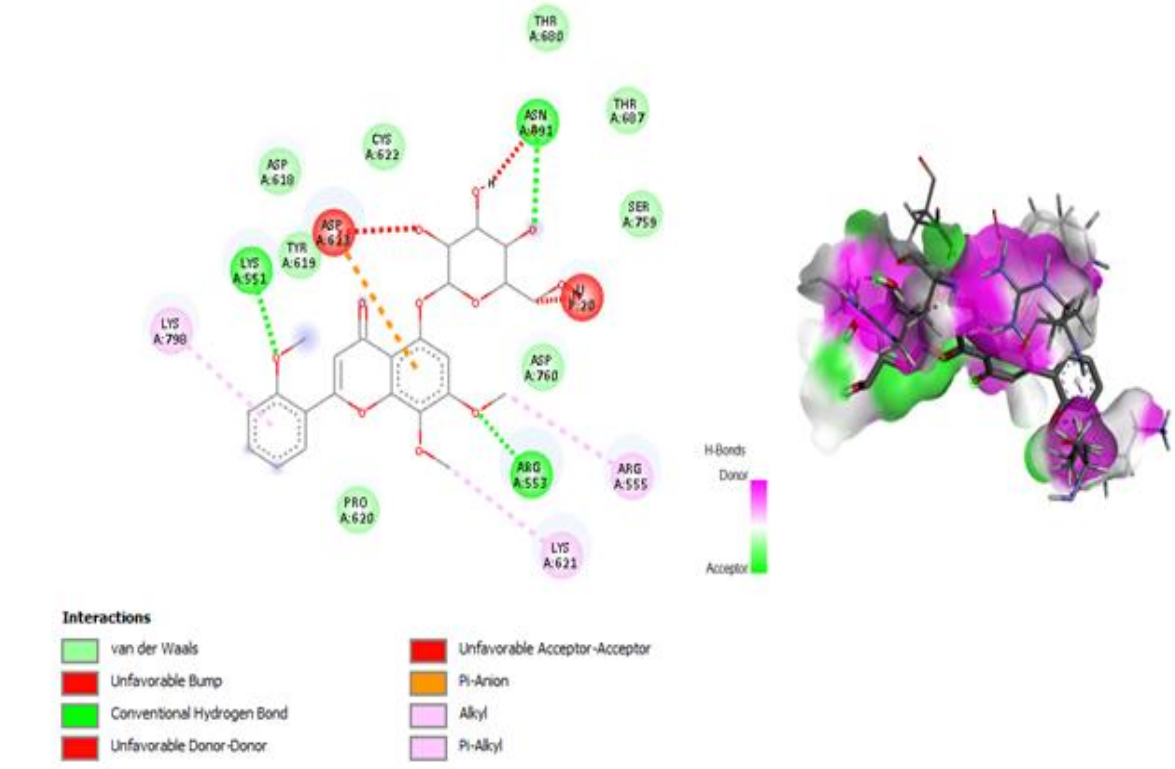

Andrographidine E

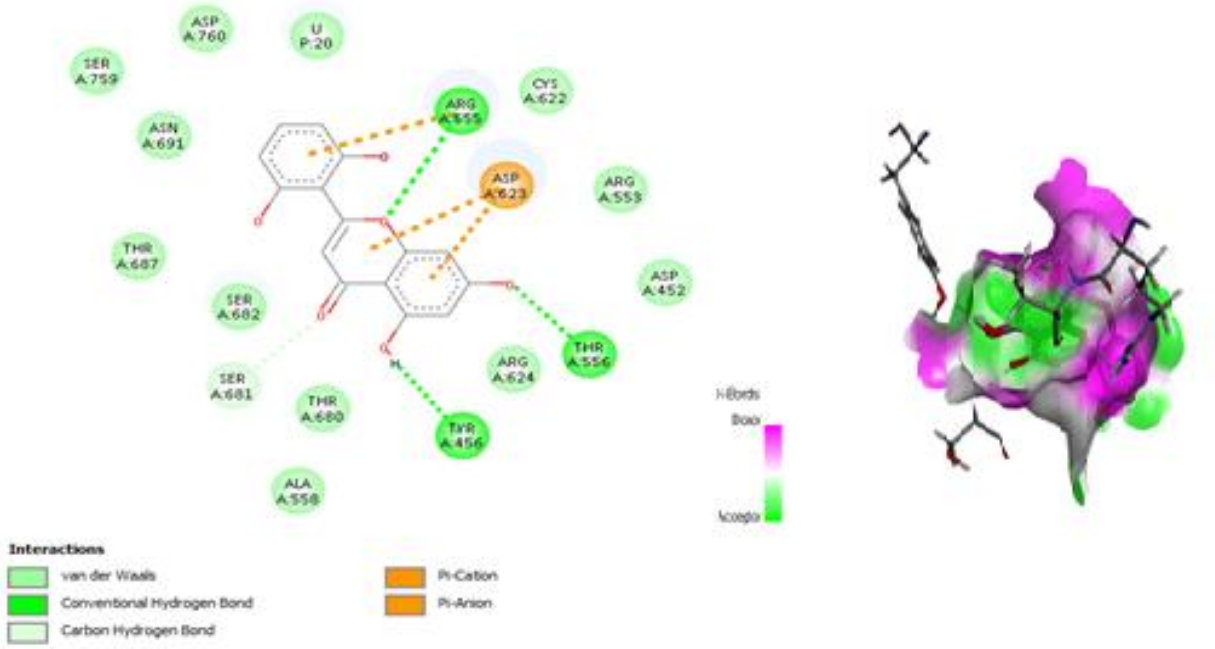

5,7,2',6'-Tetrahydroxyflavone

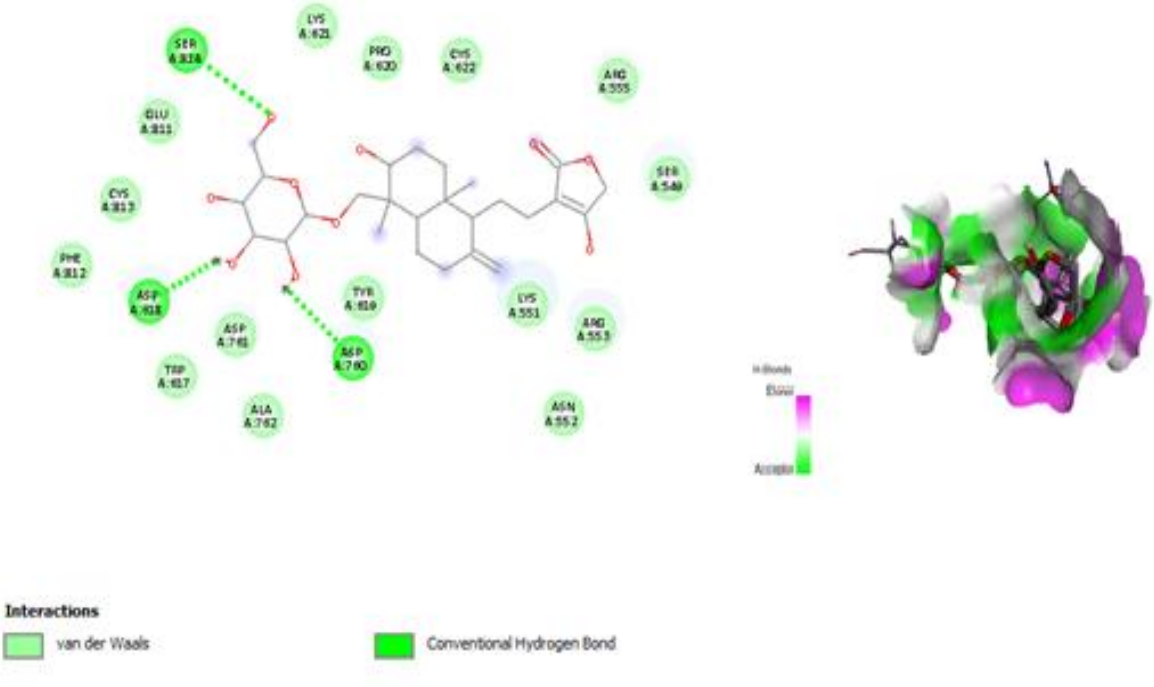

AndrographisideFigure 3.6: 2D (left) and 3D (right) views of the molecular interactions of compounds **17-22** from *Andrographis paniculata* (Table 3) with the amino-acid residues of SARS-CoV-2 protein.

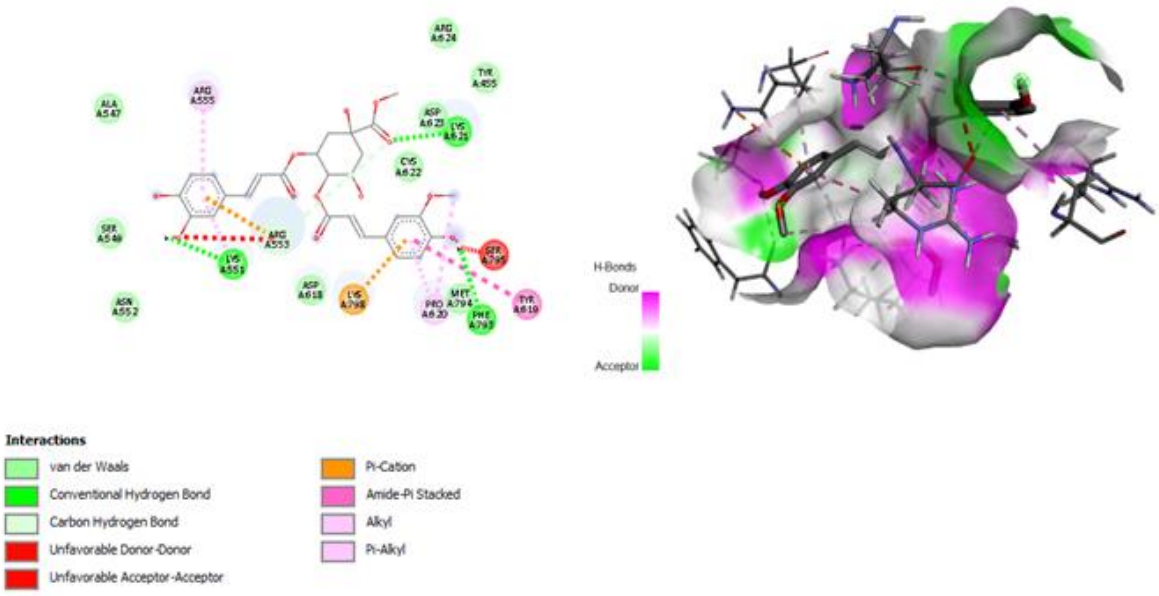

Methyl 3,4-dicaffeoylquinate

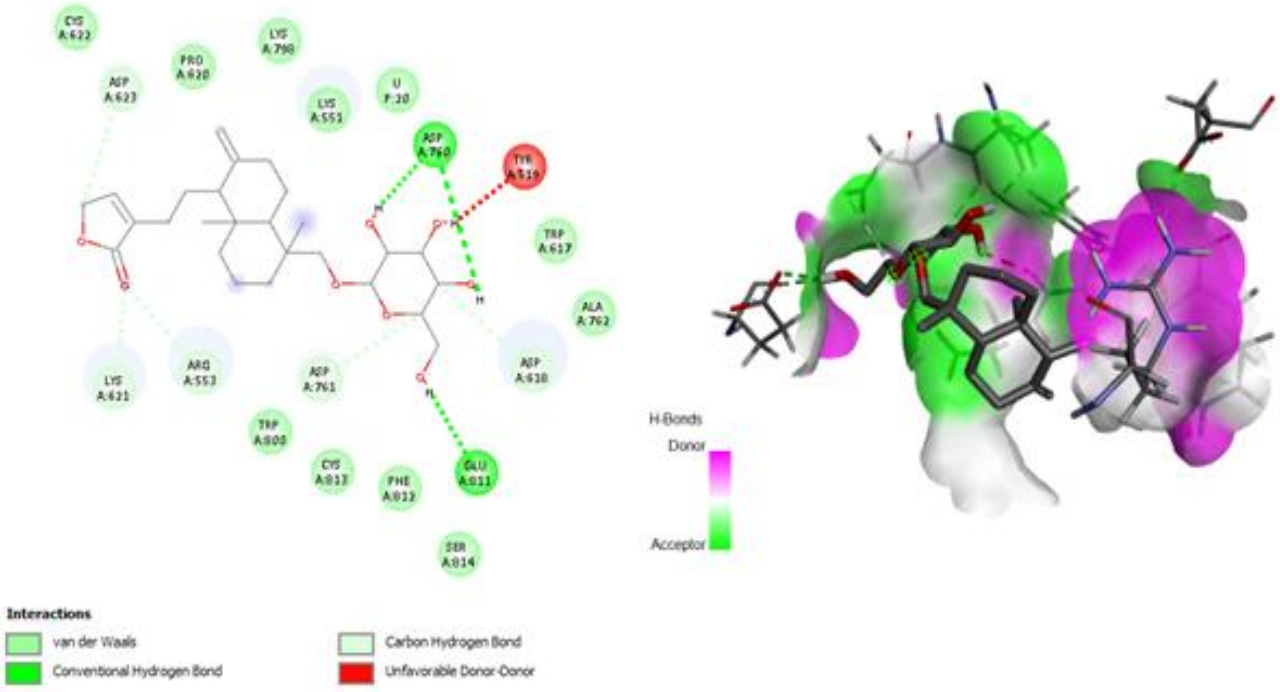

Neoandrographolide

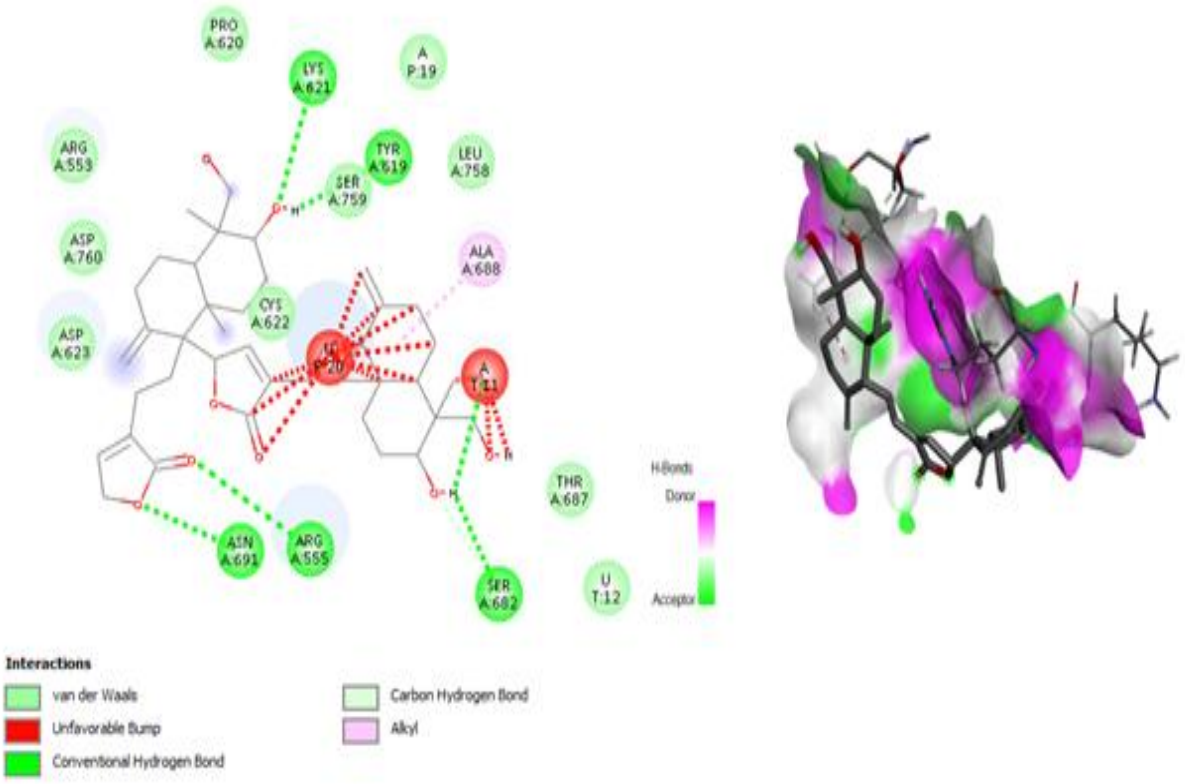

Bisandrographolide B

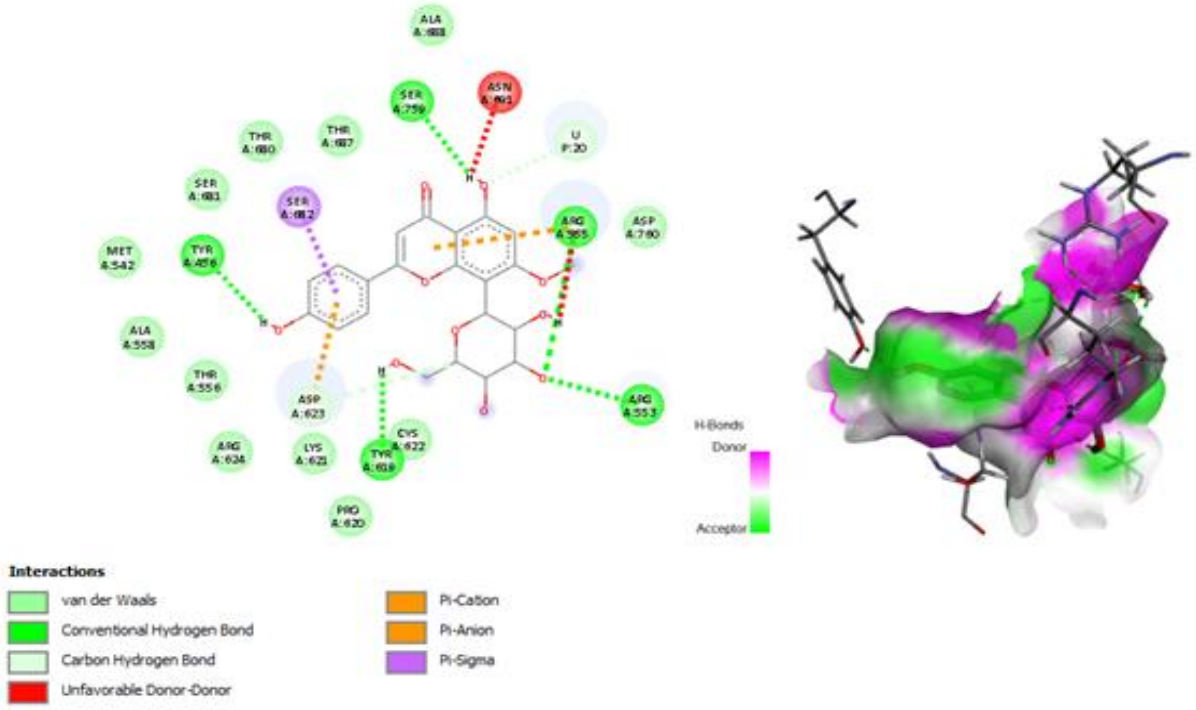

7-O-Methylvitexin

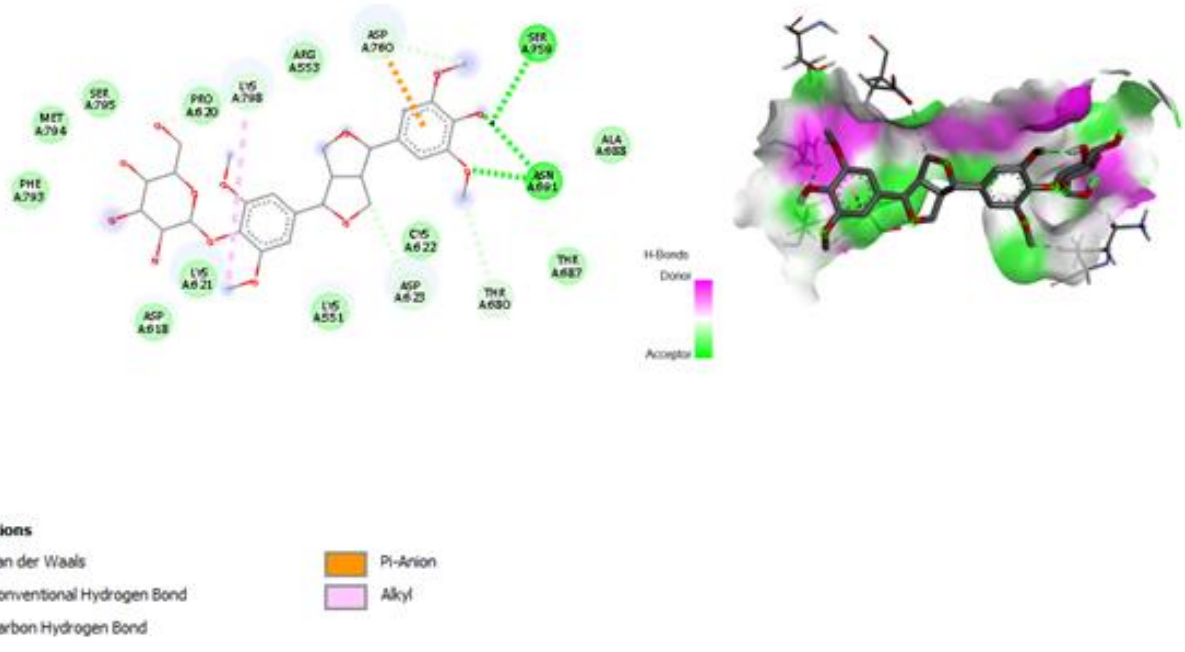

Eleutheroside E1

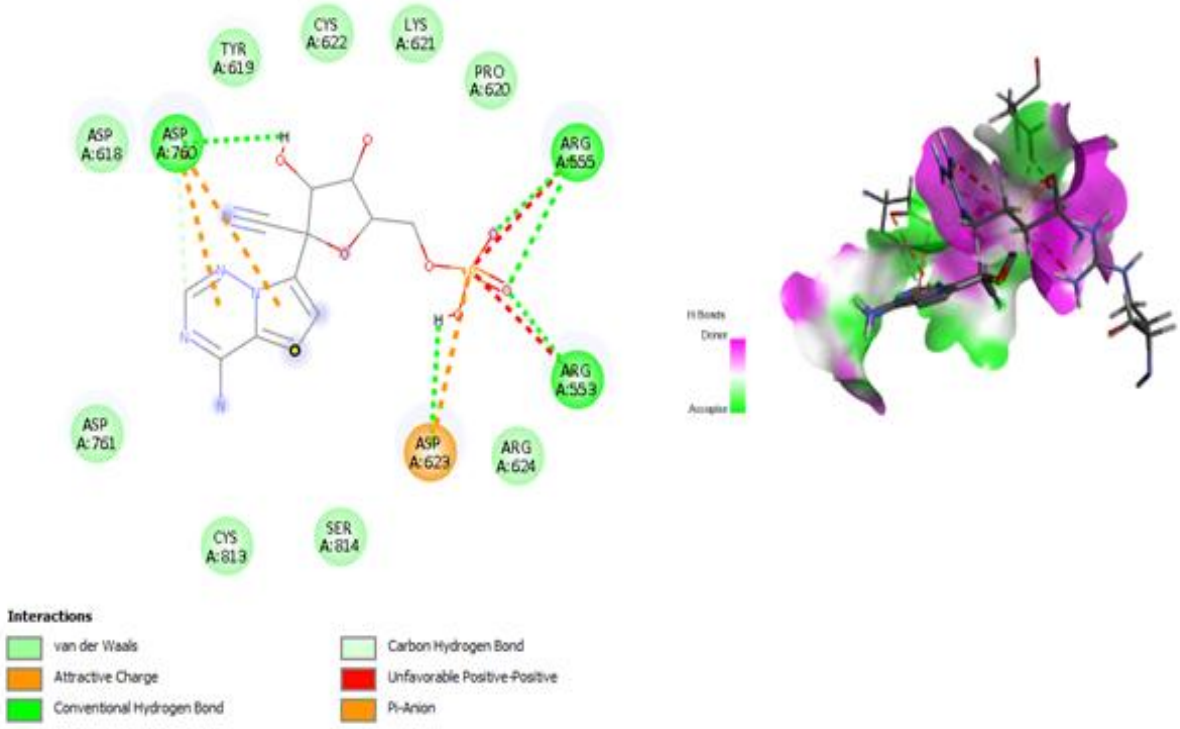

F86

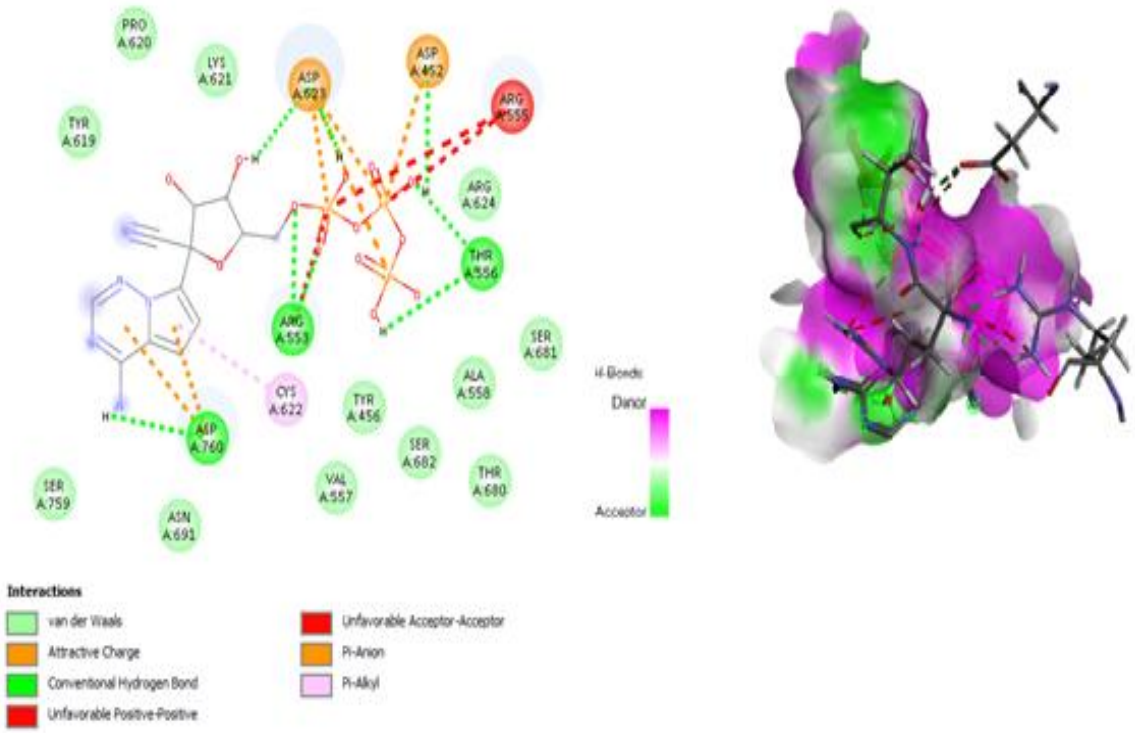

RTP

Figure 3.7: 2D (left) and 3D (right) views of the molecular interactions of compounds **23-27** from *Andrographis paniculata* as well as the co-crystallized ligand (F86) and the Standard Drug (Remdesivir Triphosphate-RTP).

Table 3.5: Showing the various types of interaction between the ligands (Andrographis paniculata compounds) and amino acids in the target protein.

S/N	Compound	Hydrogen Bond	Van der Waals Interactions	Other Interactions
1	Oleanolic Acid	-	SER795, LYS798 ASP618, PRO620 TYR619, CYS622 ASP623, ASP760 ARG555, LYS621 LYS551	Unfavorable donor-donor
2	3-O-beta-D-Glucopyranosylandrographolide	ASP618, ASN691, ASP623, ARG555	GLU811, SER814, CYS813, CYS622, TRP617, ALA762, ASP761, LEU758, SER759, ALA688	Unfavorable Acceptor-Acceptor, unfavorable bump, pi-sigma, pi-alkyl, carbon hydrogen bond
3	Andrographidin B	SER795, PHE793, TYR619, LYS621, ASP623, ARG553, ARG555	LYS551, CYS622, MET794, ASP618, ARG624	Pi-sigma, pi-cation, unfavorable donor-donor, amide-pi stacked, pi-alkyl
4	Bisandrographolide C	LEU758, CYS813, ASN691	ASP761, SER814, SER759, ARG555, ASP623, CYS622, ARG553, PRO620, LYS621, LYS551, TYR619	Unfavorable bump, carbon hydrogen bond
5	Andrographidin A	ASP760, ARG553, ARG555	LYS798, ASP618, TYR619, CYS622, SER759, THR687, SER682, ARG624	unfavorable acceptor-acceptor,pi-anion, pi-sigma, alkyl, unfavorable bump, unfavorable donor-donor
6	14-Deoxy 11,12-didehydroandrographiside	ASP760,ASN691, ARG555, LYS621	SER681, THR680, SER684, THR687, SER759, ARG553, CYS622, LYS798, PRO620, TYR619, SER795, ASP618	Carbon hydrogen bond, Unfavorable donor-donor
7	Chlorogenic Acid	MET542, THR556, ARG624,	ASP452, TYR456, ALA558, SER681, ARG555, THR680, THR687, ALA688, GLY683	Unfavorable Donor-Donor, Pi-anion, Pi-sulfur, Pi-lone pair

		ASN691, SER759, SER682		
8	2',3',4',5',7-Pentamethoxyflavone	ARG555, THR556	ASP760, ASN691, SER682, THR680, TYR456, ARG624, ASP452, ARG553, THR687	Unfavorable acceptor-acceptor, unfavorable donor-donor, carbon hydrogen bond, Pi-anion, Pi-alkyl, Alkyl
9	Echioidin	ASP623, TYR456, ARG555, THR556	ASP760, TYR619, CYS622, LYS621, ALA558, THR680, SER682, ARG553, ASN691, ARG624, THR687	Carbon hydrogen bond, pi-cation, pi-anion
10	14-Deoxyandrographoside	CYS622, ARG553, SER795	ASP760, ARG555, TYR619, LYS621, PRO620, PHE793, ASP623, PHE793, LYS798, LYS551	Carbon hydrogen bond
11	Andrographiside	SER795	ASP760, CYS622, TYR619, ASP618, LYS798, PHE793, LYS551, LYS621, ARG553, ARG555	carbon hydrogen bond
12	Quercetin	ASP760, ARG555, SER682, ASP452	SER759, ASN691, THR687, THR680, CYS622, ALA558, MET542, TYR456, THR556, ARG553	Unfavorable bump, unfavorable donor-donor, carbon hydrogen bond, pi-anion
13	Apigenin	ASP760, SER682, ARG555, THR680, THR556	THR456, ALA558, ARG624, ARG553, ASP452, THR687, ASN691, SER759	Carbon Hydrogen Bond, Pi-Cation, Pi-Anion, Unfavorable Acceptor-Acceptor, Unfavorable Bump
14	Luteolin	ASP760, ARG555, ASP452	ALA688, THR687 ASN691, SER759 SER681, THR680 ALA558, TYR456 ARG624, THR556	Pi-Anion, Carbon Hydrogen Bond, Unfavorable Donor-Donor, Unfavourable Bump
15	Apigetrin	PHE793, SER795, LYS551, ASP760, ASP618, SER814, GLU811	ALA762, TRP617, ASP761, PHE812, CYS813, MET794	Amide-Pi Stacked, Pi-Alkyl, Unfavorable Donor-Donor
16	Wogonin	TYR456,		Carbon Hydrogen

		ASP452, ARG555	ASP760, ASN691, THR687, SER682, THR680, ALA558, ARG624, THR556, ARG553	Bond, Pi-Cation, Pi-Anion
17	4,5-Dicaffeoylquinic acid	TRP617, ASP618, PHE793, SER795, LYS551, ARG553	GLU811, ASP761, ALA762, ASP760, TYR619, MET794, CYS622, ASP623, LYS621, ARG624, TYR455	Pi-cation, pi-anion, pi-alkyl
18	5-Hydroxy-7,2',6'-trimethoxyflavone	ARG555, THR556, THR680	THR687, SER759, ASP760, ASN691, LYS676, TYR456, ALA558, ARG553, ARG624, ASP452	carbon hydrogen bond, pi-anion, alkyl, pi-alkyl
19	Andrographidine C	ARG553, ARG555	LYS798, ASP618, TYR619, ASP760, SER759, ARG624, ASN691, THR687, SER682	Unfavorable bump, carbon-hydrogen bond, pi-anion, pi-donor hydrogen bond, pi-sigma, alkyl
20	Andrographidine E	LYS551, ARG553, ASN691	ASP618, TYR619, CYS622, THR680, THR687, SER759, ASP760, PRO620	Unfavorable bump, unfavorable donor-donor, unfavorable acceptor-acceptor, pi-anion, alkyl, pi-alkyl
21	5,7,2',6'-Tetrahydroxyflavone	TYR456, ARG555, THR556	SER759, ASP760, ASN691, THR687, SER682, THR680, ALA558, CYS622, ARG553, ASP452, ARG624	Pi-cation, pi-anion, carbon hydrogen bond
22	Andrographoside	SER814, ASP618, ASP760	GLU811, CYS813, PHE812, TRP617, ASP761, ALA762, TYR619, LYS621, PRO620, CYS622, ARG555, SER549, LYS551, ARG553, ASN552	-
23	Methyl 3,4-dicaffeoylquinate	LYS551, PHE793, LYS621	ALA547, SER549, ASN552, ASP618, MET794, CYS622, ASP623, ARG624, TYR455	Carbon hydrogen bond, unfavorable donor-donor, unfavorable acceptor-acceptor, pi-cation, amide-pi stacked, alkyl, pi-alkyl
24	Neoandrographolide	ASP760, GLU811	CYS622, PRO620, LYS798, LYS551, TRP800, CYS813, PHE812, SER814, TRP617, ALA762	Unfavorable donor-donor, carbon hydrogen bond

25	Bisandrographolide B	LYS621, TYR619, ASN691, ARG555, SER682	ARG553, ASP760, ASP623, CYS622, PRO620, SER759, LEU758, THR687	Unfavorable bump, carbon hydrogen bond, alkyl
26	7-O-Methylvitexin	SER759, TYR456, TYR619, ARG555, ARG553	ALA688, THR687, THR680, SER681, MET542, ALA558, THR556, ARG624, LYS621, PRO620, CYS622, ASP760	pi-cation, pi-anion, pi-sigma, unfavorable donor-donor, carbon hydrogen bond
27	Eleutheroside E1	SER759, ASN691	MET794, PHE793, SER795, PRO620, ASP618, LYS621, LYS551, ARG553, CYS622, THR687, ALA688	Pi-anion, alkyl, carbon hydrogen bond

Table 3.6: Co-crystallized ligand & standard drug interactions with amino acids on SARS-CoV protein

S/N	Compound	Hydrogen Bond	Van der Waals Interactions	Other Interactions
1	Remdesivir Monophosphate	ARG555, ASP760	PRO620, TYR619, LYS621, SER759, ASN691, TYR456, VAL557, SER682, ALA558, THR680, SER681, ARG624	Carbon Hydrogen Bond, Pi Anion, Unfavorable Positive-Positive, Attractive Charge
2	Remdesivir Triphosphate	ARG553, ASP760, THR556	ASP618, LYS621, PRO620, ARG624, TYR619, CYS622, SER814, CYS813, ASP761	Attractive Charge, Unfavorable Positive-Positive, Unfavorable Acceptor-Acceptor, Pi-Anion, Pi-Alkyl

3.5 ADMET Profiling

The results of the Physicochemical, Pharmacokinetic properties, Lipophilicity and Toxicity profiles of *Andrographis paniculata* ligands (phytoconstituents) are shown in Tables **3.7** – **3.9** respectively.

Table 3.7: Physicochemical Properties of the Phytoconstituents of Andrographis paniculata

S/N	Name of Compound	Molecular Formula	Molecular Weight	Num. Heavy Atoms	Num. Aromatic Heavy Atoms	Fraction CSP3	Num. Rotatable bonds	Num. H. bond Acceptor	Num. H. bond Donor	Molar Refractivity	TPSA (Å²)
1	Oleanolic Acid	$C_{30}H_{48}O_3$	456.7	33	0	0.9	1	3	2	136.65	57.53
2	3-O-beta-D-Glucopyranosylandrographolide	$C_{26}H_{40}O_{10}$	512.59	36	0	0.81	6	10	6	127.6	166.14
3	Andrographidin B	$C_{23}H_{24}O_{12}$	492.43	35	16	0.35	6	12	6	119.1	188.51
4	Bisandrographolide C	$C_{40}H_{56}O_8$	664.87	48	0	0.7	8	8	4	185.52	133.52
5	Andrographidin A	$C_{23}H_{26}O_{10}$	462.45	33	12	0.43	6	10	4	112.63	144.14
6	14- Deoxy-11,12-didehydroandrographiside	$C_{26}H_{38}O_9$	494.57	35	0	0.73	6	9	5	125.96	145.91
7	Chlorogenic Acid	$C_{16}H_{18}O_9$	354.31	25	6	0.38	5	9	6	83.50	164.75
8	2',3',4',5,7-Pentamethoxyflavone	$C_{20}H_{20}O_7$	372.37	27	16	0.25	6	7	0	100.38	76.36
9	Echioidin	$C_{22}H_{22}O_{10}$	446.40	32	16	0.32	5	10	5	110.58	159.05
10	14-Deoxyandrographoside	$C_{26}H_{40}O_9$	496.59	35	0	0.81	7	9	5	126.44	145.91
11	Andrographiside	$C_{26}H_{40}O_{10}$	512.59	36	0	0.81	6	10	6	127.6	166.14
12	Quercetin	$C_{15}H_{10}O_7$	302.24	22	16	0	1	7	5	78.03	131.36
13	Apigenin	$C_{15}H_{10}O_5$	270.24	20	16	0	1	5	3	73.99	90.90
14	Luteolin	$C_{15}H_{10}O_6$	286.24	21	16	0	1	6	4	76.01	111.13
15	Apigetrin	$C_{21}H_{20}O_{10}$	432.38	31	16	0.29	4	10	6	106.11	170.05
16	Wogonin	$C_{16}H_{12}O_5$	284.26	21	16	0.06	2	5	2	78.46	79.90
17	4,5-Dicaffeoylquinic acid	$C_{25}H_{24}O_{12}$	516.45	37	12	0.24	9	12	7	126.90	211.28
18	5-Hydroxy-7,2',6'-trimethoxyflavone	$C_{18}H_{16}O_6$	328.32	24	16	0.17	4	6	1	89.42	78.13
19	Andrographidine C	$C_{23}H_{24}O_{10}$	460.43	33	16	0.35	6	10	4	115.05	148.05
20	Andrographidine E	$C_{24}H_{26}O_{11}$	490.46	35	16	0.38	7	11	4	121.54	157.28
21	5,7,2',6'-Tetrahydroxyflavone	$C_{15}H_{10}O_6$	286.24	21	16	0	1	6	4	76.01	111.13
22	Andrographoside	$C_{26}H_{40}O_{10}$	512.59	36	0	0.81	6	10	6	127.6	166.14
23	Methyl 3,4-dicaffeoylquinate	$C_{27}H_{28}O_{12}$	544.5	39	12	0.3	11	12	5	135.69	189.28

24	Neoandrographolide	$C_{26}H_{40}O_8$	480.59	34	0	0.81	7	8	4	125.27	125.68
25	Bisandrographolide B	$C_{40}H_{56}O_8$	664.87	48	0	0.7	8	8	4	185.26	133.52
26	7-O-Methylvitexin	$C_{22}H_{22}O_{10}$	446.4	32	16	0.32	4	10	6	111.08	170.05
27	Eleutheroside e1	$C_{28}H_{36}O_{13}$	580.58	41	12	0.57	9	13	5	140.01	174.99

Table 3.8: Pharmacokinectics Parameters of the Phytoconstituents of *Andrographis paniculata*

S/N	NAME OF COMPOUND	GI absorption	BBB permeant	P-gp substrate	CYP1A2 inhibitor	CYP2C19 inhibitor	CYP2C9 inhibitor	CYP2D6 inhibitor	CYP3A4 inhibitor	LogKp(skin permeation) (cm/s)
1	Oleanolic Acid	Low	No	No	No	No	No	No	No	-3.77
2	3-O-beta-D-Glucopyranosylandrographolide	Low	No	No	No	No	No	No	No	-9.41
3	Andrographidin B	Low	No	Yes	No	No	No	No	Yes	-8.74
4	Bisandrographolide C	Low	No	Yes	No	No	No	No	No	-6.04
5	Andrographidin A	Low	No	Yes	No	No	No	No	No	-8.63
6	14-Deoxy-11,12-didehydroandrographiside	Low	No	Yes	No	No	No	No	No	-8.54
7	Chlorogenic Acid	Low	No	No	No	No	No	No	No	-8.76
8	2',3',4',5,7-Pentamethoxyflavone	High	Yes	No	No	No	Yes	No	Yes	-6.41
9	Echioidin	Low	No	Yes	No	No	No	No	Yes	-7.50
10	14-Deoxyandrographoside	Low	No	Yes	No	No	No	No	No	-8.42
11	Andrographiside	Low	No	No	No	No	No	No	No	-9.41
12	Quercetin	High	No	No	Yes	No	No	Yes	Yes	-7.05
13	Apigenin	High	No	No	Yes	No	No	Yes	Yes	-5.80
14	Luteolin	High	No	No	Yes	No	No	Yes	Yes	-6.25
15	Apigetrin	Low	No	Yes	No	No	No	No	No	-7.65
16	Wogonin	High	No	No	Yes	No	Yes	Yes	Yes	-5.56

17	4,5-Dicaffeoylquinic acid	Low	No	Yes	No	No	No	No	No	-8.37
18	5-Hydroxy-7,2',6'-trimethoxyflavone	High	Yes	No	Yes	Yes	Yes	Yes	Yes	-5.61
19	Andrographidine C	Low	No	Yes	No	No	No	No	Yes	-8.43
20	Andrographidine E	Low	No	Yes	No	No	No	No	Yes	-8.63
21	5,7,2',6'-Tetrahydroxyflavone	High	No	No	Yes	No	No	Yes	Yes	-6.16
22	Andrographoside	Low	No	Yes	No	No	No	No	No	-9.41
23	Methyl 3,4-dicaffeoylquinate	Low	No	Yes	No	No	No	No	No	-8.07
24	Neoandrographolide	High	No	Yes	No	No	No	No	Yes	-7.36
25	Bisandrographolide B	Low	No	Yes	No	No	No	No	No	-5.89
26	7-O-Methylvitexin	Low	No	No	No	No	No	No	No	-8.65
27	Eleutheroside e1	Low	No	Yes	No	No	No	No	No	-9.54

Table 3.9: Lipophilicity Parameters of the Phytoconstituents of *Andrographis paniculata*

S/N	NAME OF COMPOUND	LOG $P_{O/W}$ (ILOGP)	LOG $P_{O/W}$ (MLOGP)	LOG $P_{O/W}$ (SILICOS-IT)	LOG S_W (SILICOS-IT)	SOLUBILITY	SOLUBILITY CLASS	DRUGLIKENESS (LIPINSKI)
1	Oleanolic Acid	3.94	5.82	5.85	-6.12	3.45E-04	Poorly soluble	Yes; 1 violation
2	3-O-beta-D-Glucopyranosylandrographolide	2.5	-0.29	0.9	-0.93	6.04E+01	soluble	No; 2 violations
3	Andrographidin B	3.04	-2.16	0.5	-2.89	6.40E-01	soluble	No; 2 violations
4	Bisandrographolide C	3.83	3.92	6.49	-5.73	1.23E-03	moderately soluble	Yes; 1 violation
5	Andrographidin A	2.50	-0.99	0.97	-3.08	3.82E-01	soluble	Yes; 0 violation
6	14-Deoxy-11,12-didehydroandrographiside	2.56	0.39	1.49	-1.16	3.41E+01	moderately soluble	Yes; 0 violation
7	Chlorogenic Acid	0.87	-1.05	-0.61	0.40	8.94E+02	soluble	Yes; 1 violation
8	2',3',4',5,7-Pentamethoxyflavone	3.67	0.63	4.21	-6.71	7.24E-05	Poorly soluble	Yes; 0 violation
9	Echioidin	2.56	-1.39	0.89	-3.38	1.85E-01	soluble	Yes; 0 violation
10	14-Deoxyandrographoside	3.58	0.48	1.67	-1.88	6.56E+00	soluble	Yes; 0 violation
11	Andrographiside	2.12	-0.29	0.90	-0.93	6.04E+01	soluble	No;2violation
12	Quercetin	1.63	-0.56	1.54	-3.24	1.73E-01	soluble	Yes; 0 violation
13	Apigenin	1.89	0.52	2.52	-4.40	1.07E-02	moderately soluble	Yes; 0 violation
14	Luteolin	1.86	-0.03	2.03	-3.82	4.29E-02	soluble	Yes; 0 violation
15	Apigetrin	1.98	-1.61	0.35	-2.69	8.77E-01	soluble	Yes; 1 violation
16	Wogonin	2.55	0.77	3.03	-5.10	2.25E-03	moderately soluble	Yes; 0 violation

17	4,5-Dicaffeoylquinic acid	1.32	-0.35	0.69	-1.16	3.54E+01	soluble	No; 3 violations
18	5-Hydroxy-7,2',6'-trimethoxyflavone	3.38	0.70	3.6	-5.91	4.03E-04	moderately soluble	Yes; 0 violation
19	Andrographidine C	2.37	-1.18	1.44	-4.07	3.92E-02	moderately soluble	Yes; 0 violation
20	Andrographidine E	3.58	-1.46	1.51	-4.17	3.35E-02	moderately soluble	Yes; 1 violation
21	5,7,2',6'-Tetrahydroxyflavone	1.70	-0.03	2.03	-3.82	4.29E-02	soluble	Yes; 0 violation
22	Andrographoside	2.78	-0.29	0.9	-0.93	6.04E+01	soluble	No; 2 violations
23	Methyl 3,4-dicaffeoylquinate	2.81	0.05	1.81	-2.54	1.58E+00	soluble	No; 2 violations
24	Neoandrographolide	3.37	1.26	2.55	-2.7	9.54E-01	soluble	Yes; 0 violation
25	Bisandrographolide B	4.07	3.92	6.77	-6.31	3.26E-04	Poorly soluble	Yes; 1 violation
26	7-O-Methylvitexin	2.12	-1.80	0.87	-3.07	3.83E-01	soluble	Yes; 1 violation
27	Eleutheroside e1	3.70	-1.61	0.69	-2.62	1.41E+00	soluble	No; 2 violations

Table 3.10: Toxicity profile of the phytoconstituents of *Andrographis paniculata*

S/N	COMPOUND NAME	LD50 (MG/KG)	TOXICITY CLASS	HEPATO TOXICITY	NEURO TOXICITY	NEPHRO TOXICITY	RESPIRATORY TOXICITY	CARDIO TOXICITY	CARCINO GENICITY	IMMUNO TOXICITY	MUTA GENICITY	CYTO TOXICITY
1	Oleanolic Acid	2000	4	+	-	-	+	+	+	+	-	-
2	3-O-beta-D-Glucopyranosylandrographolide	590	4	-	-	+	+	+	-	+	-	+
3	Andrographidin B	5000	5	-	-	+	+	+	-	+	-	+
4	Bisandrographolide C	452	4	-	-	+	+	+	-	+	-	+
5	Andrographidin A	3000	5	-	-	+	+	+	-	+	-	+
6	14- Deoxy-11,12-didehydroandrographiside	41	2	-	-	+	+	+	-	+	-	+
7	Chlorogenic Acid	5000	5	-	-	+	+	-	-	+	-	-
8	2',3',4',5,7-Pentamethoxyflavone	5000	5	-	-	+	+	-	-	+	-	-
9	Echioidin	5000	5	-	-	+	+	-	-	+	-	-
10	14-Deoxyandrographoside	5	1	-	-	+	+	+	-	+	-	+
11	Andrographiside	590	4	-	-	+	+	+	-	+	-	+
12	Quercetin	159	3	-	-	+	+	-	+	-	+	-
13	Apigenin	2500	5	-	-	+	+	-	-	-	-	-
14	Luteolin	3919	5	-	-	+	+	-	+	-	+	-
15	Apigetrin	5000	5	-	-	+	+	+	-	-	+	-
16	Wogonin	3919	5	-	-	+	+	+	-	-	-	-
17	4,5-Dicaffeoylquinic acid	5000	5	-	-	+	+	-	-	+	-	-
18	5-Hydroxy-7,2',6'-trimethoxyflavone	4000	5	-	-	+	+	-	-	-	-	-
19	Andrographidine C	5000	5	-	-	+	+	+	-	+	-	+
20	Andrographidine E	5000	5	-	-	+	+	+		+	-	+
21	5,7,2',6'-Tetrahydroxyflavone	3919	5	-	-	+	+	-	-	-	-	-
22	Andrographoside	590	4	-	-	+	+	+	-	+	-	+
23	Methyl 3,4-dicaffeoylquinate	5000	5	-	-	+	-	-	-	+	-	-

24	Neoandrographolide	5	1	-	-	+	-	+	-	+	-	+
25	Bisandrographolide B	1000	4	-	-	+	+	+	-	+	-	+
26	7-O-Methylvitexin	832	4	-	-	+	+	-	-	-	-	-
27	Eleutheroside e1	3000	5	-	-	+	+	+	-	+	-	-

Where + = Toxic, - = Not toxic

CHAPTER FOUR

DISCUSSION

The discovery of new drugs for the treatment of SARS-CoV-2 is highly essential, as new mutant strains of the virus are constantly emerging against which Remdesivir is ineffective. *Andrographis paniculata*, a well-known medicinal plant with numerous scientifically proven benefits, is also used locally for viral diseases. The isolated compounds were subjected to molecular docking studies, which can aid in the discovery of new drugs to treat SARS-CoV-2.

Remdesivir Triphosphate (RTP) is the active metabolite of the parent drug Remdesivir, an antiviral agent that has been approved for the treatment of the virus COVID-19. RTP mimics Adenosine Triphosphate (ATP), which is a natural nucleotide responsible for RNA production and viral replication; therefore, RTP acts as a substrate for RNA synthesis and is incorporated by the viral RNA-dependent RNA polymerase (RdRp), causing termination of the viral RNA chain, inhibiting the production of new viral RNA and subsequently inhibiting viral replication.

The docking score, obtained from molecular docking analysis of ligands (compounds) against a known protein target, is used to predict the ligand's binding affinity and potential activity.

Remdesivir Triphosphate is used in this study as the standard ligand for comparative analysis, having a binding affinity of -7.7 Kcal/mol. However, a total of 90 compounds from literature sources and 23 compounds identified by GC-MS analysis of A*ndrographis paniculata,* was subjected to molecular docking. Compounds with binding affinities less than or equal to -6.9 kcal/mol were prioritized for further study. Based on these, 27 compounds were selected as potential drug candidates for further analysis.

Site-directed docking was performed by identifying the active/binding-site amino acids in the target protein (7BV2). This enabled predicting ligand activity from the number of active amino acids bound by each ligand in the target protein.

Different ligands bind to amino acids in the target protein via various interactions, including van der Waals forces, π-π interactions, and conventional hydrogen bonds.

4.1 Molecular docking

Twenty-nine (29) compounds, including the standard ligand (Remdesivir Triphosphate) and the co-crystallized ligand (F86), bound with different affinities to the target protein as shown in Tables 3.2 and 3.3. Binding affinity values of the phytoconstituents from A*ndrographis paniculata* range from -6.9 to -8.5 kcal/mol. Methyl 3,4-dicaffeoylquinate had the highest negative binding affinity of -8.5 kcal/mol, the standard drug, Remdesivir triphosphate showed a binding affinity of -7.7 kcal/mol, the co-crystallised ligand (F86) has binding affinity of -6.8 kcal/mol, 14- Deoxy-11,12-didehydroandrographiside, Luteolin, Quercetin, 7-O-Methylvitexin have binding affinities of -7.4, -7.7, -7.5 and -7.6 kcal/mol, respectively, while Apigetrin, and 4,5-Dicaffeoylquinic acid exhibited a binding affinities of -8.4 kcal/mol respectively. In contrast, 3-O-beta-D-Glucopyranosylandrographolide, 2',3',4',5,7-Pentamethoxyflavone, 5-Hydroxy-7,2',6'-trimethoxyflavone, and Neoandrographolide had the least negative binding affinity of -6.9 kcal/mol, respectively. The high negative free energy of binding scores indicates spontaneous protein-ligand binding that stabilizes the interaction (Ahsana *et al*., 2022). Notably, Bisandrographolide C, Apigetrin, 4,5-Dicaffeoylquinic acid, and Methyl 3,4-dicaffeoylquinate showed stronger binding affinity than the standard drug; this suggests that these compounds interact more effectively with the target site and may have greater potential inhibitory activity against the target protein. Overall, the binding affinity score obtained in this study were comparable to those reported by Ahsana *et al* (2022) for *A. paniculata* compounds against SARS-CoV-2 RdRp (PDB ID: 6M71), where 19 compounds exhibited binding affinities ranging between -5.72 and -8.86 kcal/mol. Additionally, better inhibitors of the SARS-CoV-2 RdRp (PDB ID: 7BV2) have been identified among selected flavonoids isolated from the genus *Erythrina,* exhibiting binding affinities ranging from -6.41 and -9.01 kcal/mol (Herlina *et al*., 2025).

As shown in Table 3.1, this study identified key amino acid residues of RdRp, such as ARG555, ASP760, ASN691, SER759, and SER814, that play a crucial role in hydrogen bonding and the active site of the target protein. The standard RTP formed one conventional hydrogen bond interaction with ASP760. The co-crystallized ligands F86, Quercetin, and Luteolin formed two conventional hydrogen bonds (traditional hydrogen interactions) with ARG555 and ASP760 within the active site of the protein. 14- Deoxy-11,12-didehydroandrographiside formed three conventional hydrogen bonds (traditional hydrogen interactions) with ASN691, ASP760, and ARG555, which appeared stronger than those formed by the standard RTP, whereas 3-O-beta-D-Glucopyranosylandrographolide formed

two hydrogen bonds with ASN691 and ARG555. Similarly, Apigetrin formed two hydrogen bonds but interacted with ASP760 and SER814. Notably, although Methyl 3,4-dicaffeoylquinate exhibited the highest binding affinity, it did not form strong hydrogen bonds with any of the active site amino acid residues of the protein. This suggests that its strong binding to the protein is likely due to other types of molecular interactions, such as hydrophobic interactions. Although RTP in this study formed a hydrogen bond only with ASP760, several other compounds exhibited hydrogen bond interactions with residues such as ARG555, ASN691, SER759, and ASP760, which support findings reported by Gado & Alagoz. (2022), which recorded that RTP formed hydrogen bonds with the same amino acid residues. This similar interaction may imply comparable binding orientations of the compounds within the protein active site, suggesting potential inhibitory activity identical to that of remdesivir triphosphate.

Hydrogen bonds promote ligand binding affinity by displacing protein-bound water molecules. Hydrogen bonds are essential for defining ligand specificity (Boss *et al*., 2003). Therefore, 14-Deoxy-11,12-didehydroandrographiside will have high ligand-receptor specificity by interacting with the target amino acids using conventional hydrogen bonds. Also, 14-Deoxy-11,12-didehydroandrographiside, Quercetin, Apigenin, Luteolin, and 5-Hydroxy-7,2',6'-trimethoxyflavone showed similar amino acid interactions as the standard drug and the co-crystallized ligand. This supports the claim that compounds from *Andrographis paniculata* possess anti-SARS-CoV-2 activity (*Khanit et al*., 2021).

4.2 ADMET Profiling

The ligands from *Andrographis paniculata* showed promising binding affinity against the protein. However, assessing the compounds' pharmacokinetic (Absorption, Distribution, Metabolism, Excretion, and Toxicity) profiles is essential to ascertain their viability as potential drug candidates and to avoid costly failures in later stages of drug development. Various rules are available to assess drug-likeness; however, the Lipinski rule of 5 was adopted for this project. The Lipinski rule of 5 states that an orally active drug must not break more than one of the following criteria: hydrogen bond acceptor ≤ 10; hydrogen bond donor ≤ 5; octanol-water partition coefficient ≤5; molecular weight <500 Daltons (*Lipinski,* 2004)

The following compounds, including the best-hit compound Methyl 3,4-dicaffeoylquinate, as well as 3-O-beta-D-Glucopyranosylandrographolide, Andrographidin B, Andrographiside, 4,5-Dicaffeoylquinic acid, Andrographoside, and Eleutheroside E1, violated Lipinski's Rule

of 5. However, all other 20 selected compounds from *Andrographis paniculata* passed the ADME drug-likeness evaluation, as shown in Table 3.7. The compounds that violate these criteria are likely to exhibit poor oral bioavailability and may require additional modifications to improve it. This finding is similar to a previous study carried out on isolated flavonoids against SARS-CoV-2 RdRp (7BV2) in which the two best hits compounds identified as Abyssinoside A and Abyssinoside B with binding affinities of -9.01 and -8.47 kcal/mol, respectively, also violated the Lipinski rule of 5 (Herlina *et al*., 2025). However, all 27 selected compounds were subsequently screened for potential toxicity to determine their safety profile.

The toxicity analysis in this study considered several parameters, including LD_{50} (mg/kg), predicted toxicity class, and organ toxicities, including hepatotoxicity, neurotoxicity, nephrotoxicity, respiratory toxicity, and cardiotoxicity. It also predicted toxicity endpoints, including carcinogenicity, immunotoxicity, mutagenicity, and cytotoxicity. Toxicity levels are classified as follows: Class I: Fatal if swallowed, $LD_{50} \leq 5$, Class II: Fatal if swallowed, $LD_{50} \leq 50$, Class III: Toxic if swallowed, $LD_{50} \leq 300$, Class IV: Harmful if swallowed, $LD_{50} \leq 2000$, Class V: Maybe harmful if swallowed, $LD_{50} \leq 5000$, and Class VI: Non-toxic, $LD_{50} > 5000$, as indicated by the LD_{50} (mg/kg) values in Table 3.9, none of the compounds were found to be non toxic and they all exhibited varying toxicity classes with 14-deoxyandrographoside and Neoandrographolide classified as class I, 14- deoxy-11,12-didehydroandrographiside as class 2, Quercetin as class 3, Oleanolic acid, 3-o-beta-d-glucopyranosylandrographolide, Bisandrographolide C, Andrographiside, Andrographoside, Bisandrographolide B, and 7-o-methylvitexin class 4, and Andrographidin B, Andrographidin A, chlorogenic acid, 2',3',4',5,7-pentamethoxyflavone, Echioidin, Apigenin, Luteolin, Apigetrin, Wogonin, 4,5-Dicaffeoylquinic acid, 5-hydroxy-7,2',6'-trimethoxyflavone, Andrographidine C, Andrographidine E, 5,7,2',6'-tetrahydroxyflavone, methyl 3,4-dicaffeoylquinate and Eleutheroside E1 as class 5.

It was observed that, except for Oleanolic Acid, all the compounds screened did not exhibit hepatotoxicity and neurotoxicity potential, as indicated in Table 3.9. Methyl 3,4-dicaffeoylquinate, which showed the highest binding affinity (-8.5) and an LD_{50} of 5000 mg/kg, was predicted to be relatively safe, with low immunotoxicity and nephrotoxicity. In contrast, Apigenin, 5-Hydroxy-7,2',6'-trimethoxyflavone, and 5,7,2',6'-Tetrahydroxyflavone, with binding affinities of -7.3, -6.9, and -7.0 kcal/mol, respectively, are also predicted to be relatively safe, with toxic effects restricted to nephrotoxicity and respiratory toxicity.

Therefore, Methyl 3,4-dicaffeoylquinate, Apigenin, 5-Hydroxy-7,2',6'-trimethoxyflavone, and 5,7,2',6'-Tetrahydroxyflavone were identified as potential good drug candidates due to their comparatively safer toxicity profile. Except for Methyl 3,4-dicaffeoylquinate, the identified compounds are highly absorbed from the GIT, making them good candidates for oral dosage forms. From Table 3.8, Apigenin and 5-Hydroxy-7,2',6'-trimethoxyflavone are moderately water soluble, while 5,7,2',6'-Tetrahydroxyflavone and Methyl 3,4-dicaffeoylquinate are water soluble, which further facilitates their oral bioavailability.

CHAPTER FIVE

CONCLUSION

This study evaluated compounds from *Andrographis paniculata* as potential inhibitors of SARS-CoV-2 protein. Using molecular docking analysis and ADMET prediction, this study revealed that all 27 compounds screened exhibited a stronger binding affinity for the target protein than the co-crystallized ligand, which had a binding affinity of -6.8 kcal/mol. This validates their potential inhibitory activity against the SARS-CoV-2 target protein (PDB ID: 7BV2). Notably, compound Bisandrographolide C, Apigetrin, 4,5-Dicaffeoylquinic acid, and

Methyl 3,4-dicaffeoylquinate revealed stronger binding affinity than the standard drug, RTP, which had a binding affinity of -7.7 kcal/mol. ADME prediction indicated that 20 compounds possessed good oral bioavailability. In contrast, toxicity predictions varied, with some compounds showing high toxicity risk and others, such as 5-Hydroxy-7,2',6'-trimethoxyflavone, 5,7,2',6'-Tetrahydroxyflavone, Apigenin, and Methyl 3,4-dicaffeoylquinate, displaying a comparatively safer toxicity profile. Therefore, these compounds emerge as promising potential leads for drug development against the SARS-CoV-2 RdRp protein.

Overall, further experimental validation through molecular dynamics simulations, *in vitro and in vivo studies, and preclinical and clinical assessments is required to* confirm their therapeutic potential as antiviral agents against the SARS-CoV-2 RdRp protein.

REFERENCES

Adedayo BC, Komolafe T, Ojueromi OO, Oboh G. (2024). Evaluation of Andrographis paniculata-supplemented Diet on the reproductive indices of Plasmodium berghei-infected mice. J Ethnopharmacol;321:117558

Agu P.C, Afiukwa C.A, Orji O.U, Ezeh E.M, Ofoke J.I, Ogbu C.O, Ugwuja E.I, Aja P.M. (2023). Molecular docking as a tool for the discovery of molecular targets of nutraceuticals in disease management. Sci rep. 13(1):13398

Ahsana D, Meily A, Pratama RR, Andika A. (2022). Discovery of SARS-CoV-2 RNA-dependent-RNA-polymerase (RdRp) inhibitor from Sambiloto (*Andrographis*

paniculata) Based on Molecular Docking and ADMET Prediction Approach. Pharm Sci Res. 9(2):81-90. Doi:10.7454/psr.v0i2.1236

Ajjarapu S. (2023). *Computer-Aided Drug Design (CADD): Types, Uses, Examples, Softwares.* Available from https://microbenotes.com/computer-aided-drug-design-cadd/

Ameh SJ, Obodozie OO, Inyang US, Abubakar MS, Garba M. (2010). A normative study of Nigerian grown "Maha-tita" (King of Bitters)- Andrographis paniculata Nees. Int J Drug Dev Res;2(1):291-9

Ameh SJ, Obodozie OO, Inyang US, Abubakar MS, Garba M. (2010). Quality control tests on Andrographis paniculata Nees (family: Acanthaceae)- an Indian 'Wonder' plant grown in Nigeria. Trop J Pharm Res. 9(4):387-94. Doi:10.4314/tjpr.v9i4.58937

Azad I. (2023). Molecular Docking in the Study of Ligand-Protein Recognition: An Overview. IntechOpen. DOI: 10.5772/intechopen.106583.

Aziz S, Waqas M, Mohanta TK, Halim SA, Amir A, Ali A, Khalid A, Abdalla AN, Khan A, Al-Harrasi A. (2023). Identifying non-nucleoside inhibitors of RNA-dependent RNA-polymerase of SARS-CoV-2 through per-residue energy decomposition-based pharmacophore modelling, molecular docking, and molecular dynamics simulation. J Infect Public Health.16(10):501-519.

Banerjee P, Eckert A.O., Schrey A.K. and Preissner R. (2018). ProTox-II: a webserver for the prediction of toxicity of chemicals. *Nucleic acids research*, *46*(W1), pp.W257-W263.

Batool M, Ahmad B, Choi S. (2019). A Structure-Based Drug Discovery Paradigm. Int. J. Mol. Sci. 20(11),2783. Available from https://doi.org/10.3390/ijms20112783

Boss C, Richard-Bildstein S, Weller T, Fischli W, Meyer S, & Binkert C. (2003). Inhibitors of the Plasmodium falciparum parasite aspartic protease plasmepsin II as potential antimalarial agents. Current Medicinal Chemistry. 10(11): 883-907.

Burley S.K., Berman H.M., Duarte J.M., Feng Z., Flatt J.W., Hudson B.P., Lowe R., Peisach E., Piehl D.W., Rose Y. and Sali, A. (2022). Protein data bank: a comprehensive review of 3D structure holdings and worldwide utilization by researchers, educators, and students. *Biomolecules. 12*(10), p.1425.

Caceres DD, Hancke JL, Burgos RA, Wikman GK. (1997). Prevention of common colds with *Andrographis paniculata* dried extract: A Pilot double blind trial. Phytomedicine. 4:101104.

Centers for Disease Control and Prevention. (2025). COVID-19 treatment clinical care for outpatients. Available from https://www.cdc.gov/covid/hcp/clinical-care/outpatient-treatment.html

Dailey JW. (2025). Pharmaceutical industry. In Encyclopaedia Britannica. Available from: https://www.britannica.com/technology/pharmaceutical-industry

Daina A., Michielin O., and Zoete V. (2017). SwissADME: a free web tool to evaluate pharmacokinetics, drug-likeness and medicinal chemistry friendliness of small molecules. *Scientific reports*, *7*(1), p.42717

Demeke CA, Woldeyohanins AE, Kifle ZD. (2021). Herbal medicine use for the management of COVID-19: A review article. Metab open. 12:100141

Drews J. (2000). Drug discovery: A historical perspective. Science. 287:1960-1964.

Dwivedi M, Mishra S, Sonter S, Singh PK. (2021). Diterpenoids as potential anti-malarial compounds from *Andrographis paniculata*. Beni-Suef Univ J Basic Appl Sci. 10:7. Doi:10.1186/s43088-021-00098-8

Ece A. (2023). Computer-aided drug design. BMC Chem. 17(1):111. Doi:10.1186/s13065-023-00939-w

Eweas AF, Maghrabi I, Namarneh AI. (2014). Advances in molecular modelling and docking as a tool for modern drug discovery. Der Pharma Chemica. 6(6):211-228.

Faluyi O. (2021). Nigeria's Medicinal Plants: Andrographis paniculata (Meje Meje). Punch Newspapers (punchng.com)

Norma F-H, Juan F, Daniel G-M. (2021). "In Silico Pharmacokinetics, ADMET Study and Conceptual DFT Analysis of Two Plant Cyclopeptides Isolated from *Rosaceae* as a Computational Peptidology Approach." *Frontiers in Chemistry,* ***9*(1)**. DOI: 10.3389/fchem.2021.708364.

Gado S, Alagoz ZA. (2022). RNA dependent RNA polymerase (RdRp) inhibitor drugs against SARS-CoV-2: a molecular docking study. J. Fac. Pharm. Ankara, Turkey. 46(1):62-77. Doi:10.33483/jfpau.963384

Ghosh R, Chakraborty A, Biswas A, Chowdhuri S. (2020). Evaluation of green tea polyphenols as novel corona virus (SARS CoV-2) main protease (Mpro) inhibitors -an in silico docking and molecular dynamics simulation study. J. Biomol. Struct. Dyn. 39 (12), 4362-4374.

Guan L, Yang H, Cai Y, Sun L, Di P, Li W, Liu G, & Tang Y. (2018). ADMET-score - a comprehensive scoring function for evaluation of chemical drug-likeness. *MedChemComm*, *10*(1), 148–157. DOI: https://doi.org/10.1039/c8md00472b

Gupta S, Mishra K.P., Ganju L. (2017). Broad-spectrum antiviral properties of andrographolide. *Arch. Virol.* 162(3):611–623. [**Google Scholar**] [**CrossRef**]

Herlina T, Nishinarizki V, Akili AWR, Hardianto A, Gaffar S, Muchtaridi M, Latip J. (2025). Exploring Erythrina flavonoids as potential SARS-CoV-2 RdRp inhbitors through virtual screening, in silico ADMET evaluation, and molecular dynamics simulation studies. Sci Rep. 15(1):14259. Doi:10.1038/s41598-025-97311-w

Jiang M, Sheng F, Zhang Z, Ma X, Gao T, Fu C, Li P. (2021). *Andrographis paniculata* (Burm.f.) Nees and its major constituent andrographolide as potential antiviral agents. J ethnopharmacol. Available from https://doi.org/10.1016/j.jep.2021.113954

Jones AW. (2011). Early drug discovery and the rise of pharmaceutical chemistry. Drug Test Anal. 3(5-6):337-344. Available from http://doi:10.1002/dta.301

Khan H. 2014. Medicinal plants in light of History. Evid based complement Alternate Med. 19(3):216-9 https://doiorg/10.1177/2156587214533346

Khanit S, Ampa S, Yongyut P, Piyanoo T, Phongthon K, Suwimon M, Charonensutthivarakul S, Wongtrakoongate P, Pitiporn S, Chaopreecha J, Kongsomros S, Jearawuttanakul K, Wannalo w, Khemawoot P, Chutipongtanate S, Borwornpinyo S, Thitithanyanont A, Hongeng S. (2021). Anti-SARS-CoV-2 activity of *Andrographis paniculata* extract and its major component andrographolide in human lung epithelial cells and cytotoxicity evaluation in major organ cell representatives. J Natural Products. 84(4):1261-70.

Kondapuram S.K., Sarvagalla S, Coumar M.S. (2021). Docking-based virtual screening using PyRx Tool: autophagy target Vps34 as a case study. In *Molecular Docking for Computer-Aided Drug Design.* Academic Press. (pp. 463-477).

Leeson PD, Springthorpe B. (2007). "The influence of drug-like concepts on decision-making in medicinal chemistry". *Nature Reviews. Drug Discovery*. **6** (11): 881–890. DOI: 10.1038/nrd2445. PMID 17971784. S2CID 205476574.

Lipinski CA, Lombardo F, Dominy BW, Feeney PJ (2001). "Experimental and computational approaches to estimate solubility and permeability in drug discovery and development settings". *Advanced Drug Delivery Reviews*. **46** (1–3): 3–26. DOI: 10.1016/S0169-409X(00)00129-0. (4):337-341

Lipinski CA (2004). "Lead-and drug-like compounds: the rule-of-five revolution". Drug Discovery Today: Technologies. Lipinski CA (2004). "Lead-and drug-like compounds: the rule-of-five revolution". Drug Discovery Today: Technologies. 1(4):337-341. Doi:10.1016/j.ddt ec

Lipinski CA (2004). "Lead-and drug-like compounds: the rule-of-five revolution". Drug Discovery Today: Technologies. 1(4):337-341. Available from Doi:10.1016/j.ddt ec

Macalino SJY, Billones JB, Organo VG, Carrillo MCO. (2020). In Silico Strategies in Tubercuolosis Drug Discovery. Molecules. 25(3):665.

Macalino SJY, Gosu V, Hong S, Choi S. (2015). Role of computer-aided drug design in modern drug discovery. Arch Pharm Res. 38(9):1686-1701.

Malin JJ, Suarez I, Priesner V, Fatkenheuer G, Rybniker J. (2020). Remdesivir for the treatment of COVID-19: A narrative review. Infection. 48(5):641-9. Available on https://pmc.ncbi.nlm.nih.gov/articles/PMC10828241

Mathieu E, Ritchie H, Rodes-Guirao L, Appel C, Giattino C, Hasell J, Macdonald B, Dattani S, Beltekian D, Ortiz-Ospina E, and Roser M. (2020). Covid-19 Pandemic. Retrieved from https://ourworldindata.org/coronavirus

Mshebelwala K, Ofokansi KC, Kennechukwu FC. (2013). Antihypertensive effect of methanol leaf extract of *Andrographis paniculata* in experimental cats. Afr J Pharm Res Dev. 5(2):109-20

Newman D.J., & Cragg G.M. 2012. Natural products as sources of new drugs over the 30 years from 1981 to 2010. Journal of natural products. 75(3):311-35

Nyeem MAB, Mannan MA, Nuruzzaman M, Kamrujjaman KM, Das SK. (2017) Indigenous king of bitter (*Andrographis paniculata*): A review, J Med Plants Stud. 7;5(2):318-24.

Okhuarobo A, Falodun JE, Erharuyi O, Imieje V, Falodun A, Langer P. (2014). Harnessing the medicinal properties of Andrographis paniculata for diseases and beyond: a review of its phytochemistry and pharmacology. Asian Pac J Trop Dis;4(3):213-222

Oprea TI, Davis AM, Teague SJ, Leeson PD (2001). "Is there a difference between leads and drugs? A historical perspective". *Journal of Chemical Information and Computer Sciences*. **41** (5): 1308–1315. DOI: 10.1021/ci010366a. PMID 11604031.

Pina A. S., Hussain A., & Roque A. C. A. (2009). An Historical Overview of Drug Discovery. *Methods in Molecular Biology*. 572:3-12.

Pattnaik S, Siddharta B. (2022). Molecular docking and molecular dynamic simulation approaches for drug development and repurposing of drugs for severe acute respiratory syndrome-Coronavirus-2. In Parihar A, Khan R, Kumar A, Kaushik A, Gohel H, editors. Computational Approaches for Novel therapeutic and Diagnostic Designing to mitigate SARS-CoV-2 infection. p207-246

Pinzi L., Rastelli G. (2019). Molecular docking: shifting paradigms in drug discovery. Int. J. Mol Sci. 20:4331. Doi:103990/ijms20184331.

Rahman HS, Aziz MS, Hussein RH, Othman HH, Omera SHS, Khalid ES, Abdulrahman NA, Amin K, Abdullah R. (2020). The transmission modes and sources of COVID-19: A systematic review. Int J Surg Open. 26:125-36. Retrieved from https://doi.org/10.1016/j.ijso.2020.08.017

Schake P., Bolz S.N., Linnemann K., Schroeder M. (2025). PLIP 2025: introducing protein-protein interactions to the protein-ligand interaction profiler. 53(W1):W463-W465. https://doi.org/10.1093/nar/gkaf361

Torres PHM, Sodero ACR, Jofily P, Silva-Jr FP. (2019). Key Topics in molecular Docking for Drug Design. Int J Mol Sci. 20(18):4574.

US Food and Drug Administration. (2018). "The drug development process". Retrieved from https://www.fda.gov/patients/learn-about-drug-and-device-approvals/drug-development-process

Verber DF, Johnson SR, Cheng HY, Smith BR, Ward KW, Kopple KD (2002). "Molecular properties that influence the oral bioavailability of drug candidates". J Med. Chem. 45(12):2615-2623.

Vijayakumar M, Janani B, Kannappan P, Renganathan S, Al-Ghamdi S, Alsaidan M, Abdelaziz M.A, Mohideen A.P., Shahid M, Ramesh T. (2022). In silico identification of potential inhibitors against main protease of SARS-Cov-2 6LU7 from Andrographis paniculata via molecular docking, binding energy calculations and molecular dynamics simulation studies. Saudi J Biol sci. 29(1):18-29

Wang X, Song K, Li L, Chen L. (2018). Structure-based drug design strategies and challenges. Curr Top Med Chem. 18(12):998-1006. Doi:10.2174/1568026618666180881311529 21.

World Health Organization. (2022). Middle East respiratory syndrome coronavirus (MERS-CoV). Retrieved from https://www.who.int/emergencies/mers-cov/en/

World Health Organization. Molnupiravir safety poster C. (2022). Available from https://apps.whp.int/iris/bitstream/handle/10665/359764/WHO-2019-nCoV-Therapeutic-Molnupravir-Poster-C-2022-1-eng.pdf

World Health Organization. (2023). Clinical management of COVID-19: living guideline.

World Health Organization. (2025). COVID-19 dashboard. Retrieved from https://data.who.int/dashboards/covid19/cases

World Health Organization. (2025). Clinical management of COVID-19: living guideline. Retrieved from https://doi.org/10.2471/B0946.

Wikipedia. (2025). Lipinski rule of five. Available from https://en.wikipedia.org/wiki/lipinski%27s_rule_of_five#

Wikipedia. (2025). Medicinal plants. Available from https://en.wikipedia.org/wiki/medicinal_plants

Wikipedia. (2025). Molnupiravir. Available from https://en.wikipedia.org/wiki/molnupiravir

Wikipedia. (2025). Nirmatrelvir/ritonavir. Available from https://en.wikipedia.org/wiki/Nirmatrelvir/ritonavir

Wu Z, Chen S, Wang Y, Li F, Xu H, Li M, Zeng Y, Wu Z, Gao Y. (2024). Current perspectives and trend of computer-aided drug design: a review and bibliometric analysis. Int J Surg. 110(6):3848-3878.

Xu CX, Tham CL. (2024). Drug discovery and development: A historical overview, current challenges and perspective. Life Sci Med Biomedicine. 8(1):137

Yin W, Mao C, Luan X, Shen D, Shen Q, Su H, Wang X, Zhou F, Zhao W, Gao M, Chang S, Xie Y.C., Tian G, Jiang H.W., Tao S.C., Shen J, Jiang Y, Jiang H., Xu, Y, Zhang S,

Zhang Y, Xu H.E. (2020). Structural basis for inhibition of the RNA-dependent RNA polymerase from SARS-CoV-2 by remdesivir. Sci.;368(6498):1499-1504

Yin Y, Wunderink R.G. (2018). MERS, SARS and Other coronaviruses as causes of pneumonia. Respirology. 23(2) pp. 130-137

Yusuf ZH, Dan VMY, Magaji Y, Onwumere GB, Emmanuel E. (2022). Antidiabetic properties of aqueous leaf and stem extracts of Andrographis paniculata on alloxan-induced diabetes in Wistar rats. UMYU J Microbiol Res.;7(1). doi:10.47430/ujmr.2271.010.

Yu W, MacKerell AD Jr. (2017). Computer-Aided Drug Design Methods. In: Sass P, editor. Antibiotics: Methods and Protocols. Methods in Molecular Biology. 1520:85-106

INDEX

Table showing canonical smiles of selected compounds of *Andrographis paniculata*

S/N	Name of compound	Canonical smiles
1	Oleanolic Acid	C[C@]12CC[C@@H](C([C@@H]1CC[C@@]3([C@@H]2CC=C4[C@]3(CC[C@@]5([C@H]4CC(CC5)(C)C)C(=O)O)C)C)(C)C)O
2	3-O-beta-D-Glucopyranosylandrographolide	C[C@@]12CC[C@H]([C@@]([C@H]1CCC(=C)[C@H]2C/C=C/3\[C@@H](COC3=O)O)(C)CO)O[C@H]4[C@@H]([C@H]([C@@H]([C@H](O4)CO)O)O)O
3	Andrographidin B	COC1=C(C2=C(C(=C1)O)C(=O)C=C(O2)C3=C(C(=CC=C3)O[C@H]4[C@@H]([C@H]([C@@H]([C@H](O4)CO)O)O)O)O)OC
4	Bisandrographolide C	C[C@]12CC[C@@H]([C@]([C@@H]1CCC(=C)[C@@H]2CC(C3C=C(C(=O)O3)/C=C/[C@H]4C(=C)CC[C@@H]5[C@@]4(CC[C@@H]([C@]5(C)CO)O)C)C6=CCOC6=O)(C)CO)O
5	Andrographidin A	COC1=C(C2=C(C(=O)C[C@H](O2)C3=CC=CC=C3)C(=C1)O[C@H]4[C@@H]([C@H]([C@@H]([C@H](O4)CO)O)O)O)OC
6	14- Deoxy-11,12-didehydroandrographiside	C[C@@]12CC[C@H]([C@@]([C@H]1CCC(=C)[C@H]2/C=C/C3=CCOC3=O)(C)CO[C@H]4[C@@H]([C@H]([C@@H]([C@H](O4)CO)O)O)O)O
7	Chlorogenic Acid	C1[C@H]([C@H]([C@@H](C[C@@]1(C(=O)O)O)OC(=O)/C=C/C2=CC(=C(C=C2)O)O)O)O
8	2',3',4',5,7-Pentamethoxyflavone	COC1=C(C(=C(C=C1)C2=CC(=O)C3=C(O2)C=C(C=C3OC)OC)OC)OC
9	Echioidin	COC1=CC(=C2C(=C1)OC(=CC2=O)C3=CC=CC=C3O[C@H]4C([C@H]([C@@H](C(O4)CO)O)O)O)O
10	14-Deoxyandrographoside	C[C@@]12CC[C@H]([C@@]([C@H]1CCC(=C)[C@H]2CCC3=CCOC3=O)(C)CO[C@H]4[C@@H]([C@H]([C@@H]([C@H](O4)CO)O)O)O)O
11	Andrographiside	C[C@@]12CC[C@H]([C@@]([C@H]1CCC(=C)[C@H]2C/C=C/3\[C@@H](COC3=O)O)(C)CO[C@H]4[C@@H]([C@H]([C@@H]([C@H](O4)CO)O)O)O)O
12	Quercetin	C1=CC(=C(C=C1C2=C(C(=O)C3=C(C=C(C=C3O2)O)O)O)O)O
13	Apigenin	C1=CC(=CC=C1C2=CC(=O)C3=C(C=C(C=C3O2)O)O)O

14	Luteolin	C1=CC(=C(C=C1C2=CC(=O)C3=C(C=C(C=C3O2)O)O)O)O
15	Apigetrin	C1=CC(=CC=C1C2=CC(=O)C3=C(C=C(C=C3O2)O[C@H]4[C@@H]([C@H]([C@@H]([C@H](O4)CO)O)O)O)O)O
16	Wogonin	COC1=C(C=C(C2=C1OC(=CC2=O)C3=CC=CC=C3)O)O
17	4,5-Dicaffeoylquinic acid	C1[C@H]([C@H]([C@@H](C[C@@]1(C(=O)O)O)OC(=O)/C=C/C2=CC(=C(C=C2)O)O)OC(=O)/C=C/C3=CC(=C(C=C3)O)O)O
18	5-Hydroxy-7,2',6'-trimethoxyflavone	COC1=C(C(=C2C(=O)CC(OC2=C1)(C3=CC=CC=C3)OC)O)OC
19	Andrographidine C	COC1=C(C2=C(C(=C1)O[C@H]3[C@@H]([C@H]([C@@H]([C@H](O3)CO)O)O)O)C(=O)C=C(O2)C4=CC=CC=C4)OC
20	Andrographidine E	COC1=CC=CC=C1C2=CC(=O)C3=C(O2)C(=C(C=C3O[C@H]4[C@@H]([C@H]([C@@H]([C@H](O4)CO)O)O)O)O)OC)OC
21	5,7,2',6'-Tetrahydroxyflavone	C1=CC(=C(C(=C1)O[C@H]2C([C@H]([C@@H](C(O2)CO)O)O)O)C3=CC(=O)C4=C(C=C(C=C4O3)O)O)O
22	Andrographoside	C[C@@]12CC[C@H]([C@@]([C@H]1CCC(=C)C2C/C=C/3\[C@@H](COC3=O)O)(C)CO[C@H]4[C@@H]([C@H]([C@@H]([C@H](O4)CO)O)O)O)O
23	Methyl 3,4-dicaffeoylquinate	COC1=C(C=CC(=C1)/C=C/C(=O)O[C@H]2[C@@H](C[C@@](C[C@H]2OC(=O)/C=C/C3=CC(=C(C=C3)O)O)(C(=O)OC)O)O)O
24	Neoandrographolide	C[C@]1(CCC[C@@]2([C@@H]1CCC(=C)[C@H]2CCC3=CCOC3=O)C)CO[C@H]4[C@@H]([C@H]([C@@H]([C@H](O4)CO)O)O)O
25	Bisandrographolide B	CC12CCC(C(C1CCC(=C)C2/C=C/C3=CC(OC3=O)C4(C(=C)CCC5C4(CCC(C5(C)CO)O)C)CCC6=CCOC6=O)(C)CO)O
26	7-O-Methylvitexin	COC1=C(C2=C(C(=C1)O)C(=O)C=C(O2)C3=CC=C(C=C3)O)[C@H]4C([C@H]([C@H](C(O4)CO)O)O)O
27	Eleutheroside E1	COC1=CC(=CC(=C1O)OC)[C@@H]2[C@H]3CO[C@@H]([C@H]3CO2)C4=CC(=C(C(=C4)OC)O[C@H]5[C@@H]([C@H]([C@@H]([C@H](O5)CO)O)O)O)OC